
**Université de Neuchâtel**
Institut de Microtechnique

# THIN FILM SOLAR CELLS OF AMORPHOUS SILICON: INFLUENCE OF I-LAYER MATERIAL ON CELL EFFICIENCY

Thèse

Présentée à la faculté de Sciences
pour l'obtention du grade de docteur ès sciences
par

Christian Hof

**UFO Dissertation Band 379**

Die Deutsche Bibliothek – CIP-Einheitsaufnahme

Ein Titeldatensatz für diese Publikation ist bei
Der Deutschen Bibliothek erhältlich

Dissertation der Universität Neuchâtel
Datum der mündlichen Prüfung: 9. 9. 1999
Referenten: Prof. Dr. A. Shah
Prof. Dr. N. de Rooij
Prof. Dr. W. Rehwald
Dr. B. Rech
Dr. P. Seitz

UFO Atelier für Gestaltung & Verlag GbR
Allensbach
Internet http://bome.t-online.de/home/ufo.medien
Maus Druck & Medien GmbH, Konstanz
Erste Auflage 1999

ISBN 3-930803-78-X

# IMPRIMATUR POUR LA THÈSE

**Thin Film Solar Cells of Amorphous Silicon: Influence of I-Layer Material on Cell Efficiency**

de M. Christian Beat Hof

---

UNIVERSITÉ DE NEUCHÂTEL

FACULTÉ DES SCIENCES

La Faculté des sciences de l'Université de Neuchâtel sur le rapport des membres du jury,

MM. A. Shah (directeur de thèse), N. de Rooij,
P. Seitz, B. Rech (Jülich D) et
W. Rehwald (Uni. Constance D)

autorise l'impression de la présente thèse.

Neuchâtel, le 2 novembre 1999

Le doyen:

J.-P. Derendinger

*One shouldn't work on semiconductors, that is a filthy mess; who knows whether they really exist.*

*Wolfgang Pauli, 1931*

*To P. & W.*

# INTRODUCTION

## MOTIVATION

There are few other topics, which I consider as being comparably fundamental but nevertheless simultaneously neglected on a large scale, as the one of the future worldwide energy supply. Actually, the international community is well aware of the problems which are going to be caused if the present policies are continued:

There is on one hand the issue of the environmental impact of conventional energy sources. Related to the usage of fossil fuels such as coal, petrol or natural gas we expect the global warming due to the greenhouse effect to be one of the principal harmful repercussions. Predicting the time scale on which its consequences are expected to bulge to dramatic dimensions is rather intricate but, nevertheless, most of the experts agree that this will happen alarmingly soon. Evaluating *realistically* the dangers of toxic or radioactive waste produced by the power generating industry is even more complex because they are connected often with accidents which are, in principle, unforeseeable. The probability of an "extraordinary event" may be small but with such disastrous results that its threat renders the actual circumstances uncomfortable.

The second major issue can be summarized with the menacing shortage of resources on which the globes' energy consumption is based. Again there exist many projections into a relatively close future and they all do essentially differ in the model describing the growth of the demand in the long run as well as in the exact figure of actual reserves. But nevertheless it is striking that they do all expect the "crunch" in the century to come. This is the case for all conventionally used non-renewable energy sources including fissionable minerals used for nuclear power plants. The option of using the comparably limitless hydrogen reserves in fusion reactors might *(if we really do master their technology one day) unfortunately only solve this* second part of the dilemma.

Renewable energy represents a real solution to the mentioned problems of conventional energy supply. Renewable energy sources do all ultimately depend on the energy radiated on earth by the sun. Taking into account that the amount of energy reaching our planet in a year is about 10'000 times more abundant in comparison with the annual consumption in the whole world one understands that if we manage to harvest even a moderate fraction of this gigantic source we would be able to satisfy more than our needs.

This work deals with solar energy converted into electricity by the means of photovoltaics. In this introduction I intend to share my vision of the role that photovoltaics could play as a part of a concept of sustainable energy supply for the world in the future which was motivating me to accomplish this work.

## TECHNOLOGICAL ASPECTS

The research domain of photovoltaics continues to be an exciting one. Extraordinary results are published in a fast pace. The success of laboratory work is partly reflected in the high solar cell conversion efficiencies [Green 1999] which have been realized using a variety of different semiconductors as well as a variety of fabrication methods. Highest conversion efficiencies under light intensities of 100 mWcm-2 (corresponding to one sun) exceed 30 % [Takamoto 1997].

Although it is for a scientist most fascinating to notice how close such a device approaches the theoretical limits, i.e. the limits dictated by the underlying physical processes, it is important to keep in mind that solar cell efficiency is only one of the important factors that decide whether a certain type of solar cell is suitable for energy conversion on a large scale. Indeed, any photovoltaic technology apt to contribute significantly to future power generation should fulfill all of the requirements summarized in table 1.

| | |
|---|---|
| raw materials: | • available in large enough amounts<br>• reasonably cheap<br>• non toxic (production, handling, end of life) |
| production processes: | • suitable for a large scale production<br>• present a low risk in the case of an accident<br>• demand low energy investments (reducing the payback time) |
| finished modules: | • high efficiency<br>• long life cycle |

*Table 1: Catalogue of requirements to be fulfilled by a photovoltaic technology contributing significantly to power generation.*

It is, however, difficult to achieve simultaneously all the cited criteria. At present there are mainly two types of solar cells that attain most of the defined goals in a satisfying way: cells based on crystalline silicon and cells based on thin films of amorphous silicon. Their market shares amount to about 85 % (crystalline silicon) and 15 % (amorphous silicon) respectively. For crystalline silicon major compromises with respect to the goals of table 1 concern the production costs and energy investments. Amorphous silicon modules suffer mainly from conversion efficiencies that are in general still too low (highest efficiencies of modules with an approximate area of 1 $m^2$ reached 10.4 % in the case of amorphous silicon after light soaking in comparison to 15.2 % for multicrystalline silicon or 22.7 % for crystalline silicon [Green

1999]). In both fields promising new concepts are intensively being studied aiming to develop a technology allowing to produce cheap, efficient solar cells. To bring down the costs of crystalline silicon based solar cells ways of producing cheaper base material (ribbon silicon [Wallace 1997], deposition of thin crystalline films on cheap substrates [Ingram 1996] etc.) are being investigated. My own work is a contribution to the second alternative which consists of increasing the stabilized cell efficiencies of amorphous silicon based solar cells.

## POTENTIAL OF STATE OF THE ART CELLS:

In the following some rough calculations are presented in order to estimate to which extent even present day's photovoltaic modules could already contribute to the generation of electricity. In order to have reliable figures to start with a restricted region is selected. Thereby the guiding idea is to discuss the situation in Switzerland (latitude: 47° N). To extend the model to other regions one would have to take into account the prevailing meteorological conditions and other local factors.

For the Swiss local climate one can expect a watt of installed photovoltaic peak power to produce about 800 Wh in a year. This is based on experience with pilot and demonstration installations [Meier 1995] as well as on comparison with monitored insolation and temperature [Kunz 1995]. The figure of 800 Wh/Wp per year can be compared to the annual consumption of electricity in Switzerland (47'882 GWh in 1995 [OFEN 1995]). If covered exclusively by photovoltaics it would correspond to a total quantity of power to be installed of 59.9 GW. Supposing a module conversion efficiency of 10 % one can calculate the surface required to cover those needs. This amounts to 599 km² respectively to 1.5 % of the total area of the country. To get an idea of the magnitude of this surface one can compare it to the current fragmentation of the land area in Switzerland [OFES 1997] as shown in table 2.

| kind of utilization | size [km²] | size [%] |
|---|---|---|
| forest | 12523 | 30.0 |
| agriculture | 15813 | 38.3 |
| building area (without industry): | 1186 | 2.9 |
| industry area | 147 | 0.4 |
| special infrastructure | 158 | 0.4 |
| parks | 125 | 0.3 |
| traffic area | 801 | 1.9 |
| lakes and rivers | 1725 | 4.2 |
| unproductive vegetation | 2473 | 6.0 |
| no vegetation | 6333 | 15.3 |
| total | 41284 | 100 |

*Table 2: Segmentation of the land in Switzerland*

One can see, that it is theoretically not necessary to reserve additional ground for huge photovoltaic power plants. Ideally the surface required for photovoltaics to satisfy the demand of electricity can be shared to a big extent for example with the building area by integrating the panels onto the building rooftops, into facades etc. A detailed study

evaluating the total building surface poteotial for photovoltaic use in Switzerland has shown that as much as 180 km² can be used with a relative solar yield higher than 80 % (with respect to an optimally inclined and orieoted surface at the same site) [Nowak 1995].

Of course photovoltaics suffers from one main disadvantage with respect to cooveotiooal sources which is related with its availability. In the far future, if photovoltaics is to play a dominant role io providing electricity, it will be oecessary to accumulate cooverted eoergy during high insolatioo periods to allow later use. However, efficieot means allowing short term storage (to grant supply during the night) or eveo looger term storage (to achieve indepeodeoce of the seasons) are not yet geoerally available. Therefore it is interesting to estimate the part of photovoltaically produced electricity which is *in phase* with the current load.

Figure 1 compares the typical productioo of electricity (in Switzerland) oo a day for each seasoo [OFEN 1995] with average insolatioo data of the correspoodiog moath [Kunz 1995]. One clearly ohserves that daily modulations of electricity coosumptioo are esseotially syochronized with potential photovoltaic power generatioo.

From this it is obvious that there does exist an large potential of usiog photovoltaics up to a certaio exteot eveo without requiring aoy storage possihilities. As cao be seeo io figure 1 the load peaks are preseotly esseotially covered hy the use of hydroelectricity. The idea would of course oot be to replace hydroelectric plaots hy photovoltaic power geoeratioo but rather to perform a shift io time and usage of the more flexihle hydroelectric power statioos. They could io fact cover a higger share of the basic oeeds and thereby replace partly conveotional oon reoewable sources.

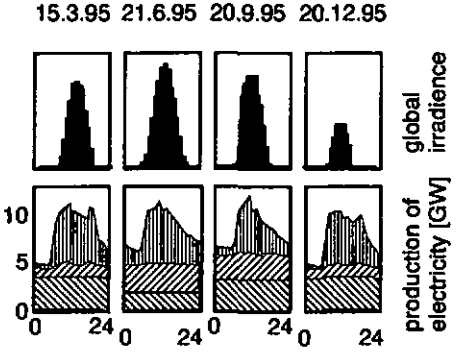


*Fig. 1: Comparison between production of electricity and averaged global insolation data for Switzerland. Electricity production is composed by (from bottom to top) conventional thermal power stations, nuclear power stations, hydroelectric (flowing water), hydroelectric (storage lakes).*

The capacity of photovoltaic power geoeratioo which is in phase with the load and which would help to flatteo the electricity demand can be estimated hy means of the same figure 1. On a first order it correspoods to the minimum peak height at midday with respect to the hase demand at night time. The total peak power that could be iostalled for this purpose would correspood to 4 GW. Part of the peak productioo is curreotly oot coosumed io the couotry itself hut exported. Nevertheless the above estimate is actually too small. The reasoos for this

are as follows. The actual height of the daytime demand peak is kept artificially low (by an increase of the costs per kWh by more than 100 % with respect to the low night tariffs). Secondly, it would be even possible to overcompensate the consumption peak at noon leading to an inversion of the curve to a certain extent. Hydroelectric power would then be required more intensively during night time. As a matter of fact as much as 10 % of the electricity needs in Switzerland could be satisfied by photovoltaics without any further construction of storage infrastructure. This would correspond to 6 GW of installed power. One understands, when comparing this figure to the statistics of world photovoltaic module shipments as presented in Fig. 2, that such an amount of photovoltaic power is colossal.

We conclude from this that technologically speaking photovoltaics is ready to contribute significantly to power production even today. The potential will doubtlessly increase in the mid-term future when we imagine that the storage problem will be solved. Or when transport of electricity over global distances becomes possible with acceptably low losses such as to allow for supply of winter regions of the earth by summer regions. Or when sociocultural changes in the society will affect also economy in such a way that improved consciousness of the value of energy and its conservation will shift electricity intensive processes to daytime (e.g. higher costs of electricity during the night than during the day) in order to favor photovoltaics. Even though such projections would open up fantastic possibilities they remain to a big extent science fiction at the present day.

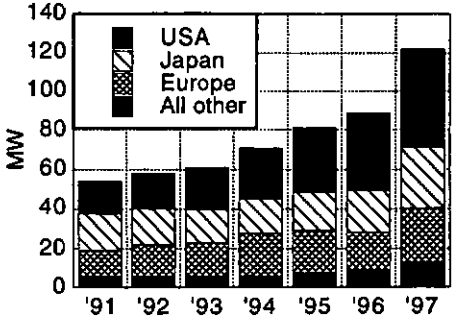


*Fig. 2: World photovoltaic module shipments in MW* [Curry 1998]

To make this dream come true sooner (and, thus, to reduce the potential damage caused to our environment by the time) a lot of work has to be done to enhance the *competitiveness* of solar electricity with respect to conventional sources. With the present work I hope to have contributed a step towards this direction.

# OUTLINE OF THIS THESIS

This thesis is structured into five individual chapters. The first three chapters constitute an approach whicb allows to increase the stabilized solar cell efficiency by an optimization of the deposition conditions leading to more stable material. The last two chapters form a reverse approach attempting to characterize the actual material quality in a completed solar cell directly by performing cell measurements. A more detailed descriptinn of each chapter is presented below:

## CHAPTER 1: CHARACTERIZATION OF AMORPHOUS SILICON LAYERS

After a brief introduction on the most important differences between amorpbous silicon and its crystalline counterpart this first chapter introduces the hasic measurement techniques which were applied for this work to characterize individual intrinsic layers. As relevant properties we estimate, therehy, first nf all the nptical absorption. Based on the standard model for electronic transport in a-Si:H we argue that as a crucial parameter for material optimization one has to consider the normalized mobility * recombination time product $\mu^0\tau^0$. In a second part of this chapter the problem nf metastability of a-Si:H is addressed. A theoretical model is presented which accounts for many of the observed phenomena and which is subsequently used as a conceptual guide on a measurement set-up which substantially accelerates the evaluation of the on the laboratory scale.

## CHAPTER 2: CHARACTERIZATION OF SOLAR CELLS

In the second chapter the standard measurement techniques are presented as they were applied in the this work to evaluate the properties of solar cells. These well-established techniques consist of measurements of the current-voltage behavior and spectral response curves. Again, a method is described to perform light soaking tests but which apply, here, to completed solar cells.

## CHAPTER 3: COMPARISON OF I-LAYER QUALITY AND CELL PROPERTIES

This third chapter constitutes the central part of the work on the correlation between transport studies performed on individual i-layers and solar cells incorporating them. In the

beginning an experimental verification is presented indicating that the earlier (in chapter ooe) presented material quality parameter $\mu^0\tau^0$ constitutes, indeed, a crucial quantity for the optimizatioo of a-Si:H layers. Subsequeotly this parameter is used for cell optimization as well as for a comparisoo of different deposition technologies.

## CHAPTER 4: THEORY OF THE PHOTOCURRENT COLLECTION

As indicated by its title this fourth chapter contains mainly *theoretical* considerations about the collection of photogenerated charge carriers in p-i-o solar cells. Several models whicb have been successfully used in literature are briefly summarized and carefully compared. An extended model is preseoted which treats analytically the more general case including a non-constant electric field. Based on this model a method is presented whicb allows - in priociple - to carry out i-layer studies directly within completed solar cells. Thereby the new i-layer quality related solar cell parameter $V_{Collection}$ is introduced.

## CHAPTER 5: VIM: MEASURING THE I-LAYER QUALITY IN THE COMPLETED CELL?

Here, an experimental study is presented which was carried out io order to apply the previously developed theory. Several consistent series of layers compared to solar cells incorporating these layers are analyzed using the VIM-method (variable intensity measurement method) for the evaluation of $V_{Collection}$. The limitations of the method are conclusively sbown.

# 1. CHARACTERIZATION OF AMORPHOUS SILICON LAYERS

Hydrogenated amorphous silicon is a solid state material made out of silicon atoms which are arranged in a lattice lacking far order. Locally, the electronic bonds between neighboring elements in the amorphous network are almost identical to their crystalline counterparts. Small distortions, however, destroy any long range periodicity. Surprisingly such a material still shows an electronic band structure which may be compared to the one of crystalline semiconductors (Fig. 1.1). But some important differences do arise. At some places the bond deformations may add up to such an extent that for an orbital no overlap with another close one is possible. This is called a "dangling bond". These dangling bonds introduce deep defect states into the bandgap unless they are saturated by an other element (hydrogen, chlorine, fluorine). The role of the hydrogen added during the deposition of a-Si:H (for example through the decomposition of silane) is primarily to reduce the dangling bond density by passivation. Unfortunately not all dangling bonds can be passivated. The remaining ones (typically $10^{16}$ cm$^{-3}$ of totally $10^{19}$ cm$^{-3}$ [Bube 1998]) can be charged either positively (by absence of an electron), they can be neutral (the energy level of such a state as shown in the band diagram

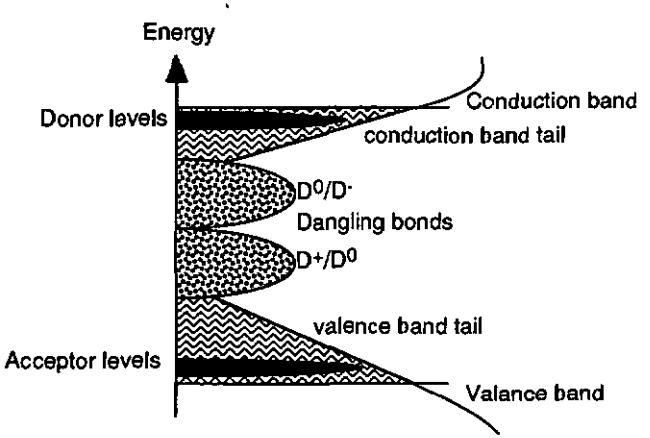


*Fig. 1.1: Schematic band diagram of a-Si:H illustrating the position of electronic states in an amorphous semiconductor. The extended states which allow electric conduction are located in the conduction band and in the valence band. The states between the band edges are localized. They do not allow electronic transport but they act on it indirectly by recombination of free carriers or via their electric charge. They also intervene in optical transitions.*

corresponds to the electronic transition $D^+/D^0$) or they can be doubly occupied (the energy level of such a state corresponds to the transition $D^0/D^-$). They affect electronic transport in two ways: First, through their action as recombination centers which is particularly effective because of their position near midgap. Secondly, they may indirectly influence electronic transport via the total electric charge associated with them. The total density of these defects in a given material is not constant: New defects can be created through breaking of weak bonds (degradation, Staebler-Wronski effect). On the other hand, thermally-stimulated structural reorganizations may reduce the total energy of the system and, thereby, the defect density (annealing). These aspects will be studied in section 1.2.

## 1.1. "STATIC" CHARACTERIZATION OF INTRINSIC LAYERS

In the present section we will imagine that our a-Si:H samples under test are frozen in a certain state (e.g. in the annealed state with a relatively low defect density or in a degraded state with a higher density of gap states). By "static" characterization we mean that the considered measurement techniques evaluate the film properties at a fixed density of dangling bonds. This is in contrast to the evaluation of the metastability addressed in section 1.2.

The standard characterization techniques which are used to analyze a-Si:H thin films can be divided into three categories depending on the kind of information that one gets by using them. A first category consists in the evaluation of optical properties. These are for example the refractive index or the absorption coefficient in the wavelength region which is of interest for photovoltaic energy conversion. A second category deals with the transport of charge carriers and with their potogeneration and recombination. These categories of characterization techniques are both equally important when judging the value of a semiconducting material as photovoltaically active layer. The third category of measurement techniques finally concerns mostly structural properties such as the way hydrogen is bonded in the material. Such knowledge is important for the understanding of the material properties of a-Si:H. But for practical device design it is of secondary interest. This is why we concentrate in the present work on optical and electronic features of a-Si:H films.

### 1.1.1. Geometrical Aspects

Before one can determine the material parameters of a given thin film it is important to know the thickness of the layer under test. To this end we used a stylus surface profiler ("alpha step" of Tencor Inc.). In order to obtain a well defined step from the substrate to the layer we applied two techniques. For many films it was possible to strip off the a-Si:H from the substrate by careful scratching with a cutter. The other technique consists in partially covering the sample with a protective resin, etching away the a-Si:H locally and then removing the resin with a

corresponding solvent. With both methods one can normally obtain measurements with a precision better than 0.05 μm whereas the thickness of the films studied amounts to typically 1 μm. This same surface profiler was also used to determine the geometry of the coplanar contacts as employed for conductivity measurements.

### 1.1.2. Optical Properties

The principle of photovoltaics is based on two individual steps which have to be regarded as equally important if a reasonable overall efficiency in energy conversion is to be obtained. The first one consists in the absorption of light in a semiconductor which will give rise to mobile charge carriers. In a second step these generated free electrons and holes have to be separated and brought to the electric terminals of the solar cell in order to be collected. The totally generated current will depend both on the fraction of photons converted into free electron hole pairs and on the fraction of the charge carriers collected. For thin cells mainly the first act is critical. Intrinsic layers using materials with lower absorption coefficients need to be thicker in order to catch most of the arriving photons. This is illustrated in the following figure (Fig. 1.2) representing thin cells made at different temperatures [Platz 1997]:

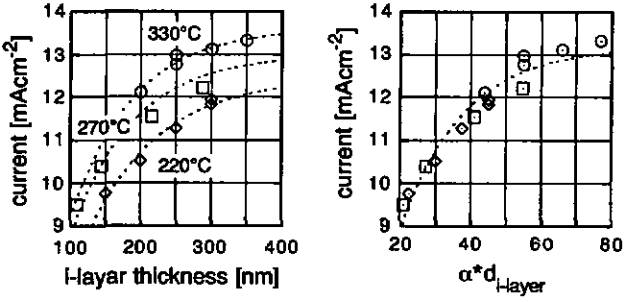


*Fig. 1.2: Thickness series of thin cells deposited at three different temperatures. Increasing the deposition temperature results in material with a higher absorption coefficient. The current of a cell incorporating an i-layer of a given material varies monotonously with its absorption coefficient and thickness. When plotted against the absorbance $A = \alpha \cdot d_{i-layer}$ the current is no longer a function of the deposition temperature. The dotted lines correspond to fits to the eqn. 1.1.*

As long as one achieves total collection the contribution of light at a wavelength $\lambda$ to the photogenerated current in a cell can be written as follows:

$$I_{photo,\lambda} = q \cdot \Phi_{\lambda,i-layer} \cdot (1 - e^{-\alpha_\lambda \cdot d_{i-layer}}), \qquad (1.1)$$

where $q$ is the elementary charge, $\Phi_{\lambda,i-layer}$ is the photon flux reaching the i-layer, and $\alpha_\lambda \cdot d_{i-layer}$ corresponds to the absorbance of the i-layer.

Generally, however, one has to make a trade off betweeo high generation (obtained by the use of a thick i-layer) and higb collectioo (obtained by the use of a thio i-layer). In thick i-layers, with a low absorption coefficient, the generated electron bole pairs are distributed over a wide zone. It is, thus, more difficult to collect them all. In the case of a-Si:H solar cells the collection of the light-generated carriers is essentially powered by the drift of the charge carriers io an electric field. Under short circuit conditions this latter corresponds on an average to the quotient of the built-in potential $V_{built-in}$ over the i-layer thickness $d_{i-layer}$:

$$E_{average} = \frac{V_{built-in}}{d_{i-layer}} \tag{1.2}$$

Materials with low absorption coefficieots lead to an increase in the necessary i-layer thickness and affect, therefore, the photocurreot collection negatively in two ways: by increasing the recombination probability since the carriers bave to travel over longer distances; and also by reduciog the driving force of charge carrier separation, i.e., by reducing the prevailing electric field.

Knowledge of the absorption coefficient of a given a-Si:H film is bence of great importance in the wavelength region that is useful for the generation of electron bole pairs. In this work we determined $\alpha(\lambda)$ of an a-Si:H layer by the measurement of the transmissioo and the reflection of a sample in a commercial spectrometer (Lambda 900 spectrometer by Perkin Elmer). Thereby, we used the following optical model for glass coated with an a-Si:H layer (Fig. 1.3):

On its passage through a sample the beam of ligbt encounters subsequently three interfaces (i-iii). We assumed that the two reflected beams from the air-glass interface (i) and

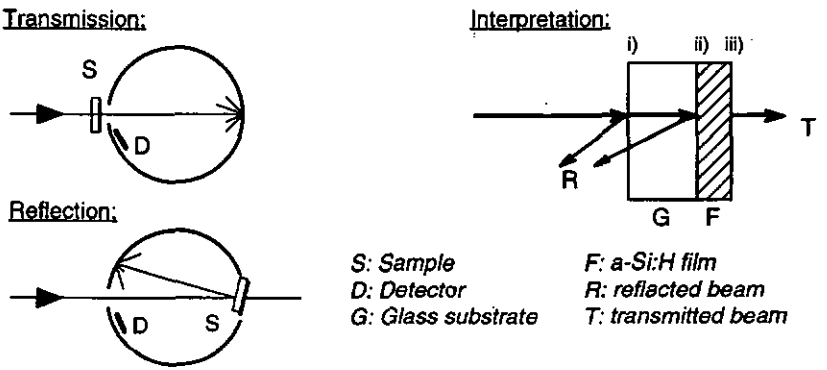


*Fig. 1.3: Reflection and transmission measurements using a commercial spectrometer equipped with an integrating sphere (Ulbricht sphere).*

from the glass-film interface (ii) are incoherent and do not interfere. We neglected the reflection from the film-air interface (iii) because this light beam is reduced in intensity by two passages through the absorbing layer before it can interfere with the light from previous reflections. In the wavelength region of interest (for which the layer is absorbing) this approximation is certainly valid. The glass substrate was assumed to be perfectly transparent. It is possible, under such simplified conditions, to write down the transmission $T_\lambda$ of such a system as:

$$T_\lambda = (1 - R_\lambda) \cdot e^{-\alpha_\lambda \cdot d_{i-layer}} \tag{1.3}$$

This equation permits one to determine the absorption coefficient $\alpha_\lambda$ (as a function of the wavelength) when the total reflection $R_\lambda$ and the i-layer thickness $d_{i-layer}$ of the sample are measured.

Eqn. 1.3 does not take into account multiple reflections (interferences). However, the precision at which the absorption coefficient can be determined with our instrument could not be enhanced even by doing so. In fact, the interferences depend sensitively on the layer thickness and, therefore, as well on the uniformity of the thin film, on the spot size of the probe beam and on its position on the sample. As reflection and transmission are measured separately and, forcefully, not exactly on the same spot of the sample it is practically impossible to compensate for interference effects.

### 1.1.3. Basic Transport and Recombination Equations

After the conversion of the energy of the incoming photons into mobile charge carriers a semiconductor would remain neutral without a mechanism leading to separation of the generated electron hole pairs. The mechanism used in photovoltaics to obtain such a separation is the insertion of an internal field sweeping selectively electrons on one side and holes on the other one and thereby giving rise to a voltage difference between the two sides. This internal field is realized by non uniform doping of the semiconductor with acceptors (p-type doping) and donors (n-type doping). In crystalline semiconductors one uses p-n diodes; here it is sufficient to have the internal field localized in the junction region, which is very narrow compared to the zone where carrier pairs are generated. The carrier pairs can, however, easily reach the junction region by diffusion because of their high mobility and their low recombination coefficient.

The mobility of free carriers in amorphous silicon is typically two orders of magnitude lower when compared to its crystalline counterpart. Furthermore, its high density of electronic states in the gap leads to fast recombination times. Therefore, one has to extend the potential step over the whole absorption region in order to stimulate carrier separation by drift. This is done by inserting an intrinsic (i-) layer as a main absorption layer between the doped layers. Such a p-i-n diode is represented in Fig. 1.4.

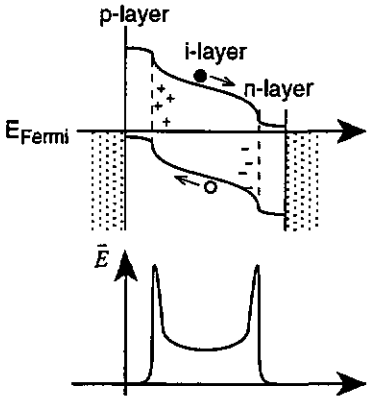


*Fig. 1.4: Schematic band diagram of a p-i-n junction and the electric field variation within the cell. Electrons (symbolized by filled dot) drift under the influence of the electric field towards the n side of the device. Holes are swept in the reverse direction. The gradient of the electric potential and hence the electric field increases towards the doped layers due to charged dangling bonds.*

Transport in intrinsic a-Si:H layer is described by the basic semiconductor equations:

$$\frac{dE(x)}{dx} = \frac{e}{\varepsilon_{Si}}\left(p_f(x) - n_f(x) + Q_{loc}(x)\right) \tag{1.4}$$

$$\frac{1}{e}\cdot j_n(x) = \mu_n^0 n_f(x)E(x) + D_n^0 \frac{dn_f(x)}{dx} \tag{1.5}$$

$$\frac{1}{e}\cdot j_p(x) = \mu_p^0 p_f(x)E(x) - D_p^0 \frac{dp_f(x)}{dx} \tag{1.6}$$

$$0 = G_n(x) - R_n(x) + \frac{1}{e}\cdot\frac{d}{dx} j_n(x) \tag{1.7}$$

$$0 = G_p(x) - R_p(x) - \frac{1}{e}\cdot\frac{d}{dx} j_p(x) \tag{1.8}$$

These are five coupled, first-order differential equations for the free carrier densities $p_f$ and $n_f$, the electric field $E(x)$ and the current densities $j_n$ and $j_p$. They contain non-linear terms introduced by the products $n_f(x)E(x)$ and $p_f(x)E(x)$, by the recombination functions $R_p(x)$ and $R_n(x)$ and by the localized charge term $Q_{loc}(x)$. Because of this they can not be solved in closed form in the general case unless additional assumptions are introduced (such as e.g. a constant electric field $E \neq f(x)$) or unless one performs e.g. a linearization restricted to a small signal case. In the above equations $D_n^0$ and $D_p^0$ stand for the diffusion coefficients and are

related to the band mobilities of free carriers by the Einstein relations : $D_p^0 = \mu_p^0 \cdot kT/e$, $D_n^0 = \mu_n^0 \cdot kT/e$.

When used as an i-layer in a p-i-n junction a-Si:H should have high carrier mobilities and low defect densities. As becomes apparent from the Fig. 1.4, dangling bonds influence the collection of photogenerated carriers in two ways: First of all the recombination of charge carriers increases with the dangling bond density. Secondly, the presence of dangling bonds may induce localized charge which, in turn, result in a screening of the electric field. The occupation function f of a localized state depends on the position of the Fermi level $E_F$. It has has been shown [Hubin 1992] by using the principle of stationarity, that under illumination and for steady state condition the ratios of neutral $f^0$, positively $f^+$ and negatively $f^-$ charged defects can be written as:

$$f^0 = \frac{1}{(p_f / n_f)\cdot(\sigma_p^0 / \sigma_n^+) + 1 + (n_f / p_f)\cdot(\sigma_n^0 / \sigma_p^-)} \tag{1.9}$$

$$f^+ = \frac{(p_f / n_f)\cdot(\sigma_p^0 / \sigma_n^+)}{(p_f / n_f)\cdot(\sigma_p^0 / \sigma_n^+) + 1 + (n_f / p_f)\cdot(\sigma_n^0 / \sigma_p^-)} \tag{1.10}$$

$$f^- = \frac{(n_f / p_f)\cdot(\sigma_n^0 / \sigma_p^-)}{(p_f / n_f)\cdot(\sigma_p^0 / \sigma_n^+) + 1 + (n_f / p_f)\cdot(\sigma_n^0 / \sigma_p^-)} \tag{1.11}$$

with $$f^- + f^0 + f^+ = 1 \tag{1.12}$$

where $n_f / p_f$ is the ratio between free carriers while $\sigma$ refers to the capture cross-sections of neutral ($\sigma^0$), positively ($\sigma_n^+$) or negatively ($\sigma_p^-$) charged dangling bonds for electrons ($n_f$) or holes ($p_f$).

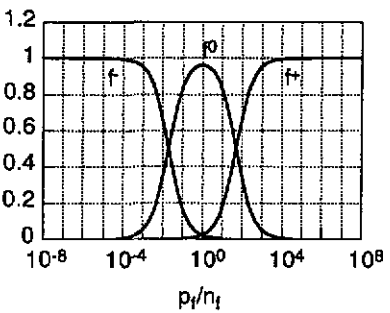


*Fig. 1.5: Calculated occupation functions depending on the ratio between free carriers (eqns. 1.9 to 1.11). It has been admitted that the capture cross-section ratios between charged and neutral dangling bonds are* $\sigma_p^- / \sigma_p^0 = \sigma_n^+ / \sigma_n^0 = 50$.

For the experimental situations considered in this work (i.e. under moderate illumination levels) the main process of recombination is monomolecular recombinatioo via dangling bonds[1]. The recombination times for electrons and boles (defined as "mean times to recombination") can then be writteo as:

$$\tau_n^R = \frac{1}{v_{th} N_{db} f^0 \sigma_n^0 + v_{th} N_{db} f^+ \sigma_n^+} \tag{1.13}$$

$$\tau_p^R = \frac{1}{v_{th} N_{db} f^0 \sigma_p^0 + v_{th} N_{db} f^- \sigma_p^-} \tag{1.14}$$

Under steady state conditions this results in a total recombination rate R :

$$R = G = \frac{n_f}{\tau_n^R} = \frac{p_f}{\tau_p^R} \tag{1.15}$$

It will be showo in Chapter 2 that this function can be simplified for the case of interest in a-Si:H solar cells. In the particular situation of predominantly neutral dangling bonds ( $f^0 >> f^+ + f^-$ ) it turns out [Hubin 1992] that this recombination function transforms into:

$$G = R = \frac{n_f}{\tau_n^0} + \frac{p_f}{\tau_p^0}, \tag{1.16}$$

where $$\tau_n^0 = \frac{1}{v_{th} N_{db} f^0 \sigma_n^0} \text{ and } \tau_p^0 = \frac{1}{v_{th} N_{db} f^0 \sigma_p^0} \tag{1.17}$$

. (Note that this result is very different when compared to the recombination function found for crystalline semiconductors. In the latter case the recombination centers are not amphoteric in nature and the recombination is described by the Sbockley-Read-Hall formula [Sze 1981].)

Intuitively it seems paradoxical (and in contradiction with equation 1.15) that electrons and boles recombine independently since they can only vanish by pairs. The formula becomes, however, evident if one considers the fact that $\sigma_p^- >> \sigma_p^0$ and $\sigma_n^+ >> \sigma_n^0$: every dangling bond

---

[1]It has been shown in work by [Rose 1963]) that defect states localized in the gap of a semiconductor can act either as traps (reemit thermally captured electrons and holes to the conduction respectively to the valence band) or as recombination centers (each capture of a free carrier is followed by a subsequent capture of a charge carrier of the opposite sign). While recombination centers lie between the so called "demarcation levels" the traps lie outside, close to the band edges. These demarcation levels coincide almost with the quasi Fermi levels. "Moderate illumination levels" means, thus, that the quasi Fermi levels embrace practically all dangling bonds without moving into the band tails (see Fig. 1.1).

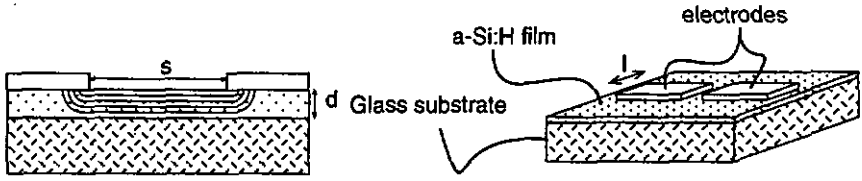


*Fig. 1.6: Configuration used to measure the transport properties of intrinsic a-Si:H layers. The electrodes were typically made of thermally evaporated aluminum. In some cases the latter did not lead to ohmic contacts. In this case the aluminum was replaced by sputtered indium tin oxide. The horizontal lines in the graph on the left schematically depict the current flow.*

catching an electron is charged negatively and will, therefore, undergo more easily a neutralization by capture of a hole. The inverse holds for the recombination of holes. In fact the intervening terms in eqn. 1.16 describe just the bottlenecks of two independent reactions.

### 1.1.4. Photoconductivity Measurements

In order to study the transport and recombination properties of a given a-Si:H material, we deposited intrinsic layers on glass substrates and used electric contacts in a coplanar configuration as illustrated by Fig. 1.6. This allowed us to determine the photoconductivity of the films as well as the ambipolar diffusion length.

The photoconductivity $\sigma_{photo}$ was measured by illuminating the area between the contacts by a widened HeNe laser beam (at the wavelength of 633 nm). Fig. 1.6 indicates that the eqn.:

$$\sigma_{photo} = \frac{1}{R} \cdot \frac{s}{l \cdot d} \tag{1.18}$$

can be used provided that $l >> s >> d$. In our experiments we used a typical geometry of $l \approx 2$ mm, $s \approx 0.5$ mm, $d \approx 1$ µm. We estimated the border effects to be negligible in this case. Assuming a linear potential drop between the two electrodes one finds from the basic transport equations 1.4-1.8 that

$$\sigma_{photo} = e \cdot \left( \mu_n^0 n_f + \mu_p^0 p_f \right) \tag{1.19}$$

One notes that $\sigma_{photo}$ basically monitors the **majority carriers** (i.e. the more numerous carriers). If both carrier densities are equal $\sigma_{photo}$ monitors the more mobile carriers. The free carrier densities $n_f$ and $p_f$ can be calculated from 1.15 which leads to a formulation of $\sigma_{photo}$ in terms of mobility * recombination time products (µτ-products):

$$\sigma_{photo} = e \cdot G \cdot \left( \mu_n^0 \tau_n^R + \mu_p^0 \tau_p^R \right) \tag{1.20}$$

Thereby, $G$ corresponds to the average generation rate within the layer (see Annex I for more details).

One realizes from equations 1.13 - 1.14 and 1.9 - 1.11 that the photoconductivity can increase by orders of magnitude as soon as the majority of dangling bonds becomes charged. When the Fermi level moves out of the midgap position, e.g. towards the conduction band, an increasing amount of dangling bonds becomes doubly occupied. Electrons in the conduction band see their recombination centers vanish and their lifetime dramatically increased. As the photoconductivity is dominated by the majority carriers it will follow accordingly. The same holds for holes in the valence band in the opposite case (with $E_F$ moving towards the valence band also leading to an increase of $\sigma_{photo}$). This means that materials with identical defect densities and band mobilities can have values of $\sigma_{photo}$ that vary over orders of magnitude, depending on the position of $E_F$. This leads in particular to an overestimation of the quality of the material that is not of truly intrinsic character, e.g. material that is contaminated by oxygen or other impurities with dopant character. Therefore, $\sigma_{photo}$ alone cannot be used as an indicator of material quality.

Because of this problem, the photogain $\sigma_{photo} / \sigma_{dark}$ rather than the photoconductivity was generally used in the past as an indicator of material quality. But the variation of $\sigma_{dark}$ with $E_F$ is in principle different than the related changes in $\sigma_{photo}$. $\sigma_{dark}$ varies proportionally with the free carrier densities which are linked to the Fermi level by Fermi-Dirac statistics. In contrast to this $\sigma_{photo}$ is governed by the dangling bond charge which fixes the free carrier density at a given generation rate by recombination. This simple normalization (i.e. to divide $\sigma_{photo}$ by $\sigma_{dark}$ is, therefore, not the ideal way to compensate for contamination-induced variations in $\sigma_{photo}$.

### 1.1.5. Ambipolar Diffusion Length Measurements

For our studies we used as a complementary measurement technique a method to assess the transport of minority carriers; this method is called the "steady state photocarrier grating method (SSPG)" (see e.g. [Sauvain 1992, Smith 1959, 1978]). We used for this purpose a setup as sketched in Fig. 1.7. The samples as prepared for $\sigma_{photo}$ measurements are illuminated using two coherent beams arriving under symmetric angles. Interference results in a periodic generation profile within the i-layer and hence in a free carrier grating modulating the local conductivity. Measuring the average conductivity allows one to determine the extent to which the diffusion of free carriers towards regions of destructive optical interference (i.e. regions with lower photogeneration) increases the locally prevailing minimum free carrier density. Varying the angles of the laser beams allows to change the grating period of the interference pattern. All measurements are made in a small-signal mode, using the lock-in technique. The characteristic length determined by this method is called the ambipolar diffusion

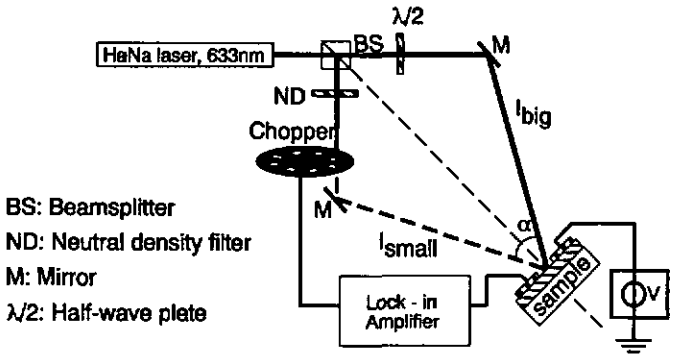


*Fig. 1.7: Sketch of the SSPG measurement set-up. To measure the ambipolar diffusion length the sample is moved along the dotted line. Together with the angle of incidence α the grating constant Λ of the interference pattern on the sample changes. If Λ is bigger than the diffusion length of free carriers $L_{amb}$ the mean conductivity of the sample is reduced by the zones with destructive interference. If Λ is in the order of $L_{amb}$ (or smaller) the carrier grating is smeared out by the diffusion and the generation profile is no longer reflected in the mean conductivity.*

length $L_{amb}$ since both types of carriers diffuse together in the semiconductor - coupled by internal electric fields[Smith 1959, 1978].

It can be shown [Shah 1997], that the basic transport equations 1.4 - 1.8 can be easily solved analytically for a small-signal situation. Under such circumstances, the equations can be linearized. Assuming implicitly that the screening length of the space charge is shorter than $L_{amb}$, i.e. that the lifetime condition is satisfied, they yield as a characteristic length:

$$L_{amb}^2 = \frac{kT}{e} \cdot \frac{\mu_n^0 \tau_n^R \mu_p^0 \tau_p^R}{\mu_n^0 \tau_n^R + \mu_p^0 \tau_p^R} \cdot (1 + \gamma + \lambda) \qquad (1.21)$$

where $G_B$ stands for the generation rate due to the constant light beam $I_{big}$ ("bias" light beam, see Fig. 1.7) whereas $\gamma$ and $\lambda$ correspond to the power law exponents of $\sigma_{photo}$ and $L_{amb}^2$, respectively. It follows from eqn. 1.21 that $L_{amb}$ monitors the minority carriers. Considering eqns. 1.9 - 1.11 and 1.13 - 1.14 one notes that $L_{amb}$ will increase substantially as the dangling bond occupation function $f^0$ for neutral dangling bonds takes over more "weight" with respect to $f^-$ and $f^+$. This is due to an increased recombination time of minority carriers as charged dangling bonds (with large capture cross - sections) are converted into neutral dangling bonds (with much smaller capture cross sections). Consequently, $L_{amb}^2$ alone cannot be used as transport quality parameter in amorphous silicon either.

### 1.1.6. The Normalized Mobility * Recombination Time Product $\mu^0\tau^0$

Formulas 1.20 and 1.21 show that $\sigma_{photo}$ and $L^2_{amb}$ depend both sensitively on the dangling bond occupation functions $f^0$, $f^-$ and $f^+$. Consequently, the mobility * recombination time products for majority carriers $\left(\mu^0\tau^R\right)_{maj}$ and for minority carriers $\left(\mu^0\tau^R\right)_{min}$ associated with them, reflect primarily the "transport character" (whether intrinsic, contaminated, doped or compensated) of a sample rather than the quality of the material.

It has, however, been pointed out by [Beck 1996] that a knowledge of both values, i.e. of $\sigma_{photo}$ and $L^2_{amb}$, allows one to determine a "normalized" mobility * recombination time product, $\mu^0\tau^0$. This parameter $\mu^0\tau^0$ is conceptually equivalent with the mobility * recombination time product that would be measured on the same layer if all dangling bonds were neutral. $\mu^0\tau^0$ takes into account the band mobility of free carriers, as well as the total defect density. It can be expressed as:

$$\mu_n^0\tau_n^0 = \mu_n^0 \frac{1}{v_{th} N_{db} \sigma_n^0} \tag{1.22}$$

$$\mu_p^0\tau_p^0 = \mu_p^0 \frac{1}{v_{th} N_{db} \sigma_p^0} \tag{1.23}$$

Experimentally it has been found that [Beck 1992, Beck 1993]:

$$\mu_n^0\tau_n^0 = \mu_p^0\tau_p^0 = \mu^0\tau^0 \tag{1.24}$$

Using this hypothesis, $\mu^0\tau^0$ can be written as:

$$\mu^0\tau^0 = \frac{\sigma_{photo}}{eG} \cdot \frac{1}{z}, \tag{1.25}$$

where z is the correction factor compensating for Fermi level dependencies of the mobility * recombination time product of majority carriers:

$$z = \frac{1}{f^0} = \left( \frac{\sigma_n^0}{\sigma_n^+} \frac{1}{b} + 1 + \frac{\sigma_p^0}{\sigma_p^-} b \right) \tag{1.26}$$

Here b is a parameter that reflects the "character" of the transport and which is defined as:

$$b = \frac{\mu_n^0 n_f}{\mu_p^0 p_f} \tag{1.27}$$

from eqns. 1.20 - and 1.15 it is found that b can be readily evaluated by:

$$\frac{b}{(b+1)^2} = \frac{L_{amb}^2 e^2 G}{kT\sigma_{photo} C} \tag{1.28}$$

For the evaluation of the correction factor z (and hence of $\mu^0\tau^0$) the capture cross-section ratios $\sigma_n^0 / \sigma_n^+$ and $\sigma_p^0 / \sigma_p^-$ are needed. There has been a lot of controversy in literature about their values. [Henry 1977] for example assumed $\sigma^\pm / \sigma^0$ to reach values up to 1000. [Street 1982], [Street 1983] reported on values of $\sigma^\pm / \sigma^0 \approx 3$ to 5. [Spear 1984] found that $\sigma_n^+ / \sigma_n^0 \geq 30$ but surprisingly $\sigma_p^- / \sigma_p^0 < 1$. [Vaillant 1986] suggested that $\sigma^\pm / \sigma^0 \approx 5$ to 50. [Wyrsch 1991] determined $\sigma_n^+ / \sigma_n^0 \approx 100$, while [Hattori 1991] published $\sigma^\pm / \sigma^0 \approx 1.8$. Throughout this work we will suppose $\sigma^\pm / \sigma^0 = 50$ a value that was determined by [Beck 1997] using two independent methods:

On one hand a series of microdoped p-layers was analyzed. It was supposed that the additional defects introduced by the dopants would vary according to $N_{db} \propto 1/\sqrt{[dopant]/[SiH_4]}$. This empirical law observed by [Stutzmann 1987] and [Street 1991] was only respected by $\mu^0\tau^0$ for a value of the capture cross-section ratio of $\sigma^\pm / \sigma^0 = 50$. On the other hand the stepwise degradation behaviour of a slightly n-type layer was studied. Here the defect density was monitored by the infrared absorbtion $\alpha_{CPM}$ as evaluated by the constant photocurrent method CPM. The changes of the $\mu^0\tau^R$ products of majority and minority carriers deduced from $\sigma_{photo}$ and from SSPG. Again a capture cross-section ratio of $\sigma^\pm / \sigma^0 = 50$ was fitted to the experimental data.

Since $\mu^0\tau^0$ is independent of the dangling bond charge it does not suffer from the drawbacks of the previously defined mobility * recombination time products. In fact it can be noted in Fig. 1.8 that $\mu^0\tau^0$ remains independent of b while $(\mu^0\tau^R)_{maj}$ and $(\mu^0\tau^R)_{min}$ vary over several orders of magnitude.

The arguments leading to the introduction of the $\mu^0\tau^0$-product as developped in the present section are purely theoretical. This material quality parameter has been widely used by our group for the optimization of deposition conditions or for the purpose of comparison of different deposition techniques. Thereby, its usefulness could be consolidated also experimentally. Some of the studies carried out using $\mu^0\tau^0$ are presented in chapter 3.

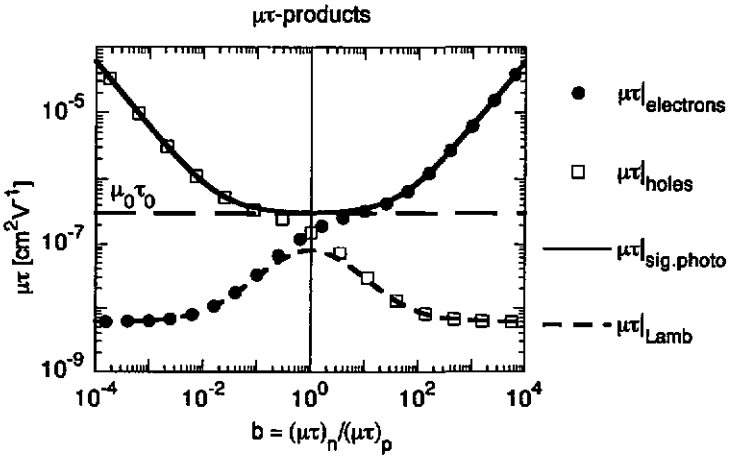


*Fig. 1.8: Calculation of mobility * recombination time products as a function of* $b = \mu_n^0 n_f / \mu_p^0 p_f$. *The normalized product was fixed at* $\mu^0\tau^0 = 3\cdot10^{-7}\ cm^2V^{-1}$ *(this corresponds e.g. to a sample with the following microscopic parameters:* $\mu_n^0 = 10\ cm^2V^{-1}s^{-1}$, $\sigma_n^0 = 10^{-15}\ cm^2$, $\mu_p^0 = 3\ cm^2V^{-1}s^{-1}$, $\sigma_n^0 = 3\cdot10^{-16}\ cm^2$, $v_{th} = 10^7\ cms^{-1}$ *and* $N_{db} = 3\cdot10^{15}\ cm^{-3}$*). Depending on the Fermi level position* $\mu_n^0\tau_n^R$ *and* $\mu_p^0\tau_p^R$ *can vary over several orders of magnitude; thereby, the* $\mu\tau$*-products as evaluated from* $\sigma_{photo}$ *and* $L_{amb}$*-measurements follow accordingly.*

## 1.2. EVALUATION OF METASTABILITY

It has been mentioned in the introduction that the density of defects in an a-Si:H layer is not fixed after its deposition. Indeed it has been observed in the very beginning of the history of a-Si:H [Staebler 1977] that the influence of light stimulates the creation of additional gap states which deteriorate the transport properties of the material. Different microscopic origins (for an overview see [Shimizu 1993]) have been thought to lead to this light-induced degradation of a-Si:H. But to the present day, none of these could be identified as being the one and only cause of this effect. Fortunately, the creation of dangling bonds does not continue indefinitely in a given layer but it saturates at a certain level. Moreover, the whole process was found to be reversible. In fact, the defect density in a film can again be reduced to its initial value by thermally annealing the sample at moderate temperatures (typically T = 180 °C during t = 2 h, followed by a slow cooling rate to prevent quenching[2] of defects).

In the long run, the performance of a given a-Si:H device will depend on its saturated defect density. It is, therefore, important that the characterization of material quality should not be restricted to the annealed state. The degraded state, however, is not unique but results from an equilibrium between creation and annealing of defects and depends, thus, sensitively on the imposed environmental conditions (temperature, illumination) and on the sample history. Consequently, we will introduce a standard degradation procedure on the basis of which different a-Si:H materials can be compared with respect to stability.

### 1.2.1 Theoretical Background

A complete and coherent theory of the underlying mechanisms of the Staebler-Wronski effect is unfortunately missing up to the present day. In the following we will nevertheless present a physical model of the defect creating process which will serve our purposes as a conceptual guide. The underlying theory has been worked out by M. Stutzmann who has shown in very detailed experimental work to what extent this theory is consistent with observation [Stutzmann 1985]. Even though this theory illustrates very well several basic features of a-Si:H material degradation there is some experimental evidence which can not be

[2]It has been observed that the equilibrium defect density of a-Si:H increases with rising temperature [Xu 1989]. If an a-Si:H layer is cooled down rapidly after annealing (e.g. by dropping the sample into liquid nitrogen) this higher defect density present at the annealing temperature can be frozen in. If a sample is allowed to cool down slowly the equilibrium defect density of room temperature can asymptotically be reached.

satisfactorily explained by it[3]. In this work no quantitative interpretation of the degradation dynamics will be based on the "Stutzmann-model". (Note that alternative models have been proposed and have been widely used to fit experimental data. The most prominent one is thereby certainly the "defect pool" model (for an overview refer to e.g. [Smith 1988]). A major drawback of this model is the fact that it leads to rather clumsy mathematical descriptions which can be treated only numerically (and thereby allowing many fit parameters). A model which is particularly successful in fitting the kinetics of degradation and annealing is the one of Redfield (see [Redfield 1992] and references therein). This model is based on rate equations of creation and removal of defects with a certain dispersion of the characteristic time constants. It leads to an analytical description of the experimentally observed degradation kinetics by stretched-exponentials. The underlying microscopic processes leading to the dispersion have been extensively discussed in literature but are still not convincingly established today. In more recent work [Walle 1996] it has been shown that a careful treatment of hydrogen diffusion (including retrapping) leads to very similar curves as the stretched exponentials. Thereby it is unnecessary to invoke statistical distributions as in Redfields' theory.)

The model quoted here has the advantage of providing a very intuitive physical picture of the underlying processes leading to predictions which are at least qualitatively well satisfied by experimental results. Its key point is the assumption that the mechanism creating a dangling bond is the direct recombination of an electron from the conduction band tail with a hole from the valence band tail providing thereby enough energy to break a weak Si-Si bond[4]. Since both, an electron as well as a hole, are required simultaneously for this transition to occur, the rate of dangling bond creation can be expressed as:

$$\frac{dN_{db}}{dt_{ill}} = c_{SW} A_t np , \tag{1.29}$$

where $N_{db}$ denotes the density of dangling bonds, $A_t np$ the number of tail to tail transitions per unit time and $c_{SW}$ a constant expressing the average efficiency of these transitions for the creation of new dangling bonds.

---

[3]As an example for the limitation of this theory the short term relaxation effects presented at the end of this section could be mentioned. Other data which is difficult to reconcile with this model is the one on thermally generated defects (quenching from elevated temperatures, see e.g. [Street 1986]).

[4]Photoluminescence data (peak emission at 1.3-1.4 eV) suggest that virtually all of the band to band recombination occurs via their tails. This is ensured by the rapid thermalization of carriers in extended states [Street 1991].

The densities of electrons and holes in the conduction and valence band are given by:

$$n = \frac{G}{A_n N_{db}} \text{ and } p = \frac{G}{A_p N_{db}}, \text{ respectively.} \tag{1.30}$$

Here G is the generation rate, $A_n N_{db}$ and $A_p N_{db}$ stand for effective transition rates of electrons and holes respectively (being trapped by dangling bonds of all possible charge states). These relations are valid as long as monomolecular recombination (e.g. via dangling bonds) is the dominant pathway reducing excess carrier densities in the bands. A more complete description (but leading basically to the same qualitative observations) is carried out in [Stutzmann 1985]. Combining eqns. 1.29 and 1.30 leads for the creation of defects to:

$$\frac{dN_{db}}{dt_{ill}} = c_{SW} \frac{A_t}{A_n A_p} \left( \frac{G}{N_{db}} \right)^2 \tag{1.31}$$

This equation reveals several interesting features connected with the described model:

1) The rate of creation of additional defects decreases with the density of already present ones: $dN_{db}/dt_{ill} \propto 1/N_{db}^2$. The creation of new dangling bonds is, thus, inhibited by already existing defects since the tail to tail recombination of electron bole pairs is bypassed by recombinations via dangling bonds[5]. Therefore the process of degradation is self-limiting; i.e. the degradation rate will forcefully decrease to a value counterbalanced by the rate of thermal annealing.

2) The saturation level, i.e. the level at which the creation rate of additional dangling bonds $dN_{db} / dt_{ill}$ reduces to a certain value, depends on the generation rate. (This is because the free carrier densities depend on the ratio $G / N_{db}$ while the creation of new defects is proportional to the free carrier densities (eqn. 1.29).)

3) The degradation rate is proportional to the square of the generation rate. (This is because both, electron and hole densities are proportional to the generation rate while the probability nf a bimolecular recombination is proportional to these free carrier densities.)

A stabilization of the degradation is obtained when the rates of dangling bond creation and thermal annealing are balanced. As a possible mathematical description of the process of thermally stimulated defect removal Stutzmann formulated the following equation:

---

[5]This particular mechanism of the stabilization is specific to the "Stutzmann-model". In the model of Redfield, for example, one has to admit explicitly a maximum density of latent defects (e.g. weak bonds).

$$\frac{dN_{db,induced}}{dt_{ill}} = -\nu \cdot N_{db,induced} \tag{1.32}$$

Thereby, $N_{db,induced}$ stands for the density of induced defects (to allow also for a certain density of stable defects) and $\nu$ is a thermally-activated decay constant:

$$\nu = \nu_0 \cdot e^{-\frac{E_a}{k_B T}} \tag{1.33}$$

The parameters $\nu_0$ and the activation energy $E_a$ can of course vary with the exact configurational situation of every metastable state. This renders quantitative predictions of the annealing dynamics impossible. Qualitatively, however, the following affirmations are implied by the model:

4) The saturation level reached by the degradation depends sensitively on the sample temperature. The equilibrium defect density is lower at high sample temperature.

5) The saturation level of the degradation is a well defined state for a material exposed to a given generation rate at a certain temperature and it does not depend on the history of the sample.

### 1.2.2. Degradation using CW Light

Since we are carrying out our material studies in view of a later incorporation of the optimized layers into solar cells, it might seem at first sight most correct to degrade the films under the same conditions as those under which the solar cells will be later exposed during operation. In a controlled experiment this would signify to irradiate the samples with an artificial light source which matches as much as possible the standard spectrum (AM 1.5, 1000 $Wm^{-2}$, see section 2.1). There are two problems associated with this kind of layer degradation:

First of all one observes that the time required to reach the saturation of the degradation is extremely long. Depending on the type of sample and on its degradation dynamics [Kleider 1995] one can be forced to wait for months before the process of defect creation starts to saturate. Several means to shorten the degradation time (i.e. the time until saturation occurs) have been proposed in literature. According to the theoretical background presented in the previous section there are basically two possibilities, as long as CW light is used: One can either raise the light intensity [Banerjee 1991, Lang 1991, Tonon 1991] or one can increase the degradation temperature [Dawson 1996, Vignoli 1996] to accelerate the onset of saturation. In both cases, one alters the equilibrium between degradation and annealing. In fact one has to be aware that the saturation of the degradation corresponds to a dynamic equilibrium which is shifted as soon as the bias conditions are changed. (In the first case of high light intensity the

degradation rate will increase while the thermally stimulated recovery remains the same; in the second case the thermally induced annealing process is enhanced). The saturated layer quality will, therefore, depend on the applied conditions and may in extreme situations not even be qualitatively representative for the state which would be obtained under a long-term exposure under standard cooditions (1000 $Wm^{-2}$ at AM 1.5). For some of our experiments we used, as a compromise, a source with about 5000 $Wm^{-2}$ at 50 °C.

The secood problem is related to the AM 1.5 spectrum. The problem is that the layers which are deposited for material analysis are generally chosen to be considerably thicker (> 1 μm) than what is typically needed for an i-layer in a solar cell (≈ 0.3 μm). Due to the strong absorptiou coefficient of a-Si:H ooe gets, therefore, an all but uniform generation within the layer. The generation rate in the part of the layer facing the light is considerably higher than deep in the material. As a result ooe gets an enhanced degradation at the surface whereas the back part of the thin film is subjected to relatively moderate defect creation. Since the transport of the carriers io a coplanar electric characterization is orthogonal to the direction of the current in the solar cells, the transport process will here primarily take place in the best zone of the layer and one tends, thus, to overestimate the material quality in its degraded state.

Ideally, one should, therefore, use a source at a photon energy sufficiently low to be absorbed uniformly within the i-layer but high enough to lead to a comparable mean generation rate as one gets in solar cells. This can be achieved with a photoo eoergy corresponding to the bandgap of the material (e.g. photons of an energy for which the absorption coefficient $\alpha \approx 10^4\ cm^{-1}$).

Tbe films which are studied do not all have the same bandgap. In a first attempt we used, therefore, a source emitting over a relatively broad wavelength range close to the typical bandgap energy of a-Si:H (1.9 eV). We selected a high pressure sodium lamp which offers the additional advantage of a long lifetime (>15'000 h), as well as a satisfying stability of light

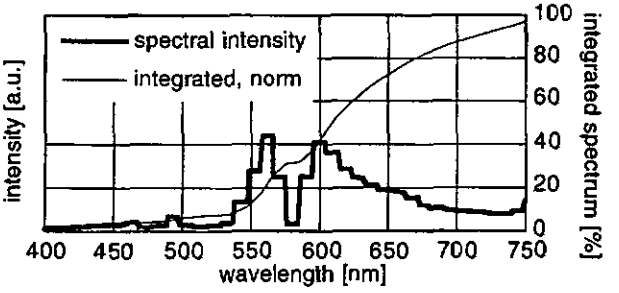


*Fig. 1.9: Spectrum of the Sodium high pressure discharge lamp used by us for CW light soaking of a-Si:H layers.*

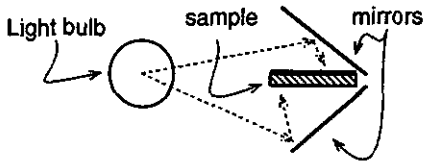


*Fig. 1.10: Degradation system with sodium lamp. Up to eight samples can be fixed for light soaking on a cylinder centered on the light bulb. Thereby symmetrical illumination of the samples from the front and the back leads to a better uniformity of the generation of carriers in the layer.*

intensity over this period of time. The spectrum of this lamp is represented in Fig. 1.9. In order to obtain a better uniformity of the generation throughout the sample it was illuminated symmetrically from both sides as indicated in Fig. 1.10. During light soaking the photoconductivity of the layer was monitored automatically; this allowed us to determine the degradation kinetics as well as the moment when a saturation of the defect creation occurred[6].

A typical curve for the degradation kinetics of an a-Si:H layer measured using this setup is presented in Fig. 1.11. One notes that it takes about $10^6$ s before the rate decelerates to less than 10% per decade i.e. before the degradation process may be considered to enter saturation.

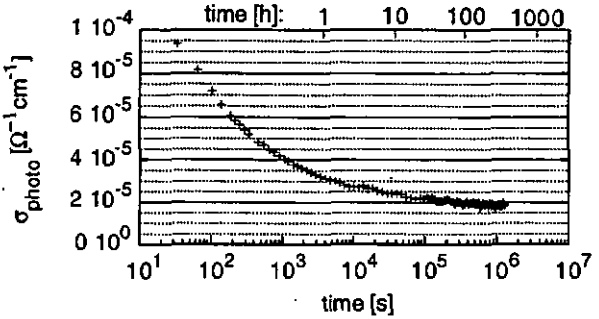


*Fig. 1.11: Typical degradation kinetics for an a-Si:H layer exposed in the sodium lamp based degradation system. Saturation occurs after approximately $10^6$ s*

[6]It is in fact a lucky coincidence that $\sigma_{photo}$ (unlike $L_{amb}$) can be measured automatically and that during degradation of intrinsic layers the changes of $\mu^0\tau^0$ are reflected by $\sigma_{photo}$ (i.e. by the $\mu^0\tau^R$-product of majority carriers). This is so because the creation of dangling bonds at midgap actually pulls the Fermi level towards midgap. It can be seen from Fig. 1.8 that $\mu^0\tau^0 \approx \mu^0\tau^R\big|_{maj}$ for b values which become smaller than the limit $\sigma^{\pm} / \sigma^0 \approx 50$. One notes (formula 1.26) that the correction factor z approaches 1 under this condition.

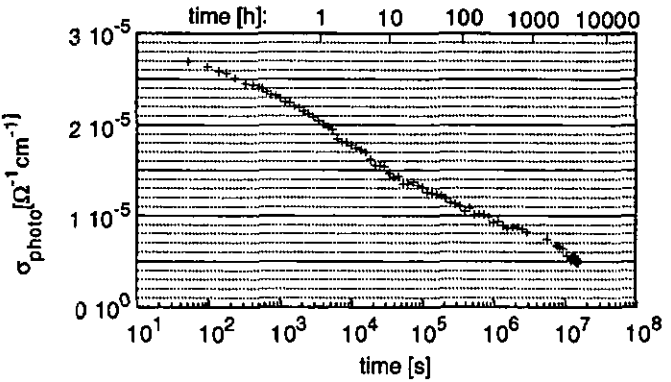


*Fig. 1.12: Typical degradation kinetics of the photoconductivity of an a-Si:H layer deposited by the Hot Wire method as measured on the sodium lamp degradation (SLD) system.*

For our standard (VHF-GD, "very high frequency glow discharge") a-Si:H films this light soaking system turned out to give satisfying and coherent results (see e.g. Fig. 1.11). However, in connection with our efforts to optimize as an alternative deposition method the Hot Wire (HW) technique, this method turned out to be insufficient. In fact, we noted that high-quality HW material presents a very different degradation kinetics when compared to GD material. A stability measurement of a HW layer as tested on the described system is presented in Fig. 1.12.

One notes that for high-quality HW layers no clear saturation of the degradation could be observed even after $10^7$ s, while in typical GD layers the saturation of the decay of the photoconductivity occurs between $10^5$ and $10^6$ s. Therefore, an alternative procedure had to be established in order to verify whether in our case, too, the HW material really possesses, as claimed by other authors ([Mahan 1991]), a better stability than standard GD layers or whether it only presents a slower degradation. This alternate degradation procedure is presented in the next section.

### 1.2.3. Accelerated Degradation under Pulsed Light

Based on theoretical considerations as presented in section 1.2.1 of the present work the idea emerged that it should be possible to degrade a sample whithin a very short time by using extremely high intensities. On the other hand, practically all the energy absorbed in an a-Si:H layer will be transformed into heat. Raising the generation rate will, therefore, inevitably result in an increase of the sample temperature. This, in turn, will shift the dynamic equilibrium of

creation and annealing of defects. To avoid this problem it is therefore of interest to work with pulsed sources at high peak intensities while keeping the average intensity low.

For pulsed sources there is a simple relation between the average intensity, $< I >$, the pulse width, $\tau_{pulse}$, the repetition rate, $\nu_{rep}$ and the peak intensity, $I_{peak}$, of the emitted light:

$$< I >= I_{peak} \cdot \tau_{pulse} \cdot \nu_{rep} \tag{1.34}$$

One notes that for a given value of $< I >$ the peak intensity increases with a reduction of the pulse width; this makes light sources with narrow pulse width particularly attractive for this purpose. Several pulsed laser sources have been compared by [Stutzmann 1991]. He found that the length of the laser pulses (and, thus, the peak power) is quite unimportant for the accelerated defect creation, as long as the pulse length remains short compared to the typical excess carrier lifetime of about $10^{-6}$s.

While pulsed lasers have been extensively used since then for accelerated aging it was only in 1994 that [Kocka 1994] proposed to use a combination of CW light together with a pulsed source for a rapid aging under realistic conditions. In their case they used for the pulsed source a ruby laser and an AM 1.5 simulator as a superimposed CW source.

To reduce problems of non-uniform degradation associated with the AM 1.5 spectrum,

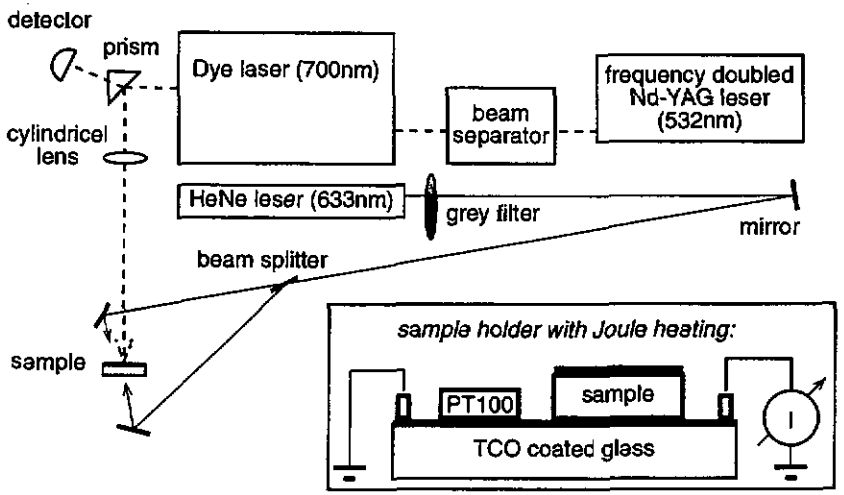


*Fig. 1.13: Schematic representation of the accelerated degradation system and magnified view of the sample holder (inset) The cylindrical lens is used to widen the beam of the pulsed laser. The optical path of the slightly diverging CW HeNe beam was chosen to be about 3 m to obtain a sufficiently large spot size for a homogeneous illumination of the sample. The sample holder allows for an active temperature control.*

as mentioned in section 1.2.1, we decided to use as the CW lightsource a HeNe laser with an intensity of 100 mWcm$^{-2}$ and a wavelength of 633 nm. For optimum uniform generation within the layer we illuminated our sample from both sides (see Fig. 1.13). Over this CW light we superimposed the beam of a Nd-YAG pumped dye laser as the pulsed source in order to accelerate the initial phase of degradation. The repetition rate of this dye laser was 20 Hz. The wavelength was chosen at $\lambda_{dye}$ = 700 nm. Its mean intensity was slightly lower than that of the CW light beam (50 mWcm$^{-2}$). The average photogenerated carrier density in the layer (as monitored by $\sigma_{photo}$) was, thus, almost entirely due to the CW light beam. Due to the low absorption coefficient of the a-Si:H at $\lambda_{dye}$ only a small fraction of the photons coming from the pulsed source were actually "seen" by our films and the incremental effect on the photoconductivity corresponded to only about 2% of the total photoconductivity. Nevertheless, since the energy was concentrated into flashes of a duration of only about 10 ns we obtained peak generation rates which were $10^5$ times higher than the average generation rate, and this lead to a substantial acceleration of the degradation process.

In Fig. 1.14 we present the kinetics of three typical degradation experiments performed with this setup. The experiments have been carried out using a sample which was thermally annealed back to its initial state after each degradation (here, annealing at 180 °C during 2h turned out to be sufficient). Each experiment consisted of an initial phase (A) where only the CW laser is present. This phase was used to cross-check the intensity of the CW beam by a measurement of the initial photoconductivity of the layer under test. The duration of phase (A)

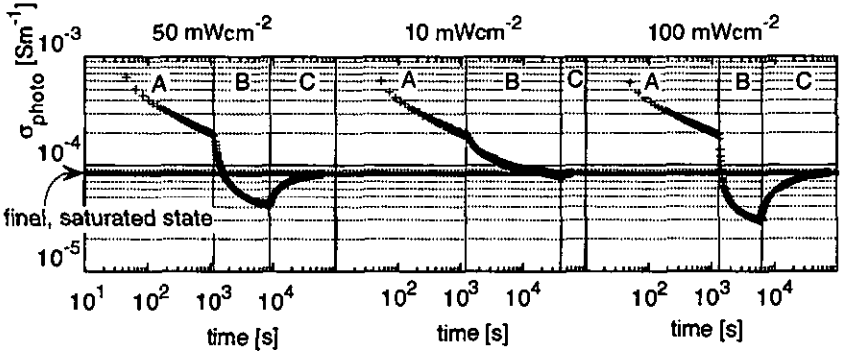


*Fig. 1.14: Three degradation experiments performed at different intensities of the pulsed source on the same a-Si:H layer. After each degradation the sample was annealed during 2h at 200 °C. In the beginning only the CW bias source is used (phase A), as soon as the dye laser is added (phase B) one observes a strong increase in the degradation rate. After saturation under the pulsed laser the latter is switched off and relaxation occurs. Note that although the saturation levels under the pulsed source depends on its light intensity one obtains the same stable state for all situations after relaxation.*

has been "exaggerated" in this series of experiments in order to demonstrate the acceleration of the degradation with the additional illumination provided by the pulsed beam at the beginning of the phase (B). Note that indeed the average intensity of the pulsed laser beam is negligible as no increase of the photoconductivity of the layer can be noted when it is switched on. For each of the three degradation experiments depicted in Fig. 1.14 a different intensity of the pulsed laser during phase (B) was chosen. This has a notable effect on the degradation rate as well as on the extrapolated saturation level during this phase. It is important to note that the saturated level of photoconductivity which is obtained just after using the pulsed laser is quite different from the one we are interested in because the high intensity of the laser pulses leads to a considerably lower value of stabilized photoconductivity. Therefore, we finish the procedure with a relaxation phase (C) using only the standard bias conditions (CW laser, layer at 50 °C).

Basically the layer can then be in either of the following three situations during this phase: Either the preceeding degradation using the pulsed source did not create the density of defects corresponding to the long term standard (CW) degradation. In this case the layer would continue to degrade under the CW source alone (this situation was not observed in the experiments depicted in Fig. 1.14). A second possibility is that the defect density obtained after the pulsed degradation exceeds the equilibrium value under standard conditions. Under these circumstances thermally-induced and light-induced annealing of the material will occur after switching off the pulsed source. Finally one may find the layer already after phase (B) in the wanted state. Then one observes a stable photoconductivity value once the pulsed source is removed.

Considering the measurements presented in Fig. 1.14 one observes that independently of the pulsed source intensity the same final, saturated photoconductivity value was obtained. This finding confirms observation 5) formulated above (section 1.2.1) and based on the defect creation model. It is interesting in the sense that this fact allows certain precautionary procedures to be simplified. It is, for example, not necessary to adjust the pulsed beam intensity in function of the infrared absorption of the layer under test. A second important remark concerns the total time required for stabilization. While for all presented experiments the saturation of degradation is reached after less than $10^5$s (i.e. less than two days) there can, in principle, occur "extreme" cases for which this duration can be substantially longer. If the pulsed source intensity is too small (<<10 mWcm$^{-2}$) the acceleration is not anymore pronounced enough. The second "extreme" case is obtained for too high dye laser intensities (>>100 mWcm-2) for which the relaxation phase starts to last longer than just few days. These two "extreme" cases have indeed been experimentally observed in our work.

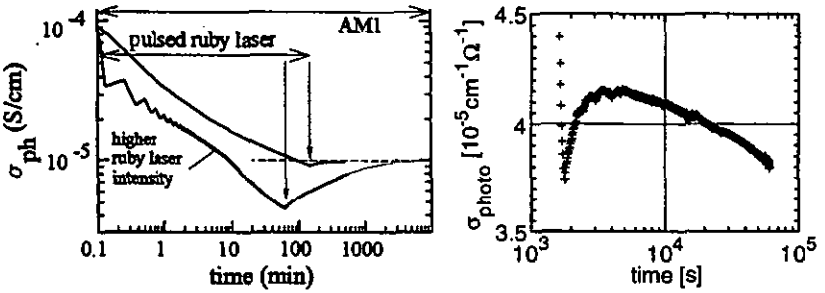


*Fig. 1.15: Two experiments illustrating the short term relaxation effects. The left picture is taken from* [Kocka 1994]. *One notes that after every individual pulse of the ruby laser* $\sigma_{photo}$ *is recovering partially resulting in a sawtooth type of degradation. The right graph is a measurement done on our setup where the pulsed illumination has been stopped too early. One observes a misleading relaxation of* $\sigma_{photo}$ *lasting more than 1000 s even though the stabilized state is not yet reached (as indicated by the ongoing degradation afterwards).*

A further important remark has to be made concerning the relaxation phase. In agreement with [Kocka 1994] we noted the existence of different types of relaxation phenomena occurring on different time scales (see fig 1.15). This behavior can not be explained by the model presented above for defect creation (section 1.2.1); it clearly shows the limitations of the model described above under certain circumstances. In fact, it seems that the high intensity degradation leads to a type of defects which differs from others by its fast recovery characteristics. While we do not have any knowledge on the underlying microscopic nature of this sort of defect it has an important consequence for the practical use of the described procedure. It means that the test whether saturation is reached or not has to be done over a sufficiently long time scale (say $> 10^4$ s) to discriminate between under- and over-degradation. In our tests we observed no further changes of the tendency after longer relaxation times.

# 2. CHARACTERIZATION OF SOLAR CELLS

In the present chapter the "standard" measurement techniques allowing to characterize the performance of solar cells are reviewed. First of all some basic definitions in the current voltage behavior of solar cells under illumination are outlined followed by some notes on the use of the spectral response measurement as used throughout this work. Finally, the conditions under which the stability of the cells under light soaking was investigated are described.

## 2.1. CURRENT VOLTAGE CHARACTERISTICS

The primary measurement technique used to characterize solar cells consists in a measurement of its current voltage behavior (i.e. IV-curve) under illumination. Since a photovoltaic device can behave either as a power source or as a dissipative element (depending on the applied bias voltage) a four quadrant measurement unit has to be used in order to accomplish a scan of such an IV-curve. A typical measurement result is presented in figure 2.1.

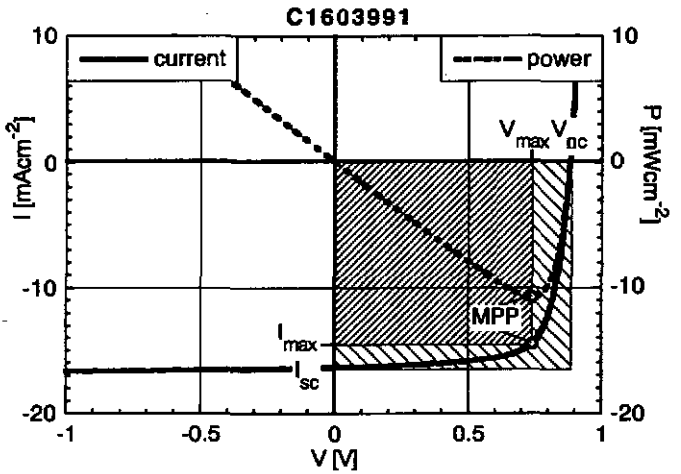


*Fig. 2.1: Typical IV-curve of an amorphous silicon p-i-n solar cell. It generates electrical power in the IV$^{th}$ quadrant (power dissipation P < 0). The electrical performance of this cell (dilution: $[H_2]/[SiH_4]$ = 2, $T_{dep.}$ = 230 °C, initial state) can be characterized by $V_{OC}$ = 880 mV, Isc = 15.1 mAcm-2 and FF = 74 %. The fill factor corresponds to the ratio of the rectangle delimited by $I_{max}$ and $V_{max}$ (maximum power point MPP) with respect to the rectangle given by $I_{SC}$ and $V_{OC}$*

The most important features of the IV-curve of a given solar cell are summarized by:

1) The open circuit voltage ($V_{OC}$), i.e. the voltage whicb builds up across the cell as long as its terminals are kept on a higb impedance forcing the electrical current to I = 0. This quantity is related to the bandgap of the semiconductor used.

2) The short circuit current ($I_{SC}$), i.e. the current whicb is generated by the solar cell if it is connected to a low impedance forcing the voltage across the device to V = 0. The current increases proportionally to the surface of the cell. Therefore it is generally normalized by the cell area and expressed as current density denoted by $J_{sc}$.

3) The fill factor (FF) corresponding to the ratio of the power which can indeed be generated by the solar cell (under maximum power conditions i.e. when it is connected to a suitable charge) to the product of $V_{OC}$*$I_{SC}$. This factor is related to the curvature of the IV-characteristics.

$$FF = \frac{J_{max} \cdot V_{max}}{J_{SC} \cdot V_{OC}} \tag{2.1}$$

These basic parameters do not only depend on the light intensity but additionally on its spectral composition. Therefore it is important to dispose of a light source which matches as close as possible the intensity as well as the spectrum of the sunlight under which the solar cells are designed to ultimately operate. This solar spectrum can be regarded as blackbody radiation emitted by a source at 5760 °K and filtered by both the suns' and the earths' atmosphere. As the latter changes locally in an unpredictable way due to the prevailing weather conditions a typical ideal sun spectrum has been defined (and is reviewed every five years) by the ASTM (American Society for Testing and Materials) Committee E-44 on Solar, Geothermal and other Alternative Energy Sources. This definition of air mass 1.5 (AM 1.5) illumination (see fig. 2.2) refers to sunlight traveling through an atmosphere 1.5 times thicker than in reality due to the actual inclined observer-sun path. Standard test conditions request to measure a solar cell under light of this spectral composition at an intensity of 1000 $Wm^{-2}$ and at a temperature of 25 °C. It is, however, impossible to generate this spectrum artificially. Nevertheless it can be reasonably approximated using a two source solar simulator (Wacom, WXS-140S-Super) as available in our laboratory. This solar simulator combines the light emitted by a Xenon short arc lamp (visible part) with the spectrum of a halogen lamp (infrared part) by means of a dichroic mirror.

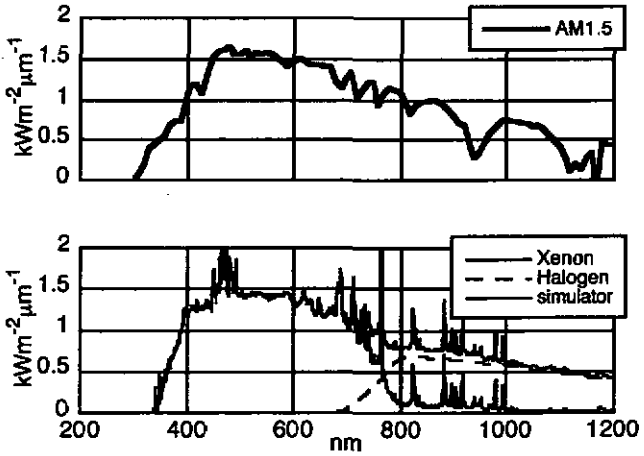


*Fig. 2.2: Comparison of the standard solar spectrum (AM1.5) with the spectrum generated by the solar simulator. The infrared part is composed by the partly reflected light of a halogen lamp while the visible part is produced by a Xenon short arc lamp (deprived of its infrared part by means of a filter).*

The density of the electrical power output of a solar cell, $P_{max}$, (measured at the maximum power point, "MPP") divided by the intensity of the incoming light, $I_{light}$, reveals the conversion efficiency:

$$\eta = \frac{P_{max}}{I_{light}} = \frac{J_{max} \cdot V_{max}}{I_{light}} \tag{2.2}$$

It becomes obvious that in order to get the highest possible conversion efficiency of a solar cell these three basic cell parameters have all to be maximized. As they contribute with an equal importance as proportional factors to the efficiency value it follows that any given relative gain in one of these parameters will result in the same relative increase of $\eta$:

$$\eta = \frac{J_{SC} \cdot V_{OC} \cdot FF}{I_{light}} \tag{2.3}$$

## 2.2. SPECTRAL RESPONSE MEASUREMENT

More insight - especially on the optical performance of a solar cell - can be gained by a measurement of its spectral response SR (or quantum efficiency QE). Physically this quantity expresses the fraction of incident photons of a given wavelength which result in an electron hole pair collected on the terminals of the cell (thus, contributing to the generated electrical current). The flux of arriving photons is expressed as:

$$\Phi(\lambda) = I(\lambda) \cdot \frac{\lambda}{hc} \tag{2.4}$$

where $I(\lambda)$ stands for the intensity of the probe beam, and $hc/\lambda$ for the energy carried by a photon of the wavelength $\lambda$. The spectral response[7] reads then as the ratio of the current increase $\Delta j_{ex}$ to the probe beams' intensity:

$$SR(V,\lambda) = \frac{\Delta j_{ex}(V,\lambda)}{\Phi(\lambda)} \tag{2.5}$$

A detailed description of the measurement setup used in this work to evaluate quantum efficiencies can be found in [Fischer 1994]. Fig. 2.3 shows a typical spectral response measurement of an a-Si:H solar cell.

Provided that SR remains constant over a large range of bias light intensities the photocurrent of a cell can be calculated for an arbitrary spectrum (and hence also for AM1.5) by the following integration:

$$J_{AM1.5}(V) = q \cdot \int_{\lambda_{min}}^{\lambda_{max}} SR(V,\lambda) \cdot \Phi_{AM1.5}(\lambda) \cdot d\lambda \tag{2.6}$$

Note that the current of a solar cell is composed by the photocurrent on one hand and the dark current of the junction diode (see section 4.3). In the forward region one has, therefore, to take into account the effect of the dark current in order to obtain the total current density:

---

[7]In fact the spectral response has to be considered as a differential quantity which varies with the bias light intensity as well as its spectrum. The most prominent changes of the spectral response curve as a function of the bias light intensity occur practically at low bias light intensities (i.e. as soon as the optical bias starts to be composed essentially of the probe beam itself. In this case, the red light response is measured under different bias light conditions than the blue light response.). All spectral response measurements performed within the framework of this thesis were, therefore, measured using white bias light (halogen lamp with an IR filter).

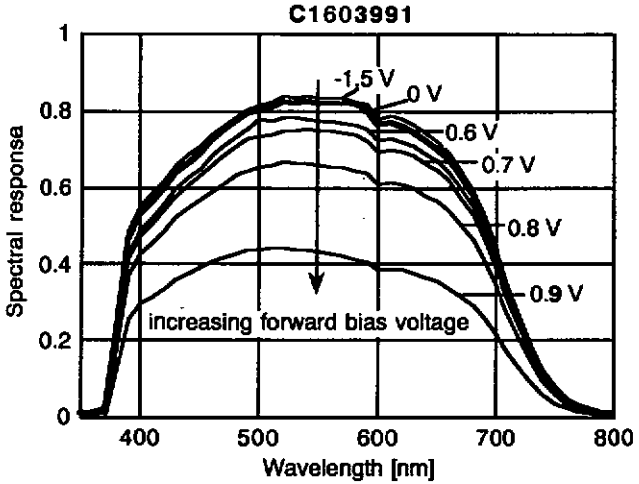


*Fig. 2.3: Spectral response measurement of an a-Si:H p-i-n junction (same as in fig. 2.1) performed at different bias voltages. The sharp drop to zero for short wavelengths is due to absorption in the ZnO front contact. In the long wavelength range the photons are not absorbed at all and do neither contribute to a current generation.*

$$J_{tot}(V,I_0) = J_{light}(V,I_0) + J_{dark}(V,I_0) \tag{2.7}$$

For short circuit conditions and reverse bias this indirect evaluation of the current is more precise than the direct measurement of the current under the simulator: The reasons are the fact that the simulator does nnt perfectly fit the AM1.5 spectrum and the required intensity. An even more important source of errors is the fact that we are nn a laboratory scale working on cells which have an area typically around 0.1 cm$^2$. Border effects[8] can, therefnre, have a relatively strong influence (the exact cell area can not be determined accurately leading to a high uncertainty in the current density).

[8]It is a common practice to assume that in a-Si:H only electron hole pairs which are generated between front and back electrode are collected (i.e. that the cell area can be defined as being the area delimited by the smaller of the two contact areas, e.g. the back contact in the case of a p-i-n diode). This is justified by the high electric resistance of a-Si:H which allows the electric current to travel over only short distances (i.e. vertically to the substrate). If highly conductive doped layers are used, however, "**lateral collectioo**" (i.e. horizontal transport of electric charge carriers in the doped layers) may become important. The relative importance of the lateral collection decreases with the cell area and is, hence, more important for small cells.

## 2.3. CONTROLLED LIGHT SOAKING OF SOLAR CELLS

In the section on light soaking of a-Si:H layers (section 1.2.2) we emphasized the importance of the uniformity of the generation rate throughout the width of a sample. The aim of the layer degradation is to create an constant defect density distribution corresponding to the degraded state to allow comparison of different materials with respect to stability. The case of light soaking of solar cells the situation is, however, more delicate:

### 2.3.1. light soaking of solar cells

In a solar cell degradation experiment one is interested in finding the device performance which would be obtained after long term exposure under natural sun light. The most reliable way to reach this degraded state is to illuminate it during a extended period with a source that matches reasonably well AM1.5. The requirements on the spectrum of the light are, thereby, less severe than they are for a precise measurement of the light IV-curve. Fig. 2.4 compares the spectra of several light sources to the AM1.5 spectrum. One notes that within the spectral

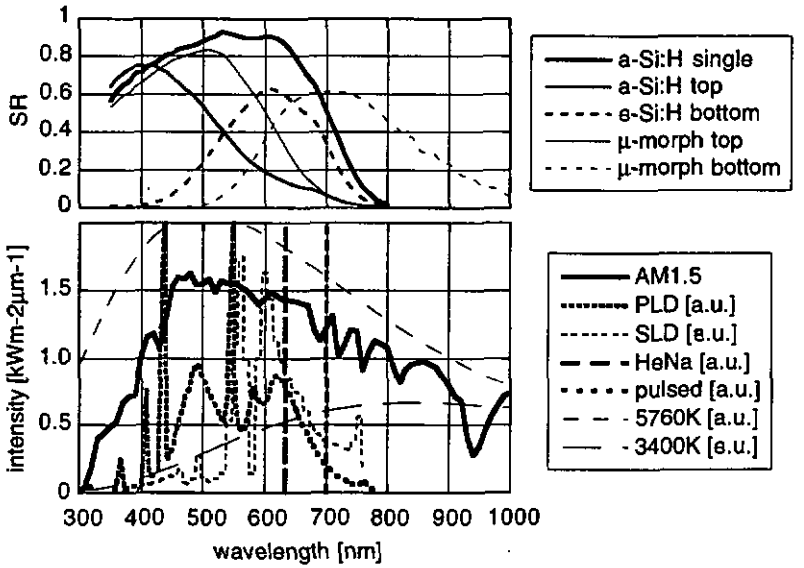


*Fig. 2.4: On the top the SR curves of various cells of interest are shown. The lower graph compares the spectral distribution of light emitted by different artificial sources to the spectrum of natural sunlight (AM1.5). PLD refers to the fluorescent tubes used for degradation of cells in this work. SLD stands for the sodium lamp degradation system used for layers which were light soaked under CW light. The 3400 K blackbody spectrum corresponds to a halogen lamp.*

sensitivity of a-Si:H cells the light of the fluorescent lamps used in our lab for degradation (Philips, PL-L 95, "natural daylight", 5300, 24 W) matches the standard spectrum AM1.5 quite well. Actually one obtains a very similar generation profile by both of these sources as observed for the case of purely amorphous tandem cells: Stacked cells which were designed to be "current-matched" under AM1.5 produced also the same top cell as well as bottom cell current under this light.

Several of these tubes were grouped as an array on the bottom within a box which was painted in white such as to provide a uniform light intensity on its cover. The cells to be degraded were fixed on this cover (with an area of about 900 $cm^2$). The temperature of this lightbox was controlled indirectly by means of a ventilator allowing a regulation of the air flow through the degradation system. Since the degradation system was installed in an airconditioned room this simple setup allowed the temperature to be kept stable at the set point value with a precision of about ±1 °C. The cell temperature amounted to 50 °C during light soaking. It was measured by platinum reference resistor "PT100" which was fixed on the back of a dummy cell that was mounted in the identical manner as the solar cells under test.

# 3. COMPARISON OF I-LAYER QUALITY AND CELL PROPERTIES

In the previous two chapters we have presented the experimental techniques which allow to characterize individual intrinsic layers and solar cells. It was argued theoretically that simple i-layers are, in view of their incorporation into p-i-n junctions, best classified by the material quality parameter $\mu\tau^{o}$ which is relevant for high collection in solar cells. In the present chapter this i-layer characterization technique will be applied to the optimization of the material produced by different deposition techniques. In the case of the VHF-GD process these layers will be incorporated into solar cells allowing to correlate tbe i-layer transport quality with cell performances.

## 3.1. I-LAYER OPTIMIZATION

In an oversimplified picture one could view a p-i-n solar cell as being composed of three layers: a p-type layer, an intrinsic layer and an n-type layer. Ideally it should then be possible to optimize each layer independently in order to be able to synthesize the most perfect solar cell which can be produced with a given technology. Unfortunately things are more complicated than that.

First of all one should be aware of the fact that the substrate on which a film is growing can play a crucial role in the determination of the film morphology and other microscopic material properties. This effect is particularly remarkable for very thin layers. It signifies e.g. that a p-type layer (with a typical thickness of 10 nm which corresponds to approximately 20 atomic layers) which is optimized on flat glass (an isolating substrate is required if the conductivity of the p-layer is to be measured) may have very different properties than when it is deposited on a TCO[9].

[9]In the case of the conventional superstrate configuration (i.e. for the configuration for which the p-, i-, and n-layer are deposited in this sequence on a transparent substrate which will face the light source during operation) the p-layer is deposited on a TCO which differs from flat glass by many aspects which influence the film growth: it is electrically and thermally conductive, it is designed to be textured (for an efficient light trapping), it has a polycrystalline structure, etc.

On the other hand there has been a lot of work published ([Rech 1995], [Arya 1986], [Xi 1994], [Platz 1996]) concerning interface treatments and interface layers which influence the solar cell properties to such an extent that one might be tempted to claim that a good solar cell is composed of optimized interfaces joining "reasonable" doped layers together with a "reasonable" i-layer.

Even though we think that the above formulated arguments are certainly to be kept in mind we are not completely pessimistic when considering such a "bottom-up approach" in the optimization of a thin film solar cell. Especially concerning the i-layer, we think that due to its thickness (typically larger than 300 nm, which corresponds to several hundred atomic layers) the substrate has only a secondary influence on the bulk properties. As to the interfaces in completed p-i-n structures there is certainly no doubt on the importance of their influence on the cell behavior. On the other hand we are convinced that especially the phenomenon of degradation can to a large extent be attributed to the bulk of the i-layer ([Wyrsch 1994]) in which case the quality of the i-layer is essential.

From this point of view we are persuaded that the optimization of simple i-layers makes sense in the perspective of realizing more efficient a-Si:H solar cells provided that the intrinsic layers are evaluated in terms of relevant properties required for high performance solar cells. In section 1.1.6 we have summarized some theoretical arguments indicating that the normalized mobility*recombination time product $\mu^{o}\tau^{o}$ fulfills the role of a pertinent material quality parameter. It will be the purpose of the following section to consolidate this statement by experimental evidence.

### 3.1.1. Assessment of the correlation between $\mu^{o}\tau^{o}$ and solar cell parameters

To experimentally verify that $\mu^{o}\tau^{o}$ does indeed reflect the material quality for photovoltaic applications a series of a-Si:H layers was deposited (thickness approximately 2.5 µm) for which the deposition temperature was varied from 120 °C to 200 °C. The $\mu^{o}\tau^{o}$-products of these layers were measured in the annealed state as well as after degradation (see section 1.2.2) in the sodium lamp degradation system (at an intensity of about 5 suns from both sides). The deposition temperature turned out to strongly influence the material quality as well as its stability as can be seen in Table 3.1.

The $\mu^{o}\tau^{o}$-product in the initial as well as in the degraded state increases monotonously with the deposition temperature. Note that in the initial state this tendency is not reflected correctly if the $\mu^{o}\tau^{R}$-products of electrons and holes are considered separately: When considering only the electrons the layer deposited at 180 °C seems to be of higher quality than the one deposited at 200 °C. This is due to a slightly higher contamination in the 180 °C layer,

| | *annealed state* | | | | *degraded state* | | | |
|---|---|---|---|---|---|---|---|---|
| | $\mu^0\tau^R$ electrons [$cm^2V^{-1}$] | $\mu^0\tau^R$ holes [$cm^2V^{-1}$] | b | $\mu^0\tau^0$ [$cm^2V^{-1}$] | $\mu^0\tau^R$ electrons [$cm^2V^{-1}$] | $\mu^0\tau^R$ holes [$cm^2V^{-1}$] | b | $\mu^0\tau^0$ [$cm^2V^{-1}$] |
| 200 °C | 1.57e-06 | 7.90e-09 | 195 | **3.21e-07** | 2.21e-08 | 1.68e-09 | 10.9 | **1.81e-08** |
| 180 °C | 1.81e-06 | 5.30e-09 | 335 | **2.34e-07** | 9.50e-09 | 1.01e-09 | 7.2 | **8.28e-09** |
| 160 °C | 1.46e-06 | 3.66e-09 | 394 | **1.65e-07** | 9.07e-09 | 8.24e-10 | 8.8 | **7.70e-09** |
| 140 °C | 2.85e-07 | 3.66e-09 | 75 | **1.14e-07** | 3.46e-09 | 4.30e-10 | 5.8 | **3.09e-09** |
| 120 °C | 1.72e-07 | 2.49e-09 | 66 | **7.38e-08** | 2.67e-09 | 3.43e-10 | 5.5 | **2.40e-09** |

*Table 3.1: Apparent mobility *recombination time products, $\mu^0\tau^R$, of electrons and holes (evaluated from $\sigma_{photo}$ and $L_{amb}$ respectively) as well as the normalized $\mu^0\tau^0$-product of intrinsic layers deposited at different substrate temperatures.*

as reflected by its higher value of b, and leading to a higher value of the photoconductivity. On the other hand, when considering only the $\mu^0\tau^R$-products of holes one gets the impression that the layers deposited at 140 °C and at 160 °C are identical. Here it is the higher contamination of the 160 °C film which lowers its ambipolar diffusion length.

The same materials were also incorporated into otherwise identical p-i-n junctions (i-layer thickness: 0.6 µm) which were characterized, too, in the initial state, as well as after degradation under white light (see section 2.4.1). In Fig. 3.1 the normalized spectral response curves of these solar cells are compared. The purpose of such a normalization is to obtain a quantity which reflects the collection quality of the i-layer. The underlying idea is thereby that at sufficiently high reverse bias voltage all photogenerated charge carriers within the i-layer are

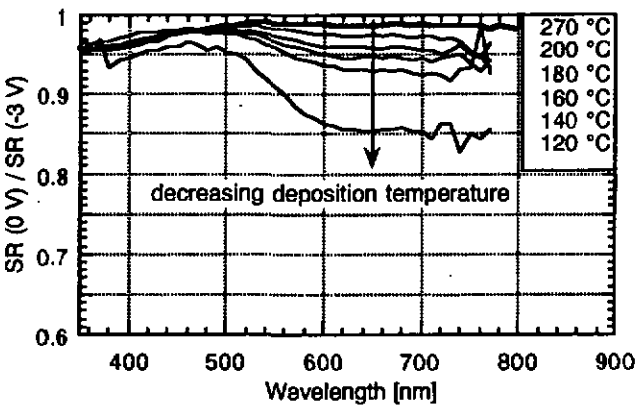


*Fig. 3.1: Normalized spectral response curves of solar cells deposited at different temperatures measured in their initial state. The spectral response curve measured at 0 V bias voltage was thereby divided by the curve measured at a reverse bias voltage of -3 V in order to obtain a collection dependent quantity.*

actually collected on the terminals of the cell. The spectral response curve at high reverse bias voltage reflects purely optical losses. Dividing the spectral response curve measured at 0 V by the one obtained at high reverse bias voltage (-3 V) yields the fraction of charge carriers which are collected under the field conditions prevailing at 0 V. By normalization one can, thus, gain some information on purely collection related losses. This fraction of collected charge carriers is somewhat wavelength dependent for short wavelengths since electron-hole pairs are generated at different locations for different absorption coefficients. In the long wavelength region, however, when the probe beam of the spectral response measurement setup is absorbed uniformly within the cell (for $\lambda > 600$ nm) this collection ratio remains constant and reveals the i-layer quality.

A comparison of the cell measurements with the layer results is presented in Fig. 3.2. The normalized spectral response has been evaluated, for this purpose, in the long wavelength range (at 650 nm) and plotted versus the $\mu^0\tau^0$-products measured in layers. In the initial as well as in the degraded state one observes, thereby, a very good correlation.

A second series of layers and cells was deposited at the temperatures of 150 °C, 170 °C, 220 °C, 270 °C and 320 °C. In Fig. 3.3 the conversion efficiencies of the solar cells are compared with the $\mu^0\tau^0$-products of the corresponding i-layers. One observes a surprisingly excellent correlation over the whole range from strongly degraded low temperature material up to high quality material in the annealed state. Only at very high temperatures (320 °C) one observes the tendency of a decreasing cell efficiency in spite of the remaining high

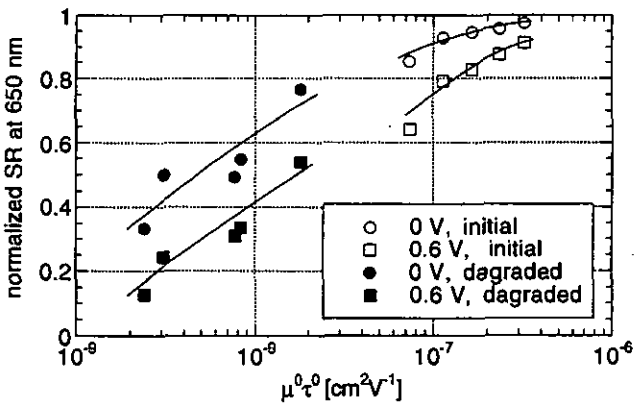


*Fig. 3.2: Relation between the normalized red light spectral response and the $\mu^0\tau^0$-product of the corresponding i-layer. The lines are guides to the eye. The cells have been light soaked under AM 1.5 white light while the layers were exposed to the light of a sodium lamp of about 5 suns total intensity.*

$\mu^o\tau^o$-product. This effect is thought to be due to interdiffusion problems which are frequently encountered when depositing cells at elevated substrate temperature (e.g. [Platz 1997]).

This nice correlation is surprising since the cells have not been degraded in the same manner as the layers (i.e. one would not expect the correlation to extend from the cells and layers in the annealed state down to the cells and layers in the degraded state). Also, it is clear that the conversion efficiency value $\eta$ contains several contributions which are not directly connected with the quality of the i-layer (such as e.g. the $V_{oc}$ or the $I_{sc}$[10] - as becomes apparent through the relation $\eta \propto J_{sc} \cdot V_{oc} \cdot FF$ - or implicit terms like e.g. the $R_s$). A correlation, as the obtained here, requires, thus, a high degree of reproducibility in the fabrication technology of the whole cell.

We concluded from these results that $\mu^o\tau^o$ does indeed reflect the potential of an a-Si:H material for its use in a solar cell. It is, nevertheless, important to bear in mind that the stabilized

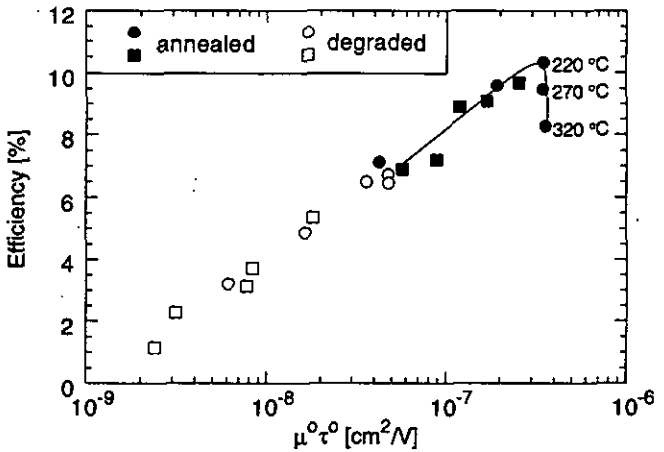


*Fig. 3.3: Correlation between solar cell efficiencies and the $\mu^o\tau^o$ products of the i-layers incorporated in these cells. The first series of layers and cells (covering the temperature range from 120 °C to 200 °C) is represented by squares. The second series (deposited between 150 °C and 320 °C) is represented by dots. The line reflects the tendency of initial state $\mu^o\tau^o$-products and cell efficiency as a function of the substrate temperature.*

[10] $V_{oc}$ tends to decrease for lower gaps (obtained when increasing the deposition temperature) while the opposite tendency is observed for $I_{sc}$.

cell efficiency which can be achieved using an i-layer with a given $\mu\tau^{o}$ value does also depend on other factors. It is, for example, well knowo that "mastering the interfaces" is crucial for obtaining high conversion efficiencies. With $\mu\tau^{o}$, we found a significant, limiting parameter in solar cells which can be optimized iodependently. Our quest for the most suitable deposition method and for the optimum depositioo parameters was, therefore, guided by $\mu\tau^{o}$.

### 3.1.2. Study of the effect of hydrogen dilution and the deposition temperature

*3.1.2.1. Material studies:*

The coocept of the evaluation of the material quality by means of the $\mu\tau^{o}$-product was applied during the optimizatioo of the hydrogeo dilutioo and the deposition temperature in the VHF-GD process. A series of layers was deposited at the substrate temperatures of 195 °C, 235 °C and 280 °C. For each temperature three layers were deposited with hydrogen dilution ratios (given by the ratio of the gas flows: $[H_2]/[SiH_4]$) of 0, 2 and 9.

The optical absorptioo data of these layers were measured using the procedure described in sectioo 1.1.2 as well as by PDS (photothermal deflection spectroscopy, for a description of the experimeotal setup used in this work refer to [Curtios 1989]). The PDS data revealed that, at a substrate temperature of 280 °C, the onset of microcrystalline growth starts already at a dilution ratio of 9 (At lower substrate temperatures, higher dilutioo ratios (>20, see [Fliickiger 1995]) are required to deposit microcrystalline silicon). This layer (280 °C, dilution 9) was therefore no longer considered in the subsequent transport studies. The absorption coefficients

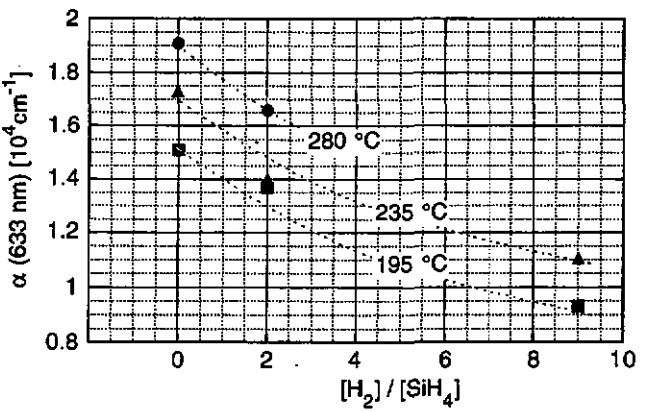


*Fig. 3.4: Absorption coefficients of a-Si:H films deposited at substrate temperatures ranging from 195 °C to 280 °C using different hydrogen dilution ratios. The lines are guides to the eye.*

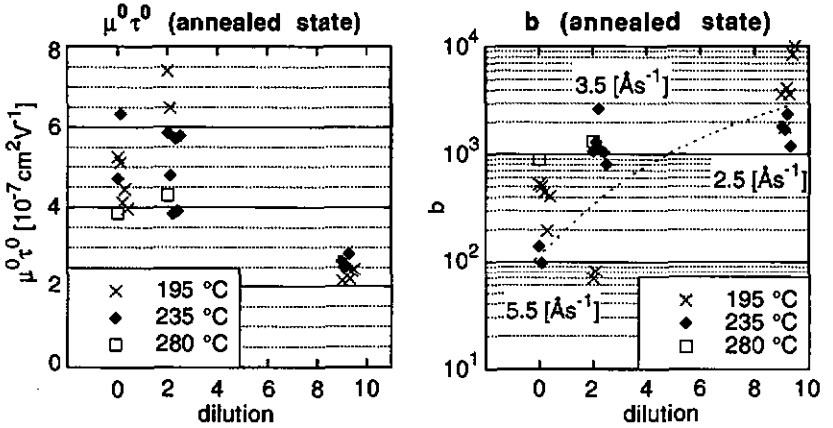


*Fig. 3.5: Comparison of the $\mu^0\tau^0$-products of a-Si:H layers deposited at different substrate temperatures and using various hydrogen dilution ratios given by $[H_2]/[SiH_4]$. Each data point corresponds to an individually contacted and measured sample. On the right the factor b of these same films is shown. The deposition rates obtained are indicated for each dilution*

measured at 633 nm (this wavelength has been chosen because the transport measurements were carried out using a HeNe laser emitting at this same wavelength) are represented in Fig. 3.4. Two general trends can be noted: First of all the absorption coefficient tends to increase with increasing substrate temperature. Secondly, the absorption coefficient decreases with increasing hydrogen dilution ratio. These observations will be important if solar cells are produced using these layers (On one hand the short circuit current depends directly on the absorption coefficient. Strongly absorbing i-layers can be made thin, leading, therefore , indirectly to an augmented cell stability. On the other hand the absorption is also related to the bandgap of a material which influences, of course, the maximum open circuit voltage which can be obtained.)

The electronic transport of these samples was afterwards analyzed by $\sigma_{photo}$ and $L_{amb}$ measurements. They allowed us to determine the $\mu^0\tau^0$-product, as well as the factor b, which corresponds to the ratio $b = \mu_n^0 n_f / \mu_p^0 p_f$. The results as they were measured after annealing (2 h at 180 °C) are represented in Fig. 3.5. The transport quality in the initial state shows a pronounced decrease at elevated hydrogen dilutions. This is to some extent correlated with the factor b, which indicates the level of contamination of a layer. One notes in Fig. 3.5 that the layers deposited using an elevated hydrogen dilution are more contaminated than the ones deposited without addition of hydrogen (the factor b is here typically ten times lower). We think

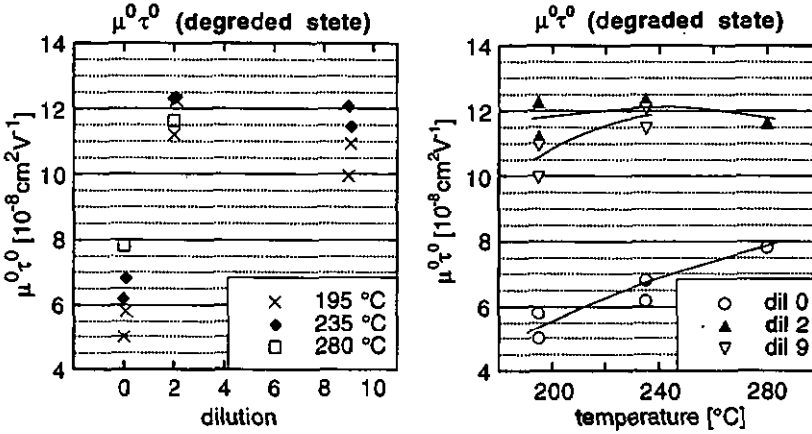


*Fig. 3.6: $\mu^0\tau^0$-products of a-Si:H layers deposited using various deposition conditions after pulsed degradation. The $\mu^0\tau^0$-products of the samples have been plotted vs. the $H_2$-dilution (left) and vs. the substrate temperature (right).*

that this is connected to the fact that the deposition rate is considerably lower when hydrogen dilution is used[11].

More important, however, than the transport quality in the annealed state is the stability under light soaking. The films have therefore been degraded with a pulsed dye laser (as described in Fig. 1.14). The results are summarized in Fig. 3.6. They show quite clearly that the quality of undiluted films increases with the deposition temperature (as has been noted previously for the temperature series presented in section 3.1.1). It is interesting to note that hydrogen dilution strongly enhances the stability. This increase in the material stability can be already observed at a dilution of 2. Diluting even further seems not to enhance the stability further. These more stable, hydrogen diluted films exhibit a less pronounced dependency of the degraded $\mu^0\tau^0$-product on the deposition temperature.

*3.1.2.2. Solar cells using the optimized i-layer material:*

Part of the films of which the optical and electrical characteristics were presented above were incorporated into p-i-n solar cells. In a first time the effect of hydrogen dilution at

[11]Thereby, we assume that the main source of contamination is the reactor itself. Indeed, if one assumes a constant outgassing rate of the reactor (which is, of course, independent of the deposition rate) and that a certain fraction of these contaminants are incorporated into the growing layer then one finds that the contamination increases at low deposition rates (see e.g. [Kroll 1995]).

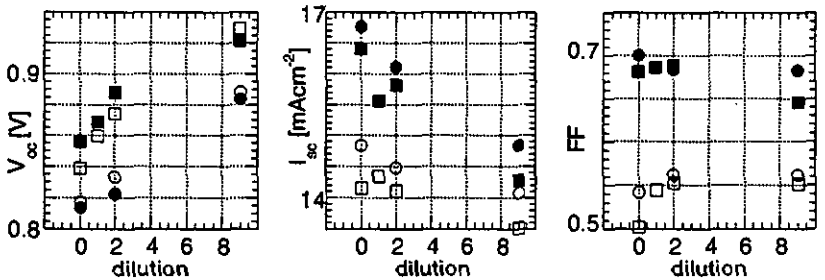


*Fig. 3.7: Solar cells (with an i-layer of 450 nm) made using the i-layer material characterized above (Fig. 3.4 to Fig 3.6). The filled symbols refer to the annealed state, the open symbols represent values after degradation. The circles represent cells deposited at 235 °C, the squares represent cells deposited at 195 °C.*

"standard" substrate temperature (i.e. at 235 °C) as well as at low substrate temperature (i.e. at 180 °C) was further elucidated directly by depositing complete solar cell structures (for a detailed analysis refer to [Platz 1996][12]). The i-layer thickness of these cells was 450 nm (i.e. thicker than what is required for optimum stabilized efficiency) in order to make the effect of the i-layer quality on the cell properties more conspicuous.

A summary of the different cell performances obtained is presented in the Fig. 3.7. Thereby several observations can be made which are directly related with the i-layer properties as presented above: First of all one notes that the tendencies that were observed in the optical absorption (increasing with the deposition temperature, decreasing with the hydrogen dilution) are reflected by the solar cells' open circuit voltages and short circuit currents. It appears that the $V_{OC}$ is higher for the cells deposited at the lower substrate temperature and tends to grow with increasing hydrogen dilution. This is related to the bandgap of the i-layer material. The effect on the short circuit current of the cells is exactly opposite. The values of $I_{SC}$ are systematically higher for the cells grown at the higher deposition temperature and tend to decrease (together with the absorption coefficient) when hydrogen dilution is applied. This difference of the $I_{SC}$-values of approximately 0.7 mAcm$^{-2}$ persists also after degradation. Concerning the stability of the cells one encounters again (as it was noted for the i-layer material alone) an improvement as soon as a hydrogen dilution of about 2 is applied. The relative increase of the fill factor amounts to about 10 % in the case of low temperature material while it is only about 4 % in the case of material grown at standard deposition temperature. As a result one obtains

[12]The deposition temperatures used in the quoted article were based on a old calibration. For comparison 220 °C there corresponds to 235 °C here, while 180 °C is equivalent to 195 °C substrate temperature.

the highest cell efficiencies at both deposition temperatures, when a bydrogen dilution is applied.

*3.1.2.3. Delicate example - optimized top cell for micromorph tandems:*

In the example above the most efficient cell (after light soaking) was found to be the one with the highest FF and hence the one incorporating the i-layer with the highest $\mu^{o}\tau^{o}$-product. This not necessarily always the case. As has been mentioned in section 2.3.2, the $\mu^{o}\tau^{o}$-product plays an increasingly important role with the i-layer thickness. For extremely narrow i-layers bad transport properties can be compensated by the higher prevailing electrical field. Additionally, one must not forget that the carrier collection (related to the fill factor) constitutes only one step in photovoltaic energy conversion. $V_{OC}$ and $I_{SC}$ have to be considered as well to calculate the efficiency. The optimum cell obtained in the dilution series above will not be the most efficient for every application as will be demonstrated below. Actually there are situations for which the *bandgap* of a material plays the crucial role. An example for this constitutes the optimization of the top cell for tandem applications:

This problem became particularly critical with the advent of a-Si:H/μc-Si:H beterojunctions [Meier 1996]. In such "micromorpb" thin film cells an amorphous and a microcrystalline silicon cell are optically and electrically series connected. Thereby both cells should generate the same current to achieve optimum performance[13]. This is difficult to realize in the case of micromorpb cells for the following reason: In any stacked cell structure the upper cell has to generate its current in only one single passage of the incident light (whereas in simple cell structures a good back reflector increases virtually the apparent i-layer thickness by a factor two)[14]. Due the extended absorption range of μc-Si:H in the infrared region (leading to a total current of ca. 26 $mAcm^{-2}$) as much as 13 $mAcm^{-2}$ have to be generated in the amorphous top cell (deprived of its back reflector). If the optimum cell (with highest stable efficiency) does not reach this threshold the overall efficiency (of the tandem) can be lower since part of the photogenerated current of the microcrystalline cell is wasted.

In this context, a study was carried out using the undiluted high temperature material which is attractive because of its high absorption value (see Fig. 3.4). A series of thin cells was

---

[13] If the so called "current matching" is not optimized the cell with the lower $I_{SC}$ (limiting cell) forces the other cell into a working point below its optimum power point lowering the total efficiency. (A slight current mismatch can sometimes be desireable if the two cells have different fill factors [Pellaton-Vaucher 1998])

[14] An interesting stacked cell design with a partially reflecting internal mirror has been presented in [Fischer 1996].

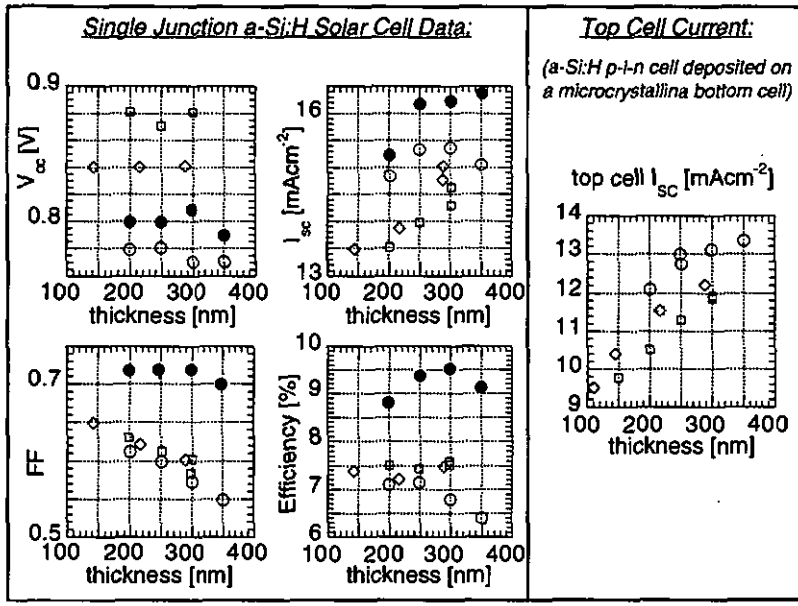


*Fig. 3.8: Solar cells made using the i-layer material characterized above (Fig. 3.4 to Fig 3.6). The filled symbols refer to the annealed state, the open symbols represent values after degradation. The circles represent cells deposited at 280 °C without $H_2$-dilution, the diamonds represent "standard" cells (deposited at 235 °C), the squares indicate optimized low-temperature (195 °C), $H_2$-diluted cells. The cells on the left include an efficient back reflector while the right cells are deposited on an absorbing bottom cell.*

deposited using this material for the i-layer. Thereby an appropriate p-i interface layer had to be developed in order to avoid a disproportionate decrease of the $V_{OC}$ and of the FF at high temperatures (for more details refer to [Platz 1997] [15]). The cell parameters of this series are summarized in Fig. 3.8, where for comparison also cells deposited at low temperature and using hydrogen dilution and cells made using "standard" deposition conditions are indicated.

One notes that -in contrast to the results presented in the previous paragrapb - for these thin cells the increased stability of the hydrogen diluted material (Fig. 3.6) has hardly an effect on the fill factors (the stabilized fill factors of cells deposited at low temperature and using hydrogen dilution are approximately equivalent to the ones made using "standard" deposition conditions.). However, when deposited on a microcrystalline bottom cell, only the high temperature material reaches the desired current of 13 mAcm$^{-2}$.

[15] The temperatures indicated in this publication are setpoint values. A value of 220 °C there corresponds to 195 °C, 270 °C to 235 °C and 330 °C to 280 °C.

### 3.1.3. Comparison of VHF and DC PE-CVD

The deposition of a-Si:H by PE-CVD using elevated excitation frequencies in the VHF band (30-300 MHz) introduced by our group [Curtins 1987] has shown to be advantageous in many aspects (high deposition rates for high quality material, low powder formation, reduced mechanical stress, etc. - for an overview see [Shah 1992]). For an industrial process, however, the DC glow discharge process can be implemented more easily (the homogeneous coupling of the electrical power at *high frequencies* into the plasma requires a careful reactor design which can be simplified when working with a DC excitation). And it has been shown on a large scale by the Solarex company [Yang 1996] that highly efficient solar cells can be made as well using this process.

The study presented in this section was carried out in order to compare these deposition techniques (VHF PE-CVD and DC PE-CVD) from the point of view of the material quality that can be obtained when employing either of the two techniques. For this purpose i-layers have been deposited with the DC PE-CVD technique using comparable substrate temperatures and hydrogen dilution ratios at which also VHF depositions had been carried out. These layers were characterized by the same methods as described in the previous section.

Regarding the optical properties (see Fig. 3.9) similar trends as the ones observed in the case of VHF deposited material were noted: Employing hydrogen dilution led to a considerable reduction of the optical absorption coefficient while raising the substrate temperature had the opposite effect.

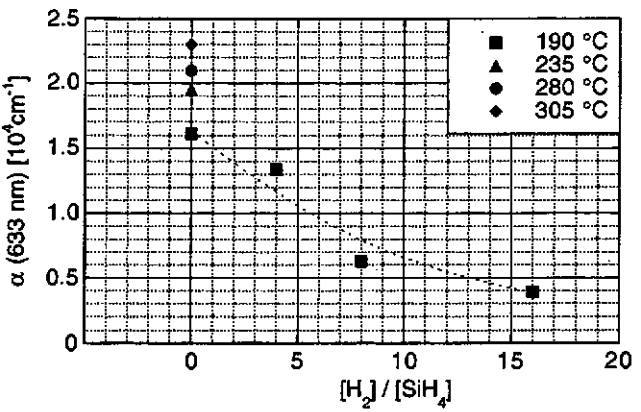


*Fig. 3.9 Absorption coefficients of a-Si:H layers deposited by DC PE-CVD at different substrate temperatures and hydrogen dilution ratios.*

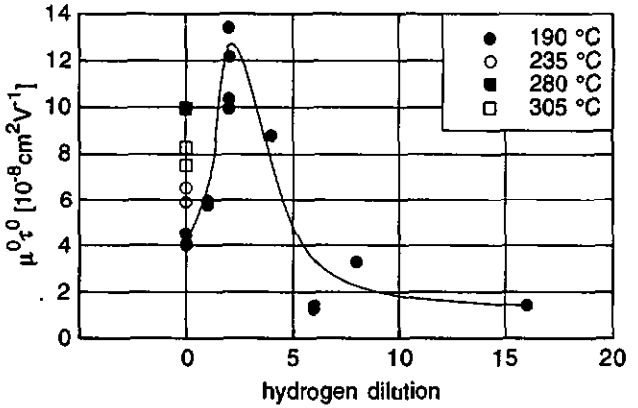


*Fig. 3.10: Material quality (as indicated by the $\mu^0\tau^0$-product) of a-Si:H layers deposited by DC PE-CVD using different substrate temperatures and hydrogen dilution ratios after degradation.*

The stability of the electrical transport properties of the DC PE-CVD deposited material has been evaluated by the $\mu^0\tau^0$-product after accelerated degradation with the pulsed dye laser. The results are plotted in Fig. 3.10. One observes that from the point of view of the stability the material quality can be enhanced by depositing the a-Si:H at higher substrate temperatures. Dilution of the feed gas by hydrogen also leads to a better $\mu^0\tau^0$-product after degradation. In contrast to the observations made in the case of VHF PE-CVD we observed here a sharp optimum for a dilution value of 2 for which the value of $\mu^0\tau^0$ is about three times higher than in the case of undiluted films. Increasing the hydrogen dilution ratio to values exceeding a factor 2 has a detrimental effect on the material quality after degradation. The $\mu^0\tau^0$-product decreases then to values which are even worse than for undiluted films. Conclusively we found it very interesting to note that optimized films deposited using DC PE-CVD as well as VHF PE-CVD have both a very similar transport quality after degradation.

### 3.1.4. Estimation of the potential of HW material

Today, RF PE-CVD (excitation frequency: $\nu_{excitation} = 13.56\,MHz$) and DC PE-CVD techniques are the only two methods which are used on a large, industrial scale for the production of a-Si:H films. Many other deposition techniques (such as magnetron sputtering, photo-CVD, microwave glow discharge, electron cyclotron resonance (ECR) plasma vapour deposition, pyrolytic CVD, etc.) have been (and continue to be) investigated on a laboratory scale [Pankove 1984]. One of them, namely the Hot Wire (HW) technique, has particularly attracted our attention after repeated claims by another group that the films deposited using this technique are more stable [Mahan 1991]. Thereby the feed gas is decomposed thermally on a

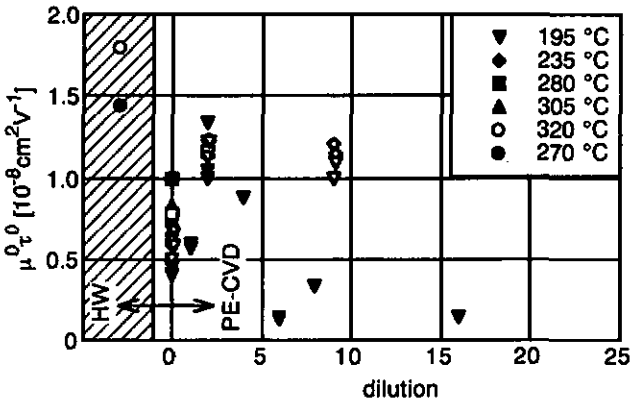


*Fig. 3.11: Comparison of $\mu^0\tau^0$-products measured on a-Si:H films produced by VHF PE-CVD (open symbols) and DC PE-CVD (filled symbols) with two optimized HW layers. All layers have been degraded using the pulsed laser.*

hot filament (consisting normally of a tungsten wire at a temperature of 1000 °C < T < 2000 °C) to form reactive species.

A deposition system has thus been devoted to the study of the HW deposition technique [Ziegler 1997]. A big effort had thereby been made to control the substrate temperature at a constant value during the whole duration of the deposition[16]. Ultimately two optimized thin films deposited at 320 °C (undiluted) and at 270 °C (with hydrogen dilution), respectively, could be characterized and compared to the previously presented PE-CVD material. Fig. 3.11 shows a comparison of the $\mu^0\tau^0$-values of these HW layers with the ones of the a-Si:H films produced by VHF PE-CVD and by DC PE-CVD from the previous sections. All the $\mu^0\tau^0$-products were measured after applying the degradation procedure using the pulsed laser. One sees, that the highest $\mu^0\tau^0$-product has been measured on the HW sample deposited at 320 °C. Its value is even higher than the one of the best films produced by PE-CVD using a slight hydrogen dilution. The transport quality in the degraded state of the second HW layer which was deposited at a somewhat lower substrate temperature (270 °C - which is still rather

[16]One major problem arises in the HW deposition technique by the fact that the depositions are generally done at lower pressure than in the case of PE-CVD. Therefore, the substrate temperature is here not controlled by thermal conductivity but starts to be increasingly dominated by radiation. During the deposition of a layer on a substrate the thermal emission of this latter changes leading to strong temperature variations during the growth.

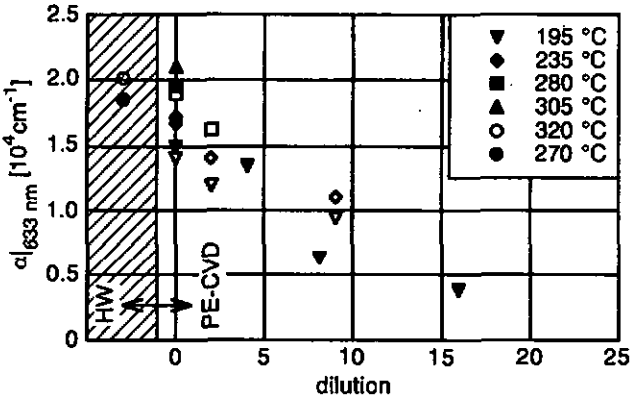


*Fig. 3.12: Optical absorption coefficients measured at 633 nm on a-Si:H films produced by VHF PE-CVD (open symbols), DC PE-CVD (filled symbols) and by HW.*

high compared to the standard deposition temperature for solar cells of 235 °C) was found to be comparable to the one of diluted PE-CVD material.

The second observation which makes these HW films even more attractive for solar cell applications is the elevated optical absorption coefficient measured on those films. Fig. 3.12 shows a comparison of the absorption coefficients of red light of a-Si:H produced using different deposition methods. One notes that the hydrogen dilution required to produce more stable material by PE-CVD has the tendency to increase the optical bandgap leading, thereby, to a reduced absorption. The HW films which also exhibit an excellent stability, however, have an absorption coefficient which is comparable to undiluted PE-CVD material.

Both, its enhanced stability combined with its high absorption coefficient make the high temperature HW material (320 °C) an interesting candidate for solar cell applications. The high deposition temperature is, nevertheless, to be considered as a major obstacle to a straightforward implementation of the film into a p-i-n diode. Problems such as the deterioration of the p-layer during the subsequent deposition of the i-layer at high temperature or the diffusion of impurities leading to an excessively contaminated i-layer have to be overcome. Up to now, we have not been able to make a solar cell demonstrating a better stabilized efficiency by incorporation of a more stable i-layer deposited by HW.

## CONCLUSIONS

In the beginning of this chapter we presented a correlation between the i-layer material quality and the solar cell parameters of devices incorporating these same i-layers. Thereby, the

variation of the $\mu^o\tau^o$-values observed in the layers was clearly reflected in the cells which were made relatively thick on purpose (in order to emphasize bulk effects). The clearly monotonous relationship between the stabilized fill factor of a cell and its i-layer $\mu^o\tau^o$-product encouraged us to apply this criterion to the optimization of the deposition conditions. Thereby, we studied the effect of the deposition temperature and of the hydrogen dilution in view of (relatively thick) single junction cells where again a nice correlation was obtained. It was also shown that the criterion of the maximization of the i-layer material quality as monitored by $\mu^o\tau^o$ does not universally lead to the most efficient cells for every usage. As a particular case we presented the optimization of (relatively thin) top cells for tandem structures where the stability of the i-layer was shown to be of secondary importance.

Comparison of different deposition technologies based on transport quality measurements by $\mu^o\tau^o$-products showed that using DC PE-CVD one is able to produce a-Si:H of comparable characteristics as the material obtained by VHF-GD. In both cases moderate hydrogen dilution had a beneficial effect on the stability. The HW technique was shown to bear an interesting potential once the obstacle of the high substrate temperature can be overcome.

# 4. THEORY OF THE PHOTOCURRENT COLLECTION IN P-I-N SOLAR CELLS

In the preceding chapter we demonstrated the usefulness of the material quality parameter $\mu\tau$ for the characterization of the i-layer in a "bottom-up approach" of the optimization of more stable a-Si:H based thin film solar cells. The cells were, thereby, characterized by two methods which have to be regarded as basic with respect to the information they provide:

- The IV-curve of a solar cell describes its global behavior under illuminated conditions (e.g. AM 1.5). It allows the maximum power point, the total current and the open circuit voltage to be determined.

- In contrast to this one can measure the external quantum efficiency with the SR setup. This permits the current density to be known. Optical losses due to reflection, absorption in dead layers (for high energy photons) or because of non absorption (for low energy photons) can be estimated with the SR as well as losses due to a bad collection.

One notes that neither of the two standard solar cell characterization tools allows a quantitative analysis of the i-layer material quality within the completed solar cell structure to be done. In order to get a complete picture of the state of the art of a given cell technology one is, however, also interested in a tool which allows this reverse analysis to be undertaken. Such a feedback is important to confirm that an i-layer performs according to its potential when incorporated in a p-i-n structure. This allows to distinguish between bulk material related limitations and other effects (such as interface recombination, shunt resistance losses etc.). Being able to measure the i-layer material quality directly within a p-i-n structure would also allow a direct comparison of material properties when grown on different types of substrates[17]

[17]Remember that the "working hypothesis" in chapter 3 was the assumption that the growth of an a-Si:H layer is essentially independent on the substrate type. We assumed that the same deposition conditions which lead on isolating corning glass substrates to the growth of thin films with an optimum transport quality (and stability) remain ideal when applied for the deposition of the i-layer of a solar cell on a substrate covered by a TCO.

In the past the FF was often used to correlate the solar cell performance with the material quality of its i-layer. The problem with this is the fact, that the FF is influenced by factors which are not directly connected with the i-layer quality as such, but which should be considered as parasitic losses. A high series resistance for example can strongly reduce the value of the FF but its origin lies in the electric contacts (too thin or not sufficiently conductive TCO, metallic grid unable to carry the current without remarkable voltage drops) rather than in the i-layer quality. On the other hand shunts may reduce the FF without being intrinsically related to the i-layer quality. They can be formed at the border of the cell when patterning the cells for the series connection or they can be located within the cell area (e.g. due to dust particles during the deposition).

In order to tackle this problem we need to deepen our understanding of the way in which the actual energy conversion takes place in a solar cell and its limiting factors. The most critical step related to the transport quality of the i-layer is, thereby , identified as being the process of the collection of photogenerated charge carriers. This process is analyzed theoretically in more detail in the present chapter. It was pointed out in section (1.13) that the basic transport equations can not be analytically solved for the general case. To get a complete picture one would, therefore, be obliged to calculate numerical solutions to the problem. Several groups have developed computer programs which allow sophisticated models to be implemented (e.g. [Arch 1991] ("AMPS"), [Hack 1985], [Smole 1992] ("ASPIN"), [Stiebig 1994], [Zeman 1997] ("ASA")). In this work, however, we preferred to gain more physical insight to solar cell physics by considering particular situations for which analytical solutions can be found. Thereby, we are conscious that the better precision of the more rigorous computer simulation is sacrificed for the sake of clarity and understanding.

We present, first of all, several models of the photocurrent collection which have been used in the past for the analysis of a-Si:H p-i-n diodes. The differences of these models are pointed out to allow for a direct comparison of the results obtained when applying each of them. One model is then extended analytically to the more general case with a non-constant electric field within the i-layer. Finally a characteristic quantity for solar cells is defined (the collection voltage, $V_{Collection}$) which is (within this theory) related to the transport quality of the i-layer of a p-i-n solar cell.

## 4.1. MODELS ASSUMING A CONSTANT ELECTRIC FIELD

In the perspective of measuring the i-layer quality directly within a completed p-i-n structure we need a model describing the influence of the transport properties of the i-layer material on the solar cell behavior.

4. Theory of the photocurrent collection in p-i-n solar cells

We will in this section concentrate on the way the drift lengths of electrons and holes influence the photocurrent collection. This is expressed by the collection function $\chi$, which is defined as:

$$\chi = \frac{Q_{collected}}{Q_{generated}} = \frac{I_{collected}}{I_{generated}} = 1 - \frac{\int R(x) \cdot dx}{\int G(x) \cdot dx} \tag{4.1}$$

### 4.1.1. Hecht collection model:

It is interesting to note that early investigations of the collection efficiencies of photogenerated mobile charge carriers were performed on isolating crystals (NaCl, AgCl, diamond, ZnS) rather than on semiconductors. [Hecht 1932] developed a single carrier collection model describing the primary photocurrent generated in macroscopic crystals which were laterally illuminated. It will be mentioned here because it presents the base for several models which were used to describe the photocarrier collection in amorphous silicon p-i-n solar cells:

He assumes that a charge carrier e that moves along the length d between two electrodes separated by the distance L corresponds to a collected charge of:

$$q = e \cdot \frac{d}{L} \tag{4.2}$$

Supposing further a decay of the total charge ($N_0$ generated at $x = 0$) following the Lenard equation he calculates the charge at a distance x:

$$N_x = N_0 \cdot e^{-\frac{x}{l_s}} \tag{4.3}$$

where $l_s$ denotes the "schubweg" (or drift length) of the generated carriers which is found to be proportional to the electric field E.

Integrating the movement of a sheet of charges generated at one extremity through the whole crystal leads to a collection efficiency of:

$$\chi = \frac{Q_{coll}}{Q_{gen}} = \frac{1}{N_0 \cdot e} \int_0^L N_0 \cdot e \cdot e^{-\frac{x}{l_s}} \cdot \frac{dx}{L} = \frac{l_s}{L}\left(1 - e^{-\frac{L}{l_s}}\right) \tag{4.4}$$

### 4.1.2. Crandalls' collection model:

It has been shown by [Crandall 1983] that a result formally identical to the Hecht equation is obtained if one calculates the collected current in a solar cell with field driven transport of

uniformly generated carriers. As simplifying assumptions to allow an analytical solution of the basic transport equations (eqns. 1.4 - 1.8) he assumes the following:

a) charge transport by diffusion can be neglected which implies that:

$$\frac{d}{dx}\left(\mu_p^0 \cdot \bar{E} \cdot p\right) = G - R \tag{4.5}$$

$$\frac{d}{dx}\left(\mu_n^0 \cdot \bar{E} \cdot n\right) = R - G \tag{4.6}$$

b) the electric field throughout the whole structure is uniform and amounts to:

$$\bar{E} = \left(V_{bi} - V_{applied}\right) / L \tag{4.7}$$

c) the recombination is described by the Shockley-Read formula [Shockley 1952] (which was deduced for the recombination on traps which may exist in either of two states differing by one electronic unit rather than on amphoteric defects as encountered in a-Si:H).

d) by the "regional approximation" he simplifies the recombination function further to:

$$R \cong \frac{p}{\tau_p} \text{ with } \tau_p = \frac{1}{v_{th} N_{db} \sigma_p} \text{ for } x > x_c \tag{4.8}$$

$$R \cong \frac{n}{\tau_n} \text{ with } \tau_n = \frac{1}{v_{th} N_{db} \sigma_n} \text{ for } x < x_c \tag{4.9}$$

These approximations lead formally to the same collection function as the one found by [Hecht 1932], however, with a different signification of $l_S$. In this case $l_S$ denotes a collection length $l_S = l_n + l_p$, where $l_n = \mu_n^0 \tau_n^R \bar{E}$ and $l_p = \mu_p^0 \tau_p^R \bar{E}$ are denoting the drift lengths of the two carriers:

$$\chi = \frac{l_S}{L}\left(1 - e^{-\frac{L}{l_S}}\right) \tag{4.10}$$

This model has been applied by [Faughnan 1984] to relate the FF of cells to the collection length of a material at zero applied voltage: $l_S(V_{applied} = 0)$. More recently [Hegedus 1997, Hegedus 1994] presented fits of I-V curves of a-Si:H and a-SiGe:H cells which were "in excellent agreement with this model".

### 4.1.3. Rechs' collection model:

A different physical model for the photocarrier collection has been proposed by [Rech 1997]. Surprisingly his model again leads to the formally identical function even though the argument is quite different: In fact, he supposes that:

a) diffusion of charge carriers is negligible with respect to the drift current

b) the electric field is constant in the i-layer and has the value given by eqn. (4.7)

c) the photocurrent is limited to holes alone which have constant collection length $l'_S$:

$$l'_S = \mu_p^0 \tau_p^R \overline{E} \tag{4.11}$$

d) the photocurrent is the integrated product of the generation rate of carriers at a location x and the probability that these charges are collected:

$$j_{ph}(\lambda) = e\int_0^L G(x,\lambda)\cdot P(x)\cdot dx \tag{4.12}$$

*The difference with respect to the two previous models is the idea that charges that move within the i-layer without being collected at one extremity do not contribute to an external current.*

e) the collection probability of charge carriers generated at x can be expressed according to the following equation:

$$P(x) = e^{-\frac{x}{l'_S}} \tag{4.13}$$

In the long wavelength limit when the generation profile is assumed to be uniform throughout the structure one obtains:

$$\chi = \frac{l'_S}{L}\left(1 - e^{-\frac{L}{l'_S}}\right) \tag{4.14}$$

in which case $l'_S = \mu_p^0 \tau_p^R \overline{E}$ denotes the drift length of holes.

### 4.1.4. Hubins' collection function:

Hubin [Hubin 1995] pointed out, that the collection function depends on the recombination model used. He underlined particularly the fact that for the case as treated by Crandall the collection in a solar cell is limited by the arithmetic sum of the drift lengths of electrons and holes (and is hence limited by the longer of the two). He recalculated the

collection of photogenerated carriers making the same assumptions as Crandall but using the appropriate formula (eqn. 1.16) describing recombination on amphoteric dangling bonds (i.e. defects that can exist in three charge states) as the ones observed in a-Si:H. To obtain an analytical solution of the transport equations he was forced to make the simplifying hypothesis that the major part of recombination occurs via neutral dangling bonds. This supposition was justified by a comparison of the numerically calculated recombination considering variable dangling bond charge to his analytical result.

For the collection function he found an expression which unlike Crandalls' was limited by the shorter of the two drift lengths. The intuitive explanation to this observation is the following: In the case of a two state recombination center carrier losses occur by sequential trapping of two charge carriers with opposite sign. This leads to a recombination time corresponding to a 'series connection' of the trapping times of individual carriers. In the case of a neutral three state recombination center trapping of a charge leads practically immediately to recombination as the cross section of capture of charged traps is bigger than the one of neutrals. As a result one finds recombination times corresponding to 'parallel connection' of the trapping times.

If both carriers have the same drift lengths (as assumed throughout this work) one deduces from Hubins' model the following equation for the collection function:

$$\chi = \frac{1}{1+\frac{L}{l_S''}} \tag{4.15}$$

where $l_S''$ stands now for the drift length of both carriers, $l_S'' = \mu_n^0 \tau_n^0 \overline{E} = \mu_p^0 \tau_p^0 \overline{E}$.

### 4.1.5. Mertens' collection function:

Yet another calculation was used in recent work of Merten [Merten 1998]. While he makes the same assumptions on the underlying physics as Hubin he uses as a further mathematical simplification of the problem a two step calculation proposed already by Crandall ([Crandall 1983]). Thereby the coupled continuity equations are solved separately (neglecting the coupling recombination term) and the resulting carrier profiles are then used in the second step to calculate the recombination. The result corresponds to a first order approximation of Hubins' collection function and reads for $\mu_n^0 \tau_n^0 \overline{E} = \mu_p^0 \tau_p^0 \overline{E} = l_S''$ as:

$$\chi = 1 - \frac{L}{l_S''} \tag{4.16}$$

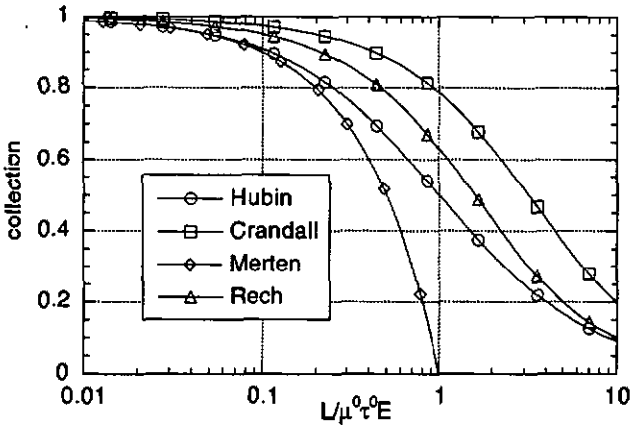


*Fig. 4.1: Comparison of the calculated photocurrent collection function depending on the drift length based on different models. Mertens' and Hubins' model are comparable for $L/\mu^0\tau^0 \le 0.1$. Crandall predicts a considerably higher collection for all drift lengths whereas Rechs' model prognosticates a collection value somewhere in between. All models converge for the high collection length limit.*

### 4.1.6. Comparisoo of the different collection models:

None of the quoted models was originally formulated based on the $\mu^0\tau^0$-product whicb can be measured in amorphous silicon layers. In the following summary we will assume symmetry of the electronic transport ($\mu_n^0\tau_n^0\overline{E} = \mu_p^0\tau_p^0\overline{E} = \mu^0\tau^0\overline{E}$, see section 1.1.6) and compare the collection models for an i-layer material with a certain $\mu^0\tau^0$-product:

1) Crandall: $\chi = \frac{l_S}{L}\left(1 - e^{-\frac{L}{l_S}}\right)$, with $l_S = \mu_n^0\tau_n^R\overline{E} + \mu_p^0\tau_p^R\overline{E} = 2\cdot\mu^0\tau^0\cdot\overline{E}$

2) Rech: $\chi = \frac{l'_S}{L}\left(1 - e^{-\frac{L}{l'_S}}\right)$, with $l'_S = \mu_p^0\tau_p^R\overline{E} = \mu^0\tau^0\cdot\overline{E}$

3) Hubin: $\chi = \frac{1}{1+\frac{L}{l''_S}}$, with $l''_S = \mu_n^0\tau_n^0\overline{E} = \mu_p^0\tau_p^0\overline{E} = \mu^0\tau^0\cdot\overline{E}$

4) Merten: $\chi = 1 - \frac{L}{l''_S}$, with $l''_S = \mu_n^0\tau_n^0\overline{E} = \mu_p^0\tau_p^0\overline{E} = \mu^0\tau^0\cdot\overline{E}$

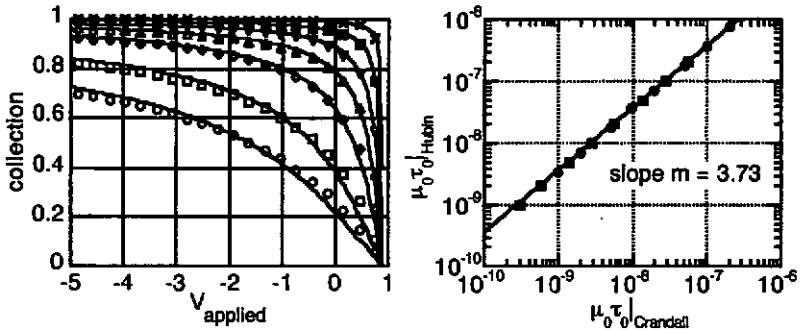


*Fig. 4.2: On the left graph the dots refer to the calculated photocurrent collection behavior according to Hubins' model. The lines correspond to best fits according to Crandalls' collection function. Strikingly good agreement can be obtained as long as the collection length is not too small On the right the relation between the (only) free parameter of each of the two models is shown.*

When plotted versus the drift length $\mu^0\tau^0 \cdot \overline{E}$ one finds that these different photocurrent collection models predict a rather different behavior of a solar cell incorporating a given i-layer material (see fig. 4.1).

For each of the mentioned models the correctness of the assumptions made for the analytical descriptions was verified by the 'quality of fits' to actual, measured data. It is interesting to note nevertheless that e.g. Crandalls' and Hubins' model - even though based on different recombination processes and yielding different analytical expressions - describe quite similar curve-shapes. This is clearly visible in fig. 4.2 where we superimpose the calculated collection behavior based on Hubins' model with best fits according to Crandall.

One notes, however, that the only free fitting parameter, $\mu^0\tau^0$, will be bigger by a factor of approximately 4 when Hubins' formula is used. One can, therefore, express the following relationship[18] between the $\mu^0\tau^0$-products when determined using the different formulas:

$$\mu^0\tau^0\big|_{Crandall} + \mu^0\tau^0\big|_{Rack} + \mu^0\tau^0\big|_{Hubin} + \mu^0\tau^0\big|_{Merten} \approx 1 + 2 + 3.73 + 4 \qquad (4.17)$$

[18]Remember that this relationship is based on the hypothesis that the transport properties of electrons and holes are symmetric. The quoted authors might not agree with this statement. As $\mu\tau$-products of electrons and holes can not be evaluated independently from the collection functions this direct comparison would not be meaningful for unequal $\mu^0\tau^0$-products of electrons and holes.

## 4.2. INFLUENCE OF THE ELECTRIC FIELD DISTORTION

In the previous section we presented different photocurrent collection models allowing to extract the i-layer material quality parameter $\mu^0\tau^0$ directly from cell measurements. It was shown that, even though the value of the $\mu^0\tau^0$ product depends on the recombination model, one obtains the same qualitative behavior for all models. Although this behavior corresponds strikingly well to measured photocurrent collection data there is one common assumption assumed for all presented models which is justified only for rather exceptional cases. This highly questionable hypothesis is the one of a constant electric field throughout the i-layer which may be satisfied only for high quality material in the annealed state (i.e. for a-Si:H with a very low defect density).

### 4.2.1. Deduction of the Analytical Expression

It will be shown in this section that the restrictions by the presumption of negligible E-field variations can be released when the recombination function for amphoteric states is used. For this case the analytical calculations can be formally extended to the case of a non-uniform electric field [Shah 1996].

Following the approach of [Hubin 1995] we assume negligible diffusion currents and that the recombination occurs mainly via neutral dangling bonds. The current equations (eqns. 1.5 - 1.6) are expressed as:

$$j_n = e \cdot \mu_n^0 \tau_n^0 \cdot \frac{n_f(x)}{\tau_n^0} \cdot E(x) \tag{4.18}$$

$$j_p = e \cdot \mu_p^0 \tau_p^0 \cdot \frac{p_f(x)}{\tau_p^0} \cdot E(x) \tag{4.19}$$

which when using the assumption of symmetric drift lengths result in a total current (which is constant over the whole i-layer) of:

$$j_{tot} = e \cdot \mu^0 \tau^0 \cdot \left( \frac{n_f(x)}{\tau_n^0} + \frac{p_f(x)}{\tau_p^0} \right) \cdot E(x) = e \cdot \mu^0 \tau^0 \cdot R(x) \cdot E(x) \tag{4.20}$$

Note that this equation expresses the fact that the recombination in a drift driven device is inversely proportional to the magnitude of the electric field. Introducing for the purpose of normalization the average electric field $\overline{E}$ according to eqn. 4.7 one obtains then by integration:

$$j_{rec} = e \cdot \int_0^L R(x) \cdot dx = \int_0^L \frac{j_{tot}}{\mu^0 \tau^0 \cdot E(x)} \cdot dx = \frac{j_{tot} \cdot L}{\mu^0 \tau^0 \cdot \overline{E}} \cdot \underbrace{\frac{1}{L} \int_0^L \frac{\overline{E}}{E(x)} \cdot dx}_{\text{form factor : } \varphi} \tag{4.21}$$

where $\varphi$ denotes a "form factor" due to the deformation of the electric field. Note that this form factor $\varphi = 1$ for a constant electric field (as assumed in the previously described models) while $\varphi \geq 1$ for any arbitrary deformation of the field at a given voltage over the structure. This indicates that any deviation of the electric field distribution from a constant value results in an increase of the recombination losses.

The collection reads as:

$$\chi = \frac{j_{tot}}{j_{tot} + j_{rec}} = \frac{1}{1 + \frac{L \cdot \varphi}{\mu^0 \tau^0 \cdot \bar{E}}} = \frac{1}{1 + \frac{L}{l_{S,eff}}} \tag{4.22}$$

with

$$l_{S,eff} = \frac{\mu^0 \tau^0}{\varphi} \bar{E} \tag{4.23}$$

*We find formally the same collection function for an arbitrary field distribution as in the case of a constant electric field but with an* effective drift length $l_{S,eff}$. This effective drift length corresponds to the previously defined drift length of free electrons and boles moving in a material with neutral defects but whicb is reduced by the form factor $\varphi$ of the field distortion.

Note in eqn. 4.23 that the experimentally measurable quantity $l_{S,eff}$ consists of tbe fraction of the drift length divided by the form factor $\varphi$. The effects on the collection of a short drift length and of a strong field deformation can, therefore, not be distinguished.

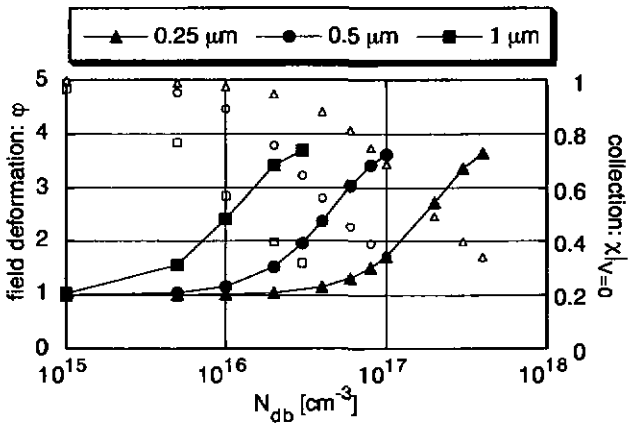


*Fig. 4.3: Calculated deformation of the electric field (expressed by φ) for solar cells with different i-layer thicknesses as a function of the defect density. The open symbols indicate the corresponding values of the collection χ calculated at a bias voltage of zero volts.*

### 4.2.2. Numerical Estimation of the Value of the Form Factor $\varphi$

In the foregoing section it was shown that, analytically, the influence of the deformation of the electric field in a p-i-n solar cell can be expressed by a simple factor $\varphi$ (see eqn. 4.21) by which the $\mu^0\tau^0$-product is reduced when calculating the collection. In order to get an idea of realistic values of this factor we performed computer simulations which resolve numerically the basic semiconductor equations (eqn. 1.4 - eqn. 1.8) for the i-layer of an a-Si:H diode. The program as well as the microscopic parameters used has been described elsewhere ([Fischer 1994]). The results are displayed in Fig. 4.3.

One notes that the field deformation factor $\varphi$ has typically a value between 1 and 2. For thick cells or for i-layers with very high defect densities $\varphi$ may even grow to values above 3. One notes, however, for such situations that the collection collapses in these cases dramatically so that even under short circuit conditions one gets a collection lower than 50 %. As a conclusion we retain that for realistic solar cells the field deformation factor has a value between $1 \leq \varphi \leq 2$.

## 4.3. IV-CURVES OF "REAL" SOLAR CELLS

It was shown in the previous paragraph that the drift length of electrons and holes, $l_{s,eff}$, influences directly the collection efficiency of a solar cell through a simple analytical relationship (eqn. 4.22). The fact that the collection efficiency $\chi$ can be written in form of an expression which does not contain the generation rate anymore implies that material related collection losses are proportional to the total generated photocurrent. This particular feature is specific to the transport limited collection losses and allows to discriminate between "material issues" (i.e. i-layer quality) and "technology issues" (series resistance, shunts, optical losses) in the cell

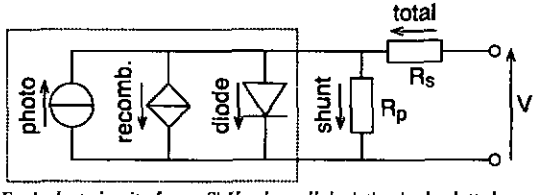


*Fig. 4.4: Equivalent circuit of an a-Si:H solar cell depicting in the dotted area on the left an idealized cell consisting of a current source (total photogenerated current, independent of the applied voltage V), a variable current sink (recombination term, depending on $I_{photo}$ and V) and the diode term $I_{diode}$ (dark current). On the right hand side the parasitic losses are summarized in a shunt resistance $R_p$ and a series resistance $R_s$.*

optimization. This becomes apparent if we use the basic equivalent circuit of an a-Si:H solar cell[19] according to fig. 4.4.

When using eqn. 4.22 to describe the difference between the photogenerated current and the recombination current ($I_{photo} \cdot \chi$) the IV-curve of a solar cell with predominant drift driven collection (according to the equivalent circuit above (fig. 4.4) can be described as follows:

$$I(V) = \underbrace{-I_{photo} \cdot \frac{1}{1 + \frac{L^2 \cdot \varphi}{\mu^0 \tau^0 \cdot (V_{bi} - [V - IR_s])}}}_{\text{generated current - recombination term}} + \underbrace{I_0\left(e^{q\frac{V-IR_s}{nkT}} - 1\right)}_{\text{injection term (dark current)}} + \underbrace{\frac{V - IR_s}{R_p}}_{\text{shunt losses}} \qquad (4.24)$$

The intervening terms have, thereby, varying importance depending on light intensity ($I_{photo}$) and bias voltage conditions. Since we are interested in the recombination losses we will define a measurement range for which the collection term dominates the IV-curve.

Concerning the bias voltage it is preferable to study the IV-curves around a fixed value ($V = 0\,V$) rather than fitting the measured collection efficiency curves over a large voltage range. The reason for this is that at increasing forward voltages the assumptions made to deduce the collection function lose their validity (drift driven current decreases and the neglected effects of diffusion start to become important) while at reverse voltages $\chi$ contains less information due to its saturation behavior. The absolute value of the photocurrent collection evaluated at $V = 0\,V$ contains essentially the information of the total generation rate (to which it is proportional). A term measurable in solar cells and which can be linked to the material quality is the *variation* of the photocurrent with the bias voltage. This quantity is given by the "short circuit resistance" which is defined as:

$$R_{SC}^{-1} = \left.\frac{\partial I}{\partial V}\right|_{V=0} \qquad (4.25)$$

Concerning the intensity range for which this quantity can be related to $\chi$ one has to calculate the derivative of eqn. 4.24 (a detailed calculation is presented in annex II). Thereby

---

[19] All the authors quoted in section 2.3.1 treat the solar cell in this same way. We will use the approach given by Merten who seperated the photocurrent in a photogeneration part which is paralleled with a recombination current sink. In Rechs' equivalent circuit this recombination current is implicitly contained in a voltage dependent photocurrent. Crandall measures directly the photocurrent by chopped illumination (see e.g. [Faughnan 1984]). Hubin also adresses directly the photocurrent alone by restricting his treatment to measurement conditions for which the IV-curve is dominated by the collection term (reverse bias).

ooe finds that the functioo $R_{SC}^{-1} = f(I_{photo})$ of a typical solar cell can be oaturally divided into three regimes: a low, a moderate and a high light intensity regime. In the following these three cases will be analyzed in detail.

### 4.3.1. The low level intensity regime:

In this regime $R_{SC}$ is determined by the terms of the injection current and the shunt losses. Due to the low saturatioo curreot in the wide gap material a-Si:H the dark diode term is, thereby, (at V = 0 V) normally negligible with respect to the parallel resistance losses. Derivation yields:

$$R_{SC}^{-1} \approx \frac{1}{R_p} + \frac{I_0}{n\frac{kT}{q}} \approx \frac{1}{R_p} \tag{4.26}$$

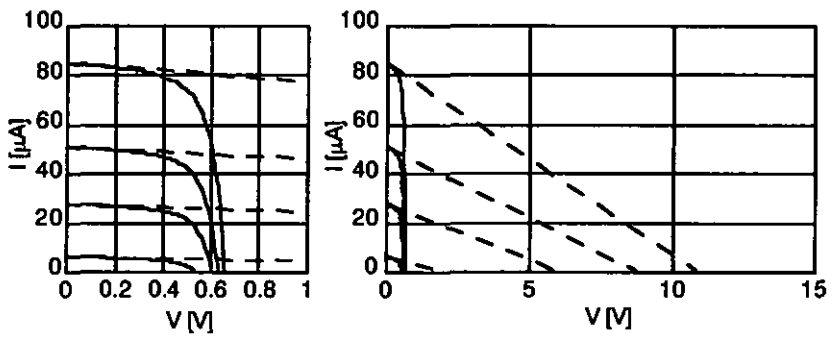


*Fig. 4.5: IV-curves [µA] of a typical a-Si:H solar cell (surface: 0.2 cm$^2$) measured at low light intensities (0.2 - 2 mWcm$^{-2}$). The dotted lines correspond to tangents fitted at V = 0 V with a slope of $R_{SC}^{-1}$.*

### 4.3.2. The medium inteosity regime:

For medinm light intensities the short circuit resistance $R_{SC}$ is limited by the collection term and decreases proportionally to the inverse of the photocurrent:

$$R_{SC}^{-1} \approx I_{photo} \cdot \chi' \approx I_{photo} \cdot \frac{L^2\varphi}{\mu^0\tau^0 \cdot V_{bi}^2} \cdot \frac{1}{\left(1+\frac{L^2 \cdot \varphi}{\mu^0\tau^0 \cdot V_{bi}}\right)^2} \tag{4.27}$$

Therefore the tangents to the IV-curves at V = 0 intersect the x-axis in a siogle point $V_{Collection}$ which can be connected to the transport properties of the material (the interpretation of this "collectioo voltage" will be given latter in this section). It is in this illuminatinn regime that the i-layer material quality can be measured via an IV-curve analysis.

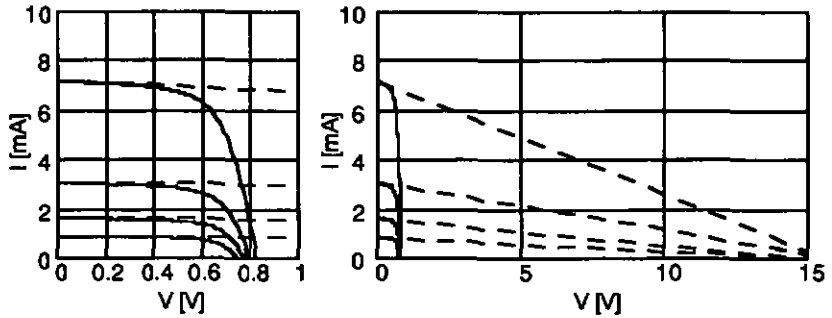


*Fig. 4.6: IV-curves [mA] of a typical a-Si:H solar cell (surface: 0.2 $cm^2$) measured at medium light intensities (25 - 200 $mWcm^{-2}$).*

### 4.3.3. The high intensity regime:

At high intensities the influence of the series resistance starts to deform more and more the IV-curves. Its main influence on the short circuit resistance $R_{SC}$ is via the voltage shift by $\Delta V = I \cdot R_S$ of the diode voltage with respect to the terminal voltage. $R_{SC}$ is, therefore, reduced to an expression given in annex II which converges to $R_S$ at very high intensities:

$$R_{SC} = \left(\frac{\partial I}{\partial V}\right)^{-1} \xrightarrow{I_{phot} \to \infty} R_s \qquad (4.28)$$

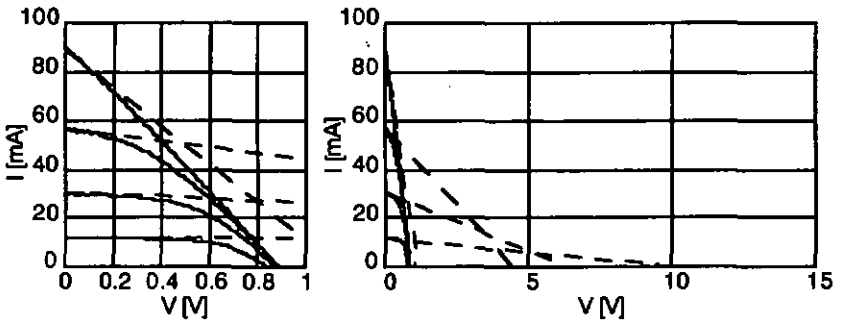


*Fig. 4.7: IV-curves [mA] of a typical a-Si:H solar cell (surface: 0.2 $cm^2$) measured at high light intensities (300 - 1000 $mWcm^{-2}$).*

### 4.3.4. The "collection voltage":

It has been shown in the previous analysis that for a typical field driven solar cell an illumination range exists for which the IV-curve is dominated by the collection function of the photocurrent. Under such illumination conditions the slope of the photocurrent at V = 0 V, $R_{SC}^{-1}$, was shown to be proportional to total photogenerated current (and hence to the short circuit current which is given by $I_{SC} = I_{photo} \cdot \chi|_{V=0}$). This proportionality implies that the tangents of the IV-curves intersect the x-axis at one single voltage - the collection voltage, $V_{Collection}$ - which can be determined as:

$$V_{Collection} = \chi|_{V=0} \cdot \left( \frac{d\chi}{dV}\bigg|_{V=0} \right)^{-1} = I_{SC} \cdot R_{SC} \tag{4.29}$$

Replacing eqn. 4.22 in formula 4.29 yields:

$$V_{Collection} = V_{bi} \cdot \left( \frac{\mu^0 \tau^0 V_{bi}}{\varphi L^2} + 1 \right) = V_{bi} \cdot \left( \frac{l_{s,eff}}{L} + 1 \right) \tag{4.30}$$

Measuring the collection voltage in a p-i-n solar cell provides, therefore, information on the effective drift length of its i-layer material (under an applied potential of $V_{bi}$).

Note that this concept of the collection voltage is more general than the particular case for which its microscopic description has been explicitly calculated here (within the framework of Hubins' model discussed earlier, in section 4.1.4). Actually the intersects of the tangents to the IV-curves at any fixed bias voltage should intersect the V-axis at a constant voltage while the intensity is varied provided that the photocurrent of a solar cell can be described by a collection function $\chi$ which is *independent* of the light intensity. Note that this property holds for all collection functions deduced by the different analytical models presented (in section 4.1.). It is, however, in striking contrast to the idealized crystalline silicon solar cell [Green 1982]. Here, the IV-curve has in its most basic analytical description a fixed shape which is simply shifted by the value of the photocurrent. This results in a collection voltage which (over the range with negligible series and parallel resistance) would increase proportionally to the short circuit current.

# 5. VIM[1]: MEASURING THE I-LAYER QUALITY IN THE COMPLETED CELL?

In the previous chapter theoretical considerations were presented which aim to relate an experimentally accessible, characteristic quantity of a p-i-n solar cell (i.e. the collection voltage $V_{Collection}$) to the transport properties of its bulk material. Thereby, some simplifying assumptions had to be admitted in order to allow analytical calculations to be carried out. The purpose of the investigations presented in the present chapter is to cross-check for the practical applicability of the theory developed above. In order to do so, we describe, first of all, several procedures that allow $V_{Collection}$ to be determined. These methods are, then, used to scrutinize the collection behavior of carefully selected p-i-n diodes of which the i-layer material was analyzed apart (allowing for a direct comparison of the i-layer quality as measured in the cell with the quality as measured on the isolated i-layer) or which formed a consistent thickness series (which allows the *relative* collection behavior to be studied as a function of the i-layer thickness).

## 5.1. THE EXPERIMENTAL TECHNIQUES:

The theoretical considerations in chapter 4 revealed that the material quality of the i-layer, $\mu^0\tau^0$, affects the IV-curve of a solar cell in a way which can be characterized by the collection voltage $V_{Collection}$. This quantity corresponds geometrically to the intersection of the tangents of the IV-curves (measured under short circuit conditions at intermediate light intensities) with the voltage axis. It was shown that $V_{Collection}$ is, therefore, identical to the constant of proportionality relating $R_{SC}$ to $I_{SC}^{-1}$ (eqn. 4.29). Experimentally the collection voltage is, thus, accessible in different ways which will be described in this section.

### 5.1.1. DC-VIM[20] method: The Merten approach:

The most direct way to determine the collection voltage consists in measuring first the IV-curves of a solar cell at various light intensities of uniformly absorbed, i.e. red, light (in

[20]The term "VIM" stands for "variable illumination measurement". It has been introduced by Merten [Merten 99g] who used this approach to directly determine an "effective μτ-product" using his collection function.

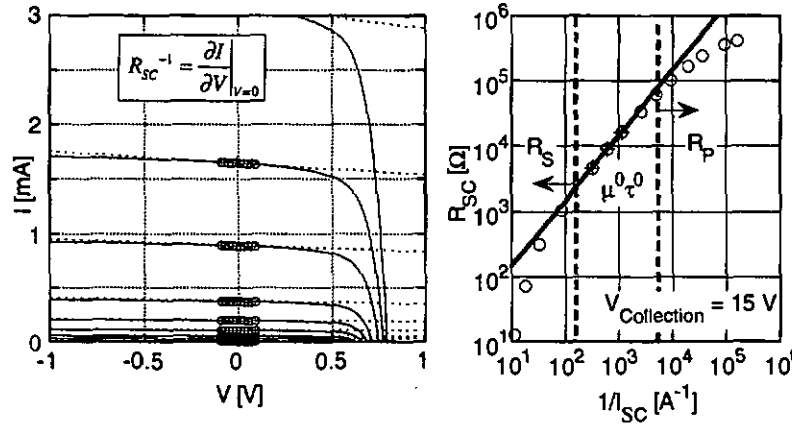


*Fig. 5.1: Measurement of $R_{SC}$ by linear fits to IV curves at V = 0 V (left graph). The right plot shows $R_{SC}$ plotted against $I_{SC}^{-1}$ for an a-Si:H solar cell (i-layer thickness: 0.3 µm, surface: 0.2 cm²). The left dotted bar indicates the high intensity region where the IV-curve is $R_S$ limited. The right dotted line delimits the low intensity regime in which the IV-curves are $R_P$ limited. In between the IV-curve is limited by the transport. A linear fit in this region yields $V_{Collection}$ = 15 V.*

order to be able to establish a direct link with the theory of the photocurrent collection which was deduced for a *constant generation rate* throughout the i-layer). For each individual curve $R_{SC}$ can then be determined by performing a linear fit to the IV-data measured within a voltage range close to V = 0 V. This procedure has to be done for several light intensities to determine the illumination range for which the cell behavior is collection limited. The information that for a given intensity range the solar cell is indeed collection limited is provided by the observation that for this regime $R_{SC} \propto I_{photo}^{-1}$. This relation extends for a typical a-Si:H solar cell for photocurrents varying over several orders of magnitude.

Note that the $\mu^0\tau^0$-product corresponding to the 0.3 µm thick p-i-n cell of Fig. 5.1 with the collection voltage of 15 V amounts to about $1 \cdot 10^{-8}$ $cm^2V^{-1}$ (see eqn. 4.30, assuming that $V_{bi} \approx 1.1$ V and $\varphi \approx 1$). Such a low value of the $\mu^0\tau^0$-product is, however, rather exceptional for device quality a-Si:H (see Fig. 3.3). Typical, device quality material was measured to have a $\mu^0\tau^0$-product of up to a factor 10 higher after degradation. Provided that the VIM-method does, indeed, measure the $\mu^0\tau^0$-product of the bulk material of solar cell we expect the necessity to dispose of a method which is able to measure accurately much higher collection voltages.

It is obvious that the method presented above is not appropriate to tackle this task if one aims to characterize cells incorporating a very good i-layer (having a big $V_{Collection}$). With standard IV-curve measurement equipment tiny current variations around V = 0 V can not be

resolved. Or they may be covered by the noise (as indicated in fig. 5.2)[21]. Therefore we developed the AC-VIM method which will be introduced in the following section. This new method can yield the desired information with an enhanced precision required under such circumstances.

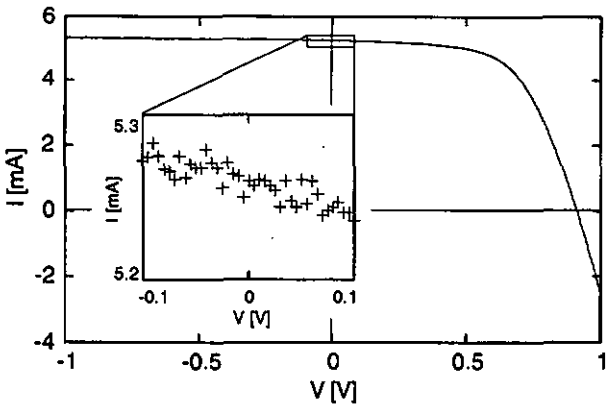


*Fig. 5.2: IV-curve of an a-Si:H cell with a good saturation behavior ($V_{Collection}$ = 40 V). For such good cells $R_{SC}$ and hence the collection voltage can not be accurately determined using the DC-VIM approach*

### 5.1.2. AC-VIM method:

The precision of the determination of $R_{SC} = f(I_{photo}^{-1})$ can be increased by performing a direct measurement of the short circuit resistance using the AC-VIM method (see fig. 5.3).

Thereby the device under test is DC biased at zero volts and a small AC signal is superimposed. As the applied voltage signal and the corresponding AC-current can both be measured directly this method allows a direct (and precise) determination of the short circuit resistance $R_{SC}$. Several practical considerations have to be taken into account nevertheless when applying this method:

On one band the measurement resistor $R_{meas}$ has to be selected high enough to get a sufficiently high current voltage conversion ratio. On the other hand one has to apply an external voltage of $V_{ext} = I_{SC} \cdot R_{meas}$ to get a bias potential of zero volts over the solar cell. $I_{SC}$ fluctuations will be amplified to bias voltage variations of $\Delta V = \Delta I_{SC} \cdot R_{meas}$ on the device under

[21] For a detailed analysis of the error estimation refer to annex III.

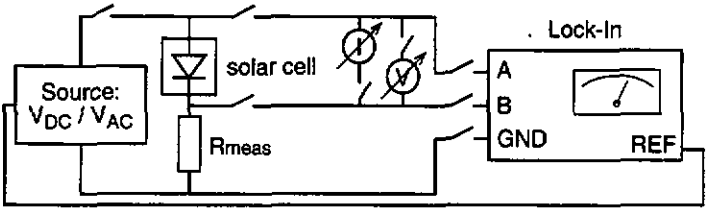


*Fig. 5.3: In the AC-VIM measurement set-up an AC signal ($V_{pp}$ = 50 mV) is applied to the cell under zero volts bias. This bias voltage is verified using the DC voltmeter. An Ampère meter con be optionally connected for an $I_{SC}$ measurement. The voltage variation ΔV can be measured on the Lock-in by measuring the difference of the signals A-B. The corresponding current variations are accurately measured via the voltage drop on $R_{meas}$ which is connected to channel B.*

test. To keep this error small $R_{meas}$ has to be selected in such a way that the working point of the solar cell remains voltage-controlled. In practice it has to be adapted to the bias light conditions.

The signal measured on $R_{meas}$ which is used to measure the AC-current through the solar cell is very small (especially for good cells). On the lock-in this signal has to be measured in the direct mode rather than io the differential mode (i.e. in figure 5.3 the device uoder test and the measurement resistor $R_{meas}$ can not be interchanged). In fact, the AC-voltage measured on $R_{meas}$ is typically several orders of magnitude smaller than the AC-voltage over the solar cell. For measuremeots io the differeotial mode the common mode rejection ratio of typical lock-in amplifiers (e.g. CMRR = 100 dB for the model "SR530" by Stanford Research systems) is oot enough for all situations.

An additional problem arises through the junction capacitance of the solar cell to be measured. For alternative currents this capacitance presents an impedance which is short circuiting the solar cell under test. The junction capacitance of typical devices is rather high. For a-Si:H it can be estimated by the following formula:

$$C \approx \frac{A\varepsilon_{Si}}{d} \tag{5.1}$$

With $\varepsilon_{Si} \approx 12 \cdot \varepsilon_0 \approx 10^{-12}\ AsV^{-1}cm^{-1}$ one fiods for a 300 om thick cell a sample capacitance of $C \approx 30$ nFcm$^{-2}$ (In the case of μc-Si:H solar cells the effective sample capacitance is typically bigger than this calculated value of the geometrical capacitance [Beck 1997].). As a result one measures with the AC-VIM method an *apparent* short circuit resistance $R_{SC}^{*}$ which corresponds to the parallel connection of the actual value $R_{SC}$ with the junction capacitance (see fig. 5.4):

$$R_{SC}^{*} = R_{SC} \cdot \frac{1}{\sqrt{1 + (2\pi\nu)^2 R_{SC}^2 C^2}} \tag{5.2}$$

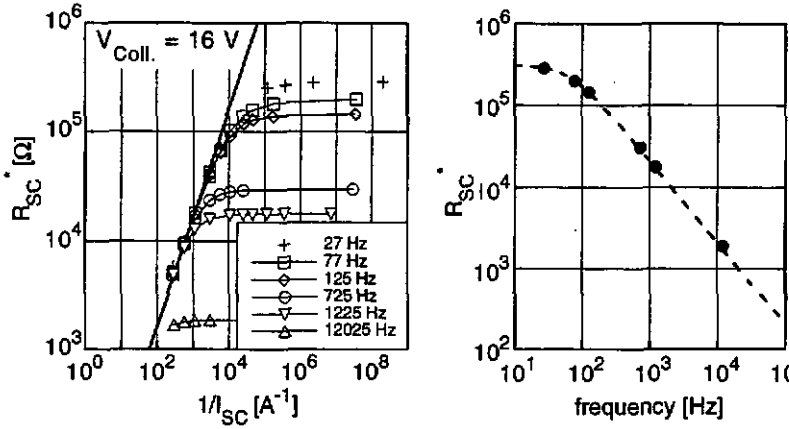


*Fig. 5.4: Influence of the measurement frequency on the apparent short circuit resistance $R_{SC}^{*}$. The low intensity limitation occurs through the junction capacitance rather than through the shunts of the cell under test (p-i-n, a-Si:H), 0.3 µm, 0.2 cm$^2$). The graph on the right is obtained by plotting the low intensity limit of $R_{SC}^{*}$ versus the measurement frequency. The dotted line corresponds to a best fit to eqn. 5.2 with $R_{SC} = 3 \cdot 10^5\ \Omega$ and $C = 8$ nF.*

To get an accurate determination of the collection voltage the excitation frequency has to be chosen small (e.g. ν = 10 Hz).

As a conclusion we claim that as long as the cited precautions are taken into account the AC-VIM method is capable of measuring higher collection voltage values (of "good" solar cells) with a higher precision than the DC-VIM method; a statement which can be readily understood when calculating an error estimation (see annex III). A disadvantage of this method with respect to the original approach is the fact that it reveals exclusively the dependency of $R_{SC}$ as a function of the light intensity (knowledge of extended IV-curves at different light intensities sometimes turns out to be useful for the analysis of problems such as the creation of shunts during the measurement etc.). Another limitation comes by the influence of the junction capacity which restrains a precise measurement of the parallel resistance of a cell to a certain maximum value (inversely proportional to the measurement frequency).

### 5.1.3. VIM on strongly shunted cells - the SR-VIM method:

The short circuit resistance of a typical solar cell is normally limited by the collection term of the equivalent model over several orders of magnitude of light intensity. In bad cases, however, shunts may limit the cell up to intensities at which the series resistance starts to affect the IV-curve. In such situations no linear region can be found in the $R_{SC} = f(I_{photo}^{-1})$ plot (see

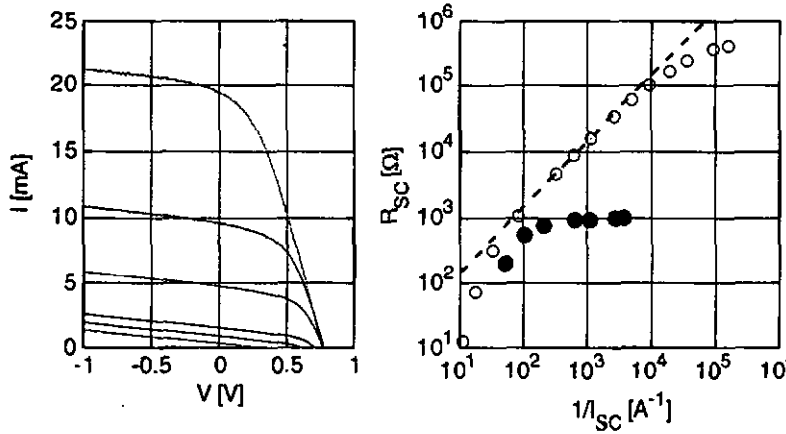


*Fig. 5.5: IV-curves of a shunted a-Si:H cell. The cell is the same as in fig. 5.1 (open circles) but purposely short circuited with a 1 kΩ resistor leading to an apparently bad collection (filled symbols). In the* $R_{SC} = f(I_{photo}^{-1})$ *plot there is no linear region and the collection voltage can, thus, not be determined.*

fig. 5.5). The collection voltage can, thus, not be determined using the described approaches. A minimum value of $V_{coll.}$ can sometimes be estimated nevertheless using SR measurements at variable bias voltage around zero volts.

The principle of this measurement is based on the fact that the SR allows a direct measurement of the photocurrent. One notes in eqn. 4.24 that the injection current (dark diode) or the shunt losses do not contribute to the signal obtained by a modulation of the photocurrent. Their magnitude depends on the applied bias voltage alone (provided that $R_S$ can be neglected). This is normally the case because of the low intensity of the probe beam in SR measurements (the probe beam induced photocurrent is for red light typically about $10^{-5}$ A). Ideally it is, therefore, possible to measure the collection gradient around zero volts in spite of the presence of shunts. As this method consists in an evaluation of the variation of the collection function around zero volts the same considerations concerning measurement accuracy apply as presented for the DC-VIM method (see annex III). Since the precision of the SR measurement is lower than the one of the current measurement the use of this technique is limited to cells with relatively low collection voltages (i.e. a-Si:H cells in the degraded state).

As an example this method has been applied to the bypassed solar cell of fig. 5.5. The red light SR measurements were performed at -0.1 V and +0.1 V. Thereby the collection variation associated with this bias voltage change was sufficiently large to be resolved with our SR set-up. It allowed a collection voltage of $V_{coll.} = 16\ V \pm 10\ \%$ to be determined (fig. 5.6) which is in accordance with the value determined by the standard VIM technique (fig. 5.1).

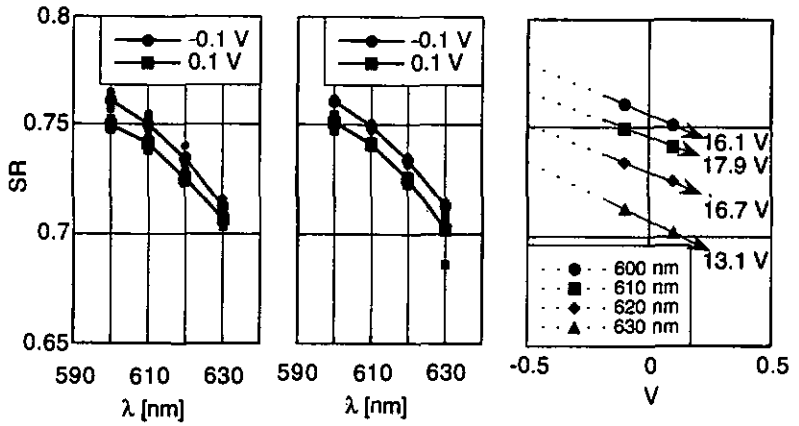


*Fig. 5.6: The two graphs on the left show red light spectral response measurements of the cell of fig. 5.5 with (center) or without (left) external shunt resistor (1kΩ). Obviously the SR measurement is not affected by such a parallel resistance. On the right these SR data are plotted against the bias voltage. This representation allows a collection voltage of* $V_{coll.} = 16\ V \pm 10\ \%$ *to be evaluated.*

## 5.2. MEASUREMENTS

In the previous section we presented several experimental techniques which allow the collection voltage $V_{Collection}$ to be measured on p-i-n diodes. In chapter 4 it was shown how this quantity can be related, theoretically, to the $\mu^0\tau^0$-product of the i-layer incorporated in this cell. The key equation is thereby eqn. 4.30 indicating the following relation:

$$\mu^0\tau^0 = \frac{\varphi L^2}{V_{bi}}\left(\frac{V_{Collection}}{V_{bi}} - 1\right) \tag{5.3}$$

It will be the purpose of the present section to investigate to which extent the VIM-method for the determination of i-layer $\mu^0\tau^0$-products leads experimentally to consistent results. For the measurements presented we used systematically the DC-VIM approach (which has the advantage of revealing the whole IV-curves rather than just $R_{SC}$-values at different light intensities, which allows to "follow" the cells during the measurements) unless stated otherwise. The AC-VIM approach was used to increase the measurement precision in the case of cell presenting a high collection voltage. The light used to perform the VIM-analysis was (unless mentioned) the focused beam of a 250 W halogen lamp filtered by a RG630 edge filter ("high pass" with a cut-off wavelength of $\lambda_{cut-off} = 630\ nm$) in order to obtain a reasonably uniform generation rate in the cells combined with a heat-absorbing filter (KG1) to avoid an excessive rise of the cell temperature during the measurement.

For the numerical calculation of the $\mu^0\tau^0$-values we will assume for all a-Si:H cell a built-in potential of $V_{bi} = 1.1\,V$. The deformation of the electric field will not be taken into account ($\varphi = 1$).

The i-layer material quality related collection voltage $V_{Collection}$ of eqn. 5.3 was defined as being the voltage at which the tangents to the IV-curves measured at different intensities intersect the V-axes. Such a unique intersection voltage exists according to the theory *provided that the IV-curves are purely collection-limited* (i.e. provided that the influences of series resistance and shunts can be neglected at the selected intensity range) and under the condition that the collection function $\chi$ is independent of the light intensity (see section 4.3.4.). In the original work of [Merten 1998] the intensity range over which this relation holds was determined in the doubly logarithmic plot of $R_{SC}$ vs. $I_{SC}$ as the region for which $\ln(R_{SC})$ varies linearly with $\ln(I_{SC})$. Such a representation is somewhat misleading since the logarithmic function "compresses" graphically the deviations from the ideal behavior. Moreover a linear fit over several orders of magnitude of data distributed uniformly in a doubly logarithmic plot strongly emphasizes the big values and does, hence, not constitute a correct average value.

Therefore, we prefer to represent on a *linear* scale directly the intersections of the tangents to the IV-curves with the V-axis as function of the logarithm of $I_{SC}^{-1}$. The requirement of this intersection voltage to be constant over a certain light intensity range has to be regarded as a more severe criterion allowing to verify more critically the actual behavior of the measured cells. In Fig. 5.7 a set of data is represented for comparison in both manners. One notes that the intensity range over which the actually measured data seem to deviate from the ideal curve is

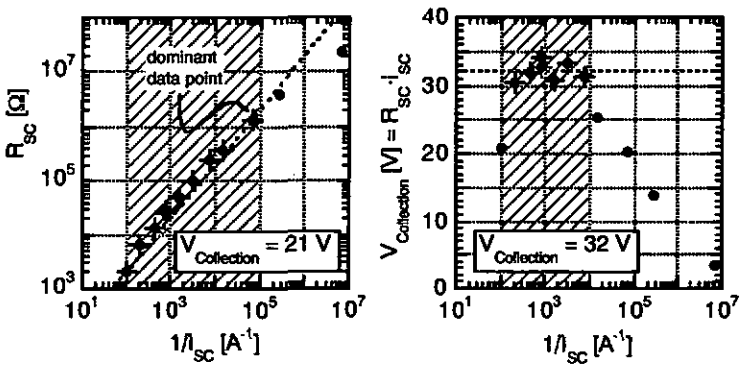


*Fig. 5.7: The VIM-technique applied to an a-Si:H cell of 0.4 µm thickness. The two plots are different representations of the identical data. The gray area indicates the range over which the model can be considered to fit the experimental points well. The crosses mark the retained data for the determination of the collection voltage.*

smaller in the first plot. When performing a linear fit through the data retained by only the data in the gray area ooe obtains as a result a value of the collection voltage which is giveo exclusively by one dominant point. In the secood representation ooe observes that this point actually does not belong to the actual plateau region of the collection voltage and it rejected. This second, more objective representation will, thus , be selected to depict all $V_{Collection}$ measurements shown in this chapter.

### 5.2.1. dilution series

First of all, a number of cells were measured of which the i-layer material bad beeo already extensively characterized in previous studies. For this purpose the layers and cells presented earlier in this work (chapter 3) were perfectly suited. Here we preseot $V_{Collection}$ measurements as evaluated on the cells of the dilution series (see Fig. 5.8). The average $\mu^{O}\tau^{O}$-products as measured io the corresponding layers are repeated in table 5.1.

| $\mu^{O}\tau^{O}$-product | dilution 0 | dilutioo 2 | dilution 9 |
|---|---|---|---|
| initial state | $4.6 \cdot 10^{-7}$ | $7.0 \cdot 10^{-7}$ | $2.3 \cdot 10^{-7}$ |
| degraded state | $5.4 \cdot 10^{-8}$ | $1.2 \cdot 10^{-7}$ | $1.0 \cdot 10^{-7}$ |

*Table 5.1: Average values of the $\mu^{O}\tau^{O}$-products [$cm^2V^{-1}$] as measured on a-Si:H films deposited at low temperature (195 °C) using various hydrogen dilution ratios in the initial state as well as after accelerated degradation.*

Comparisoo of the cell and layer analysis sbows that in the initial as well as in the degraded state the same tendencies are observed: The $\mu^{O}\tau^{O}$-product in the initial state is highest for the material deposited using a dilution of 2. It is by about a factor two lower for the high bydrogen dilution and it is about 30 % lower in the case of undiluted film growth. Similarly we observe on films and cells that the undiluted material sbows the strongest degradation.

It is striking that the $\mu^{O}\tau^{O}$-products as measured in the cells are by a factor 20 (in the initial state) and by a factor 10 (io the degraded state) lower than the ones measured in films. Sucb a huge deviation can not be attributed to the deformation of the electric field giveo by $\varphi$ (which was assumed to be 1 for the calculatioo of the $\mu^{O}\tau^{O}$-products using VIM) as can be seeo from the numerical simulations of typical values (see section 4.2.2). An additional argument forcing us to reject the explanation of the field distortioo being responsible for the big difference of $\mu^{O}\tau^{O}$-products measured in film with respect to the ones measured in the cells is that $\varphi$ tends to iocrease with the density of defects in the material and is, bence, expected to increase duriog degradation. The fact that we observe a smaller relative degradation of $\mu^{O}\tau^{O}$-products measured by VIM in cells than directly in layers is in contradictioo to this.

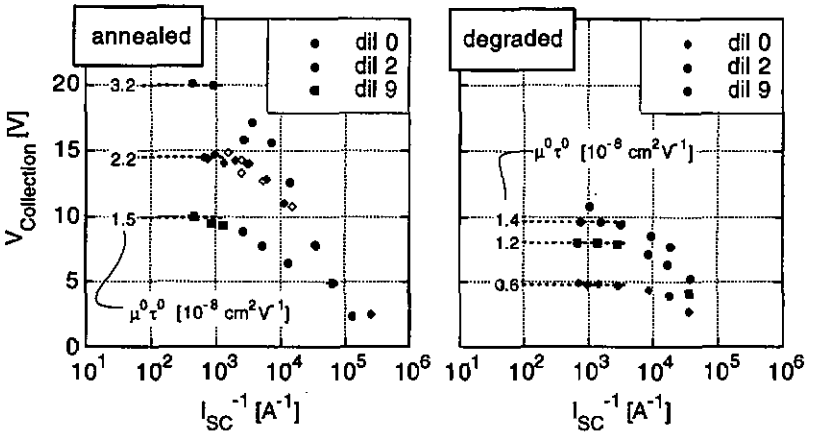


*Fig. 5.8: Collection voltages of a-Si:H cells deposited at low temperature (195 °C) using different hydrogen dilutions. The i-layer of these cells has a thickness of 450 nm. Compare also with Fig. 3.7.*

As will be seen throughout all the VIM-measurements presented in this work the observation that $\mu^0\tau^0$-products measured in cells are by about a factor 10 lower than the ones measured in films seems to be of general nature. Up to now we can only speculate on the reason of this difference. One possible explanation could be connected with defective zones close to the interfaces. They would have an effect on the collection function similar to the one observed in our actual measurements. Such defective zones which might considerably enhance the recombination in cells would in principle not be seen to the same extent[22] in coplanar transport studies as the ones presented in chapter 1. The existence of such defective zones has been postulated to explain PDS measurements carried out on thickness series of a-Si:H films on certain types of substrates. Film measurements have indicated that a defective zone extends from the interface between the substrate and the layer in which the defect density decreases gradually over a thickness of about 0.8 µm [Favre 1993]. Such defective material in the interface material could also be imagined to have a less pronounced relative degradation than the bulk material. This would explain the observed less important *relative* degradation of the $\mu^0\tau^0$-products measured in cells with respect to the ones of the corresponding layers.

[22] A measurement of the photoconductivity and the ambipolar diffusion length in a inhomogeneous film can be thought to characterize the best part of the film. In contrast to this the electronic transport in a solar cell traverses necessarily also the defective interface layers in which the recombination may be important.

On the other hand we recall that different physical models (which all lead to an expression of a collection function which is independent of the light intensity - a statement which directly implies the existence of a constant collection voltage over a certain range of light intensities) deduced for a given set of data $\mu^0\tau^0$-products differing by a factor 4. This observation encouraged us to check experimentally whether the VIM-method interpreted in terms of the collection voltage indicates at least correct *relative* tendencies even though it leads to too low numerical values of $\mu^0\tau^0$-products.

### 5.2.2. standard deposition vs. low-temperature hydrogen dilution:

In contrast to the relatively thick cells from the dilution series we measured the considerably thinner cells used as top cells for tandem structures (see section 3.1.2.3). The layer results are summarized in table 5.2. The VIM-results are shown in Fig. 5.9.

| $\mu^0\tau^0$-product | low Temperature (195 °C), $H_2$-diluted | standard temperature (235 °C), undiluted |
|---|---|---|
| initial state | $7.0 \cdot 10^{-7}$ | $5.5 \cdot 10^{-7}$ |
| degraded state | $1.2 \cdot 10^{-7}$ | $6.5 \cdot 10^{-8}$ |

*Table 5.2: Average values of the $\mu^0\tau^0$-products as measured on a-Si:H films deposited at low temperature (195 °C) using hydrogen dilution ratios compared to standard material (undiluted, deposited at 235 °C) in the initial state as well as after accelerated degradation.*

Even more pronounced than in the case of the 450 nm cells shown above we note on one hand an enormous difference in the $\mu^0\tau^0$-values measured in cells and in layers. On the other hand we observe, as previously, a much smaller relative degradation of the $\mu^0\tau^0$-products measured directly in the cells. While the $\mu^0\tau^0$-product of the low temperature, hydrogen diluted material measured in the film degrades by a relative factor of about 6 this ratio is much smaller when measured by VIM directly in the cell. It amounts to only about 1.3 for the 200 nm cell and to about 1.4 for the 250 nm cell. Similarly, one notes in the case of the standard material a relative degradation of about a factor 8 while the $\mu^0\tau^0$-product of the same material, when measured in a cell, degrades only by about a factor 1.6 (in the case of the thinner, 220 nm cell) and by about 1.9 (in the case of the 290 nm cell). Again this observation would be favoring our speculation from above that defective interfaces have a big importance on the collection function: the influence of such interfaces would indeed become more important as the cell thickness shrinks resulting in a less pronounced relative degradation of the bulk material.

Another argument in favor of this hypothesis is supplied by the observation that the $\mu^0\tau^0$-products as determined by VIM on cells incorporating identical i-layer material of various

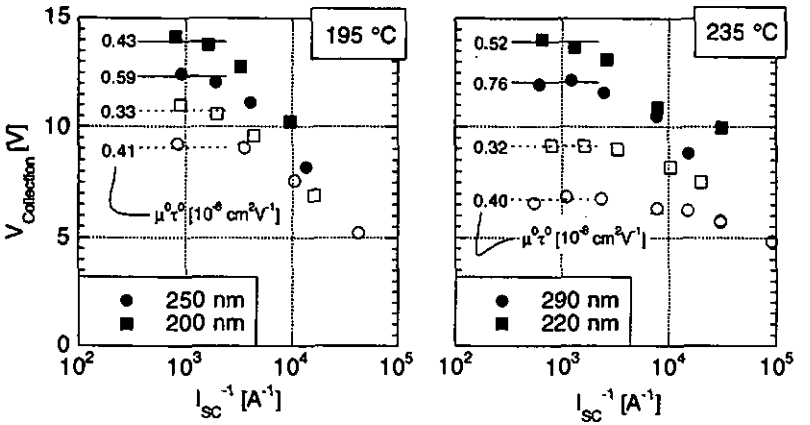


*Fig. 5.9: Collection voltage measurements carried out on a-Si:H p-i-n solar cells in the annealed (filled symbols) and in the degraded state (open symbols). The cells on the left were deposited at 195 °C using hydrogen dilution. The cells on the right were deposited at 235 °C without hydrogen dilution. These cells originate from series presented earlier in Fig. 3.8.*

thicknesses differ only by about 20 % in the degraded state while this difference is more important in the initial case (about 40 %).

### 5.2.3. high substrate temperature series:

It has been noted above that when comparing by the VIM-technique a-Si:H p-i-n cells incorporating the same i-layer material but with different thicknesses the $\mu^0\tau^0$-products are (in the degraded state) comparable within about 20 %. As a cell series for which the i-layer thickness variation covered a larger domain we selected the high substrate temperature series from section 3.1.2.3. Again, comparison of the $\mu^0\tau^0$-products measured in the film (initial state: $3.9 \cdot 10^{-7}$ $cm^2V^{-1}$, degraded state: $7.8 \cdot 10^{-8}$ $cm^2V^{-1}$, see Fig. 3.6) to the ones measured directly in the cell shows that the VIM-method indicates substantially lower values of $\mu^0\tau^0$ (Fig. 5.10).

Concerning the behavior of the collection voltage as a function of the cell thickness it is, however, interesting that, here again, similar $\mu^0\tau^0$-products (within 20 %) are measured for 200 nm, 300 nm and 350 nm cells in the degraded state. In the initial state the variation of $\mu^0\tau^0$-products as a function of the i-layer thickness is more important (ca. 60 %). This affirmation was checked on a thickness series covering an even larger range of i-layer widths shown in the following subsection:

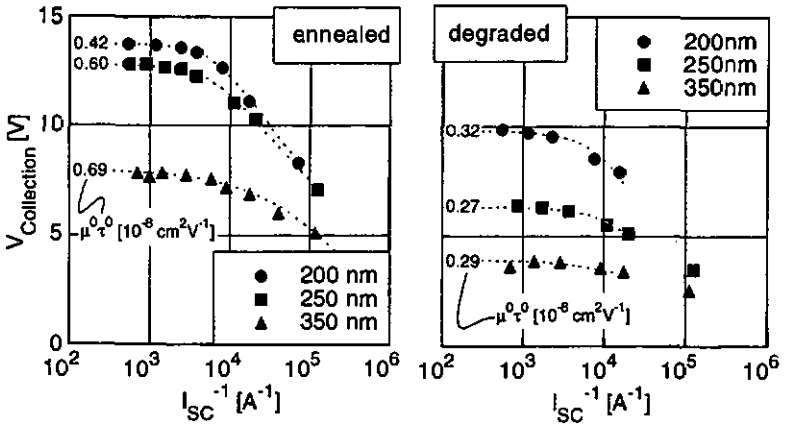


*Fig. S.10: VIM-measurements carried out on a thickness series of a-Si:H p-b-i-n diodes deposited at the high substrate temperature of 280 °C. The left plot indicates measurements carried out in the annealed state. On the right the cells are shown after degradation. These cells are the same as the ones presented in Fig. 3.8.*

### 5.2.4. Thickness series of cells and layers

In order to compare the relative values of the $\mu^0\tau^0$-products measured in layers and cells with varying thickness we deposited four cells with i-layers (with a hydrogen dilution of 2, at a temperature of 195 °C) measuring 300 nm, 600 nm, 1 µm and 2 µm. As these four cells were otherwise identical we expected to observe the effect of the i-layer thickness variation to be notable primarily on the short circuit current of the cells. As can be seen in table 5.3 which summarizes the different characteristics of these four cells the $V_{OC}$ and, even more dramatically, also the FF are affected as well especially at i-layer thicknesses ≥ 1 µm. The short circuit current, on the other hand, exhibits a continuous increase only for the thicknesses up to 1 µm. In the case of the 2 µm cell the low electric field leads to a decrease of collection (as indicated by the low FF) resulting in an even lower short circuit current of this cell in spite of its higher absorption.

| cell thickness | FF | $V_{OC}$ | $I_{SC}$ | $SRI_{sat.,\ 730\ nm}$ |
|---|---|---|---|---|
| 300 nm | 0.732 | 0.867 V | 15.82 mAcm$^{-2}$ | 0.17 |
| 600 nm | 0.738 | 0.862 V | 16.81 mAcm$^{-2}$ | 0.29 |
| 1000 nm | 0.700 | 0.858 V | 17.61 mAcm$^{-2}$ | 0.38 |
| 2000 nm | 0.65 | 0.842 V | 16.65 mAcm$^{-2}$ | 0.50 |

*Table 5.3: Solar cell performances (fill factor, open circuit voltage, short circuit current and spectral response evaluated at 730 nm for reverse bias) of four a-Si:H p-i-n diodes (which differ exclusively in the thickness of the i-layer material) in the initial state.*

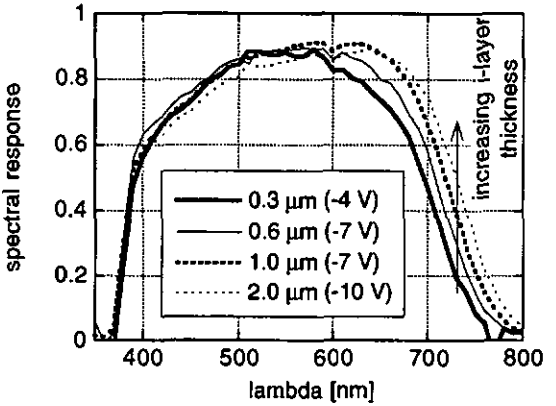


*Fig. 5.11: Spectral response curves of a-Si:H solar cells with different i-layer thicknesses. All measurements were carried out at reverse bias conditions in order to approach complete collection. Note that for thin cells a saturation can relatively easily been obtained while the reverse bias would still have to be increased in the case of the 2 µm cell to extract all photogenerated charge carriers. Here the bias voltage was limited by the measurement equipment.*

That the i-layer absorption is, as expected, increasing monotonously with the i-layer thickness in this series is demonstrated by the saturated spectral response measurements as shown in Fig. 5.11. Indeed, one observes at high negative bias voltages an increasing infra red spectral response which scales to some extent with the i-layer thickness.

The VIM-results evaluated on these cells in their annealed state are presented in Fig. 5.12. One notes that $V_{Collection}$ does not remain constant over a certain plateau at high intensities in the case of the thicker cells. Actually $V_{Collection}$ shows a maximum at low light intensities. In a first attempt this observation was thought to be due to the inhomogeneous generation of the charge carriers within the i-layers of the thick cells since light of a halogen lamp filtered by a RG630 edge filter was used. Therefore, the measurements were carried out again, however, using a better suited optical filter in order to obtain a more uniform charge carrier generation throughout the i-layer. In the case of the 1 µm cell an a-Si:H layer was used which reduced the short circuit current to 10 % of the value obtained with the RG630 filter. For the 2 µm cell a combination of a-Si:H layers was used to filter the halogen lamp reducing the $I_{SC}$ to about 1 %. Comparable curves were, however, obtained for the variation of $V_{Collection}$ over the overlapping range of intensities. This suggests that the collection function of cells of which the i-layer exceeds a certain thickness behaves differently with respect to what can be observed in thin cells. Due to the low electric field conditions space charge effects may have a big importance leading to a field deformation factor $\varphi$ that increases with the totally generated

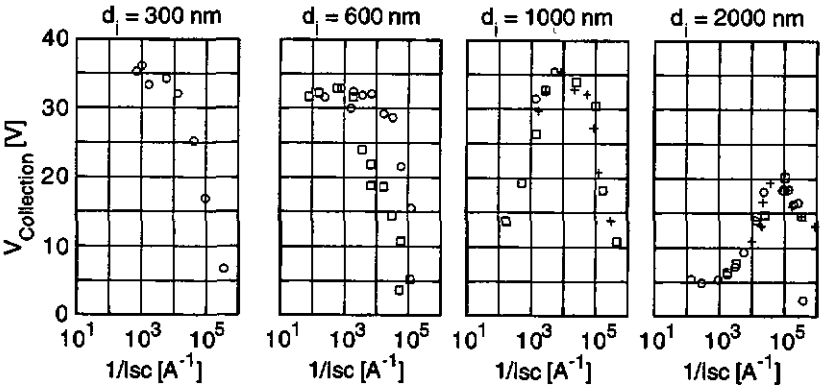


*Fig. 5.12: Collection voltages as measured on a-Si:H p-i-n diodes with different i-layer thicknesses in the annealed state. Different symbols indicate measurements made on different cells. The crosses indicate measurements which were carried out using a-Si:H as optical filter (see text).*

charge carrier densities. While this is only a speculation to explain the observed behavior of the collection voltage as a function of the light intensity it is obvious to me that for such thick cells the VIM-method can, apparently not be applied as a reliable method to determine the i-layer bulk properties.

Comparing the 0.3 µm cell and the two times thicker cell one notes that both have a similar collection voltage. This is in striking contrast to the theory which predicts a variation of the collection voltage approximately proportionally to $V_{Collection} \propto 1/L^2$ (Eqn. 4.30). According

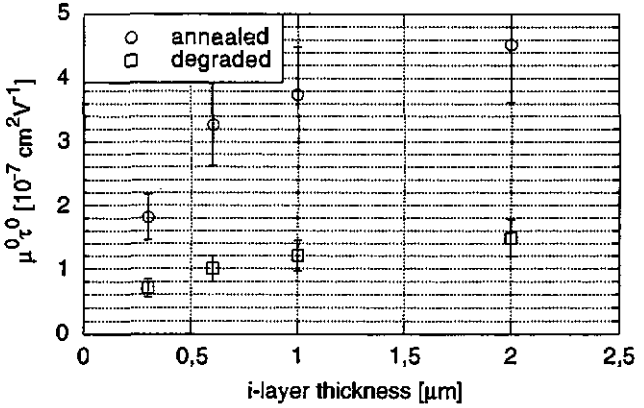


*Fig. 5.13: $\mu^0\tau^0$-products of a-Si:H films in the initial state and after accelerated degradation. The films correspond to the i-layers of the cells of Fig. 5.12.*

to this equation the collection voltage of the thin cell should be about a factor 4 higher than the one of the two times thicker cell. On the other hand, it could also be possible that the thinner i-layer has, indeed, a lower average $\mu^{o}\tau^{o}$-product (by about a factor 4) due to the bigger relative importance of a hypothetical interface layer of very low quality.

In order to cross-check whether this small collection voltage of the 0.3 μm cell can be attributed to such a defective interface layer this cell series was compared to a thickness series of films consisting of the same i-layers deposited on glass.

These layers were characterized in the way presented in chapter 1. The measurements are summarized in Fig. 5.13. It is interesting that in the initial state and although in a less pronounced manner we do, indeed, observe an increase of the average coplanar transport quality as measured by $\mu^{o}\tau^{o}$ with an increase of the i-layer thickness. This enhancement is, however, not sufficient to explain the collection voltages which were measured in the cells. A difference by a factor four would be expected between the $\mu^{o}\tau^{o}$ products of the two thinnest layers to account for an identical collection voltage. The results presented here suggest that, at least in the initial state, the VIM-method does not indicate bulk properties of the a-Si:H cells.

Fig. 5.14 indicates the measurements of the collection voltages measured on this same thickness series of solar cells *after extended degradation* (1000 h, AM1.5, according to section 2.3). The collection voltage of the 600 nm cell (5.5 V, corresponding to a $\mu^{o}\tau^{o}$-product of $1.3 \cdot 10^{-8}$ $cm^{2}V^{-1}$) is now considerably lower than the one of 300 nm cell (14.5 V, corresponding to a $\mu^{o}\tau^{o}$-product of $1.0 \cdot 10^{-8}$ $cm^{2}V^{-1}$). This factor of 1.3 between these two $\mu^{o}\tau^{o}$-products measured after degradation in the cells of moderate thickness is similar to what has been evalnated on the i-layers alone. Regarding the thicker cells, we observe also in the

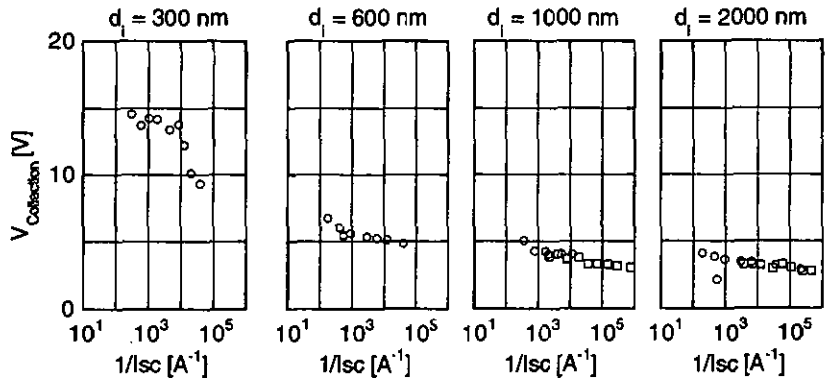


*Fig. 5.14: Collection voltages as measured on a-Si:H p-i-n diodes with different i-layer thicknesses in the degraded state.*

degraded state a collection behavior which can apparently not be reconciled with the model developed in chapter 4: Although in the degraded state the collection voltage is now even for the thick cells almost constant over a relatively large intensity range it is intriguing that both cells have approximately the same collection voltage (of about 4 V, leading to a $\mu^0\tau^0$-product of $2.4 \cdot 10^{-8}$ $cm^2V^{-1}$ in the case of the 1 µm cell and to about $9.6 \cdot 10^{-8}$ $cm^2V^{-1}$ in the case of the 2 µm cell.). Again, we think that this could be due to the extreme thickness of the cells.

### 5.2.5. Second thickness series

Two observations made on the thickness series presented above indicated that the concept of the collection voltage can apparently not be related to the bulk quality of *thick* cells: in the initial state the collection voltage is not constant over certain intensity range but it shows a maximum at relatively low light levels. In the degraded state it is identical for a 1 µm and for a 2 µm cell.

A second thickness series cells (deposited at the KFA, Jülich) was thus analyzed to study more carefully the thickness range of *thin* cells (up 1 µm). The cells were in principle ideotical except their i-layer, which varied in thickness. Table 5.4 summarizes the cell performances measured on these cells after annealing. The 480 nm thick solar cell has clearly a lower $V_{OC}$ compared to the rest of the series. On the other hand its short circuit curreot is higher than the one of the 720 nm cell. A closer look at the depositioo coodltions revealed that the i-layer of this cell was the only ooe to be deposited nsing a gas heater. We think that this could be responsible for a slightly higher gap of this i-layer.

| cell thickness | FF | $V_{OC}$ | $I_{SC}$ | $SR|_{0\ V,\ 730\ nm}$ |
|---|---|---|---|---|
| 240 nm | 0.73 | 0.825 | 12.199 | 0.096 |
| 360 nm | 0.73 | 0.844 | 13.061 | 0.122 |
| 480 nm | 0.72 | 0.806 | 14.256 | 0.202 |
| 720 nm | 0.71 | 0.841 | 14.054 | 0.238 |
| 1080 nm | 0.69 | 0.826 | 14.579 | 0.285 |

*Table 5.4: Solar cell performances of a-Si:H p-i-n diodes with different i-layer thicknesses after annealing.*

In spite of this difference in the i-layer of the 480 nm cell the VIM-method was applied to the whole series of cells. The collection voltages measured on the different cells in their annealed state are shown in Fig. 5.15.

Again the measurements are in strong contrast to the expected behavior of the collection voltage with the cell thickness which, according to eqn. 4.30, is expected to vary like $V_{Collection} \propto 1/L^2$. Again this result suggests that in the initial state the collection voltage does not

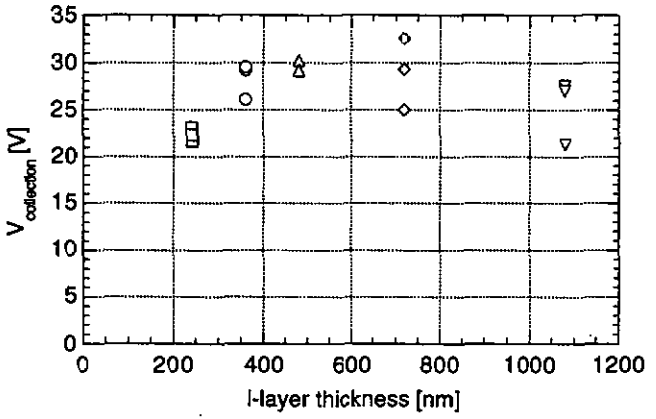


*Fig. 5.15: Collection voltages measured on a-Si:H solar cells with varying i-layer thickness after annealing. Three different cells were measured for each i-layer thickness.*

reflect i-layer bulk properties. The observation, that the collection voltage is approximately constant with the i-layer thickness and that it corresponds to much lower $\mu^0\tau^0$-products than the ones which are typically measured in intrinsic films indicates that additional recombination does take place which reduces the photocurrent collection. We think that defective zones within the i-layer adjacent to the p-i and to the n-i interfaces could be screening the actual bulk recombination at the bias voltage V = 0 V (at which the collection voltage is measured) *especially in the initial state*. After degradation one could then imagine that in the case of thick enough cells the reduced quality of the bulk dominates again the total recombination.

Fig. 5.16 shows VIM-results measured on the cells of the thickness series after degradation. It is interesting to note that now, in the degraded state, the collection voltage depends on the i-layer thickness to a certain extent as expected by eqn. 4.30. Indeed the evaluated collection voltages correspond in the case of three cells (360 nm, 480 nm and 720 nm) to quite similar $\mu^0\tau^0$-products. This could be an indication that in these situations the recombination is dominated by the bulk properties. As to the 240 nm cell its collection voltage (which does not clearly extend over a definite intensity range) would correspond to a $\mu^0\tau^0$-product of $0.8 \cdot 10^{-8}$ $cm^2V^{-1}$ which is considerably lower with respect to the values measured in the thicker cells. One could speculate that in the case of this thin cell the interface recombination could still have a dominant importance even after degradation. The 1080 nm cell, on the other hand, has a collection voltage after degradation which is approximately identical to the one measured the 720 nm cell. Additionally the intensity dependency of $V_{Collection}$ of this cell reflects an atypical behavior (with a maximum at relatively low intensities). This is again an indication that for this thick cell the collection could enter a different regime and

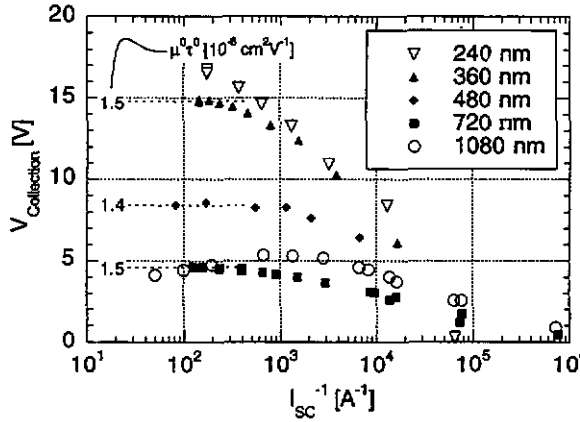


*Fig. 5.16: VIM-results obtained on the second thickness series of a-Si:H solar cells after degradation. The solid symbols correspond to the cells for which the $\mu^0\tau^0$-product is indicated. For explanations refer to the text.*

that the collection voltage is not an appropriate quantity to characterize the bulk properties of its i-layer.

### 5.2.6. Concluding remarks

Within the framework of this work a large number of a-Si:H solar cells has been evaluated using the VIM-technique. A part of these cells (of which the i-layer material had been measured apart or which formed a consistent thickness series) were presented in this chapter. The highest collection voltages measured amounted to less than 40 V (The limit of the AC-VIM set-up is considerably higher as was shown in annex III. This could also be verified experimentally on crystalline diodes on which collection voltages exceeding 100 V were measured.). $V_{Collection}$ was generally observed to increase monotonously with the short circuit current before stabilizing at a constant value at high intensities over a plateau of one to two orders of magnitude. A reduction of $V_{Collection}$ due to the series resistance at high intensities was observed exclusively on larger (> 0.25 cm$^2$) cells of the reversed n-i-p structure which were contacted by ITO.

The cell measurements presented in section 5.2 lead to the following observations:

1) The $\mu^0\tau^0$-products measured directly in cells are considerably lower than the ones measured in corresponding i-layers. In the degraded state the difference amounts to about a factor 10. In the initial state it is generally even more dramatic and values of

$\mu^0\tau^0$ up to a factor 100 higher (e.g. high temperature series) were sometimes measured in the films with respect to the cells.

2) The relative degradation of the $\mu^0\tau^0$-products measured in the cell (by VIM) was often lower than the relative degradation observed in the corresponding layer. The relative degradation was particularly low in thin cells for which the absolute value of $\mu^0\tau^0$, also, was low.

3) For thick cells (thickness $\geq 1$ µm) $V_{Collection}$ followed a different intensity dependency than for thinner cells. Rather than remaining constant over a certain range this quantity reached, here, a maximum at relatively low intensities.

4) Solar cells differing exclusively by the thickness of their respective i-layers displayed in the degraded state generally the expected $V_{Collection}$ vs. thickness behavior. In the initial state this relation was sometimes respected (e.g. section 5.2.2. or in section 5.2.3.). In other situations $V_{Collection}$ was merely independent of the cell thickness (e.g. section 5.2.4. and section 5.2.5).

These observations lead us to the affirmation that the VIM-concept as it has been presented and deepened in chapter 4 and chapter 5 of the present work can not be used under all circumstances to gain the desired feedback in the process of cell optimization as explained earlier. We have not found convincing evidence that the newly introduced quantity $V_{Collection}$ can, in any case, really be connected to the bulk properties of an i-layer incorporated into an a-Si:H p-i-n diode.

It seems, nevertheless, that in some particular situations $V_{Collection}$ is related, at least qualitatively to the i-layer of a-Si:H solar cells. The systematic way in which the measurements deviate from the expected behavior (deviations are pronounced more strongly in the initial state and for thin cells) indicate that additional recombination in defective regions close to the interfaces could be responsible for this. We think that a complementary measurement technique sensitive for interface recombination could - when used in combination with VIM - allow to distinguish between interface and bulk effects.

# ANNEX I

## Error estimation lo the $\mu^o\tau^o$ evaluation

In this paragraph we estimate the experimental error committed in the determinatioo of the $\mu^o\tau^o$-product according to the procedure described in section 1.1.6. This parameter is calculated according to eqn. (A1):

$$\mu^0\tau^0 = \frac{\sigma_{photo}}{eG}\cdot\frac{1}{z} \tag{A1}$$

with the correction factor z being determined from:

$$z = \frac{1}{f^0} = \left(\frac{\sigma_n^0}{\sigma_n^+}\frac{1}{b} + 1 + \frac{\sigma_p^0}{\sigma_p^-}b\right) \tag{A2}$$

where the value of b required for this correction factor is accessible through a measurement of the photoconductivity and of the ambipolar diffusioo length:

$$\frac{b}{(b+1)^2} = \frac{L_{amb}^2 e^2 G}{kT\sigma_{photo}C} \tag{A3}$$

In the following we will for the sake of clarity consider two situations:

*1.) truly intrinsic materials:*

These considerations apply to material with very low cootamination or layers which have been extensively light soaked and for which the Fermi level has a midgap position. Under these circumstances the correction factor z can be approximated by $z \approx 1$. The $\mu^o\tau^o$-product is then exclusively determined by the photoconductivity $\sigma_{photo}$ and the generation rate $G$:

$$\mu^0\tau^0 = \frac{\sigma_{photo}}{eG} = \frac{1}{R}\cdot\frac{s}{l\cdot d}\cdot\frac{1}{e}\cdot\frac{1}{G} \tag{A4}$$

The quantities that have to be measured are in this case the total sample resistance R, the electrode spacing s, the electrode length l, the sample thickness d and the generatioo rate which is evaluated froro an intensity measurement:

$$G = I_0\cdot(1-R)\cdot\frac{\lambda}{hc}\cdot\frac{1}{d}\cdot(1-e^{-\alpha d}) \tag{A5}$$

The relative error of $\mu^0\tau^0$ in the initial state can therefore be estimated to be:

$$\frac{\Delta(\mu^0\tau^0)}{\mu^0\tau^0} = \left|\frac{\Delta R}{R}\right| + \left|\frac{\Delta s}{s}\right| + \left|\frac{\Delta l}{l}\right| + \left|\frac{\Delta d}{d}\right| + \left|\frac{\Delta G}{G}\right| \tag{A6}$$

Clearly the most important error source is thereby identified as the generation rate which is affected by the imperfection of the collimation, the evaluated absorption coefficient, as well as the thickness. Totally the incertainty of the generation rate is estimated to be about 20 %. The contributions of the measurement errors of the other paramaters are estimated to be about 1 % in the case of R, 5 % in the case of s, 2 % in the case of l and 2 % in the case of d.

As a result in the case of truely intrinsic samples (i.e. in the degraded state) the value of $\mu^0\tau^0$ can be determined with a accuracy of about 30 %. Note that the most important errors are partly systematic (expecially the correct evaluation of the light intensity). Therefore it is often possible to observe correct tendencies even if the $\mu^0\tau^0$-product varies less.

*2.) extrinsic material:*

Under these circumstances two distinct situations may occur. The transport can be dominated either electrons or boles.

In the first case (n-type sample) the following relation holds:

$$b >> \frac{\sigma_p^-}{\sigma_p^0} >> 1 \tag{A7}$$

It follows that:

$$\frac{b}{(b+1)^2} \approx \frac{1}{b};\quad z \approx \frac{\sigma_p^0}{\sigma_p^-} b \tag{A8}$$

whereas in the opposite situation (p-type sample):

$$b << \frac{\sigma_n^0}{\sigma_n^+} << 1 \tag{A9}$$

leading to:

$$\frac{b}{(b+1)^2} \approx b;\; z \approx \frac{\sigma_n^0}{\sigma_n^+}\frac{1}{b} \tag{A10}$$

In both cases it turns out that $\mu^0\tau^0$ can be expressed as:

$$\mu^0\tau^0 = L_{amb}{}^2 \cdot \frac{e}{k \cdot T \cdot C} \cdot \frac{\sigma_p^-}{\sigma_p^0} \qquad \text{(A11)}$$

It follows that with a measurement precision of about 5 % for $L_{amb}$ (see e.g. [Sauvain 1992]) and neglecting the uncertainty in the cross-section ratio which constitutes a systematic error (since it is supposed to be the same for all samples) one finds that $\mu^0\tau^0$ can be ideally measured with an accuracy of about 10 %. In practice however this precision can not always be obtained since the degradation of the sample during the measurement can be sometimes important even at low light intensities.

# ANNEX II

## Calculation of $R_{SC}$

Based on the equivalent circuit of paragraph 4.3 it has been found that the total current of a p-i-n solar cell under illumination can be expressed as:

$$I(V) = -I_{photo} \cdot \chi(V - I \cdot R_S) + D(V - I \cdot R_S) + S(V - I \cdot R_S) \tag{A12}$$

In this equation $\chi$ refers to the collection given by:

$$\chi(V - I \cdot R_s) = \frac{1}{1 + \dfrac{L^2 \cdot \varphi}{\mu^0 \tau^0 \cdot (V_{bi} - [V - IR_s])}} \tag{A13}$$

D stands for the diode term:

$$D(V - I \cdot R_s) = I_0 \left( e^{q\frac{V - IR_s}{nkT}} - 1 \right) \tag{A14}$$

S corresponds to the parallel resistance losses:

$$S(V - I \cdot R_s) = \frac{V - IR_s}{R_p} \tag{A15}$$

Calculating the derivative of expression (A12) while taking into account that I(V) is actually an implicit function one finds:

$$\frac{\partial I}{\partial V} = \left\{ -I_{photo} \cdot \chi' + D' + S' \right\} \cdot \left[ 1 - \frac{\partial I}{\partial V} \cdot R_s \right] \tag{A16}$$

The short circuit resistance $R_{SC}$ can then be written as:

$$R_{SC}^{-1} = \frac{\partial I}{\partial V} = \frac{1}{\dfrac{1}{\left\{ -I_{photo} \cdot \chi' + D' + S' \right\}} + R_s} \tag{A17}$$

Since the term in brackets of expression (A17) contains a contribution which is proportional to the photogenerated current it follows that the high intensity limit of $R_{SC}$ is given by

$$R_{SC} = \left(\frac{\partial I}{\partial V}\right)^{-1} \xrightarrow{I_{photo} \to \infty} R_s \tag{A18}$$

At light intensities sufficiently low to have

$$1 >> \frac{\partial I}{\partial V} \cdot R_s \tag{A19}$$

$\partial I/\partial V$ can be approximated by

$$\frac{\partial I}{\partial V} = \left\{-I_{photo} \cdot \chi' + D' + S'\right\} \tag{A20}$$

Derivation yields the following contributions to $\partial I/\partial V$ at V = 0 V (here the influence of $R_s$ has been assumed to be negligible):

$$I_{photo} \cdot \chi' \approx I_{photo} \cdot \frac{L^2 \varphi}{\mu^0 \tau^0 \cdot V_{bi}} \cdot \frac{1}{\left(1 + \frac{L^2 \cdot \varphi}{\mu^0 \tau^0 \cdot V_{bi}}\right)^2} \tag{A21}$$

$$D' \approx \frac{I_0}{n\frac{kT}{q}} \tag{A22}$$

$$S' \approx \frac{1}{R_p} \tag{A23}$$

This results in the expressions given in section 4.3 for the medium and low level intensity regimes.

# ANNEX III

## PRECISION CONSIDERATIONS FOR THE VIM METHOD

### A) DC-VIM method

In the following an estimation of the precision at which the collection voltage $V_{coll.}$ can be evaluated using the DC-VIM approach is presented. For the calculation we admit that the collection function $\chi$ is the quantity which is measured. Practically one measures in fact either the current of a cell or its spectral response which are both proportional to $\chi$. And the considerations could be formulated accordingly - leading to the same result.

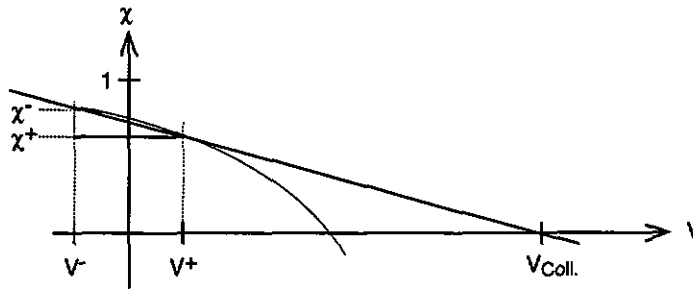


*Fig. (A.1): Determination of the collection voltage $V_{coll.}$ by the evaluation of the collection function $\chi$ at the voltages of $V^+$ and $V^-$.*

Geometrically one sees in fig. (A.1) that the collection voltage $V_{coll.}$ can be calculated as:

$$V_{coll.} = \frac{\chi^+ + \chi^-}{2} \cdot \frac{V^+ - V^-}{|\chi^+ - \chi^-|} \tag{A24}$$

The relative error in the $V_{coll.}$ determination amounts to:

$$\frac{\Delta V_{coll.}}{V_{coll.}} = \frac{1}{V_{coll.}} \left( \left| \frac{\partial V_{coll.}}{\partial \chi^+} \right| \Delta\chi^+ + \left| \frac{\partial V_{coll.}}{\partial \chi^-} \right| \Delta\chi^- \right) \xrightarrow{\Delta\chi^+ = \Delta\chi^- = \Delta\chi} \frac{\Delta\chi}{\chi(0)} + \frac{2 \cdot \Delta\chi}{|\chi^+ - \chi^-|} \tag{A25}$$

where $|\chi^+ - \chi^-|$ can be estimated as:

$$|\chi^+ - \chi^-| \approx \frac{V^+ - V^-}{V_{coll.}} \cdot \chi(0) \tag{A26}$$

The relative error in the collectioo voltage determination can then be estimated to be:

$$\frac{\Delta V_{coll.}}{V_{coll.}} \approx \frac{\Delta\chi}{\chi(0)} + 2\cdot\frac{\Delta\chi}{\chi(0)}\cdot\frac{V_{coll.}}{V^+ - V^-} \approx 2\cdot\frac{\Delta\chi}{\chi(0)}\cdot\frac{V_{coll.}}{V^+ - V^-} \qquad \text{(A27)}$$

This means that the relative error committed in the determination of $\chi$ is magnified two times by the magnitude of the lever $V_{coll.}/(V^+ - V^-)$. In the case of a-Si:H solar cells it is acceptable to keep this lever relatively small by selecting $V^+ - V^- = 0.2\ V$. Would we like to measure the collectioo voltage of a cell with $V_{coll.} = 20\ V$ with a precision of 10 % under these conditions then our set-up should be able to measure $\chi$ with a relative error smaller than 0.05 %.

For comparison this can be compared to the specified accuracy of the source measure unit (Keithley, smu 236) which we use for the IV-curve acquisition. Under ideal conditions (short, blinded terminals, apparatus thermally stabilized) an accuracy of ±0.035 % can be obtained with this instrument. In practice more than just two points of $\chi$ are used for the determination of $V_{coll.}$ as one is actually fitting a straigbt line through a set of measurement points. The precision would then approximately increase with the square root of the number of measurement points.

### B) AC-VIM method

In the previously presented DC-VIM technique the variation of the collection functioo $\chi$ was evaluated as the difference of two separately measured quantities. With a decrease of this difference its relative error increases dramatically. In the AC-VIM approach this problem can be strongly reduced.

Here one disposes of a separate measurement of the collection variation $\tilde{\chi} = \chi^+ - \chi^-$ around the origin and the collection $\chi$ itself. The collection voltage $V_{coll.}$ is determined from these two measurements as above:

$$V_{coll.} = \frac{\chi}{\tilde{\chi}}\cdot\left(V^+ - V^-\right) \qquad \text{(A28)}$$

In this case the relative error committed in the evaluation of $V_{coll.}$ corresponds simply to the sum of the relative errors:

$$\frac{\Delta V_{coll.}}{V_{coll.}} = \frac{1}{V_{coll.}}\left(\left|\frac{\partial V_{coll.}}{\partial\chi}\right|\Delta\chi + \left|\frac{\partial V_{coll.}}{\partial\tilde{\chi}}\right|\Delta\tilde{\chi}\right) = \frac{\Delta\chi}{\chi} + \frac{\Delta\tilde{\chi}}{\tilde{\chi}} \qquad \text{(A29)}$$

To measure the same cell as in the example above with the same precision then it would be sufficient to measure $\chi$ and $\tilde{\chi}$ both with an relative accuracy of 5 %.

# ABBREVIATIONS

| | |
|---|---|
| AM1.5: | air mass 1.5 spectrum - spectrum of sun rays after their passage through an atmosphere 1.5 times as thick as ours (i.e. under an angle) |
| amphoteric state: | defect state which can have three different charge states (positively charged, neutral negatively charged) |
| a-Si:H: | hydrogenated amorphous silicon |
| CW: | continuous wave, i.e. not pulsed |
| $E_F$: | Fermi level |
| FF: | fill factor |
| GD: | glow discharge, i.e. plasma enhanced chemical vapor deposition |
| HeNe: | helium-neon laser (the gas lasers used in this work are operated at a wavelength of 633 nm) |
| HW: | hot-wire deposition method |
| Isc: | short circuit current |
| KG1: | type of Shott glass used as heat absorbing filter |
| $L_{amb}$: | ambipolar diffusion length |
| MPP: | maximum power point |
| Nd-YAG: | neodyme doped yttrium-aluminium garnet based solid state laser |
| $\mu^o\tau^o$: | normalized mobility recombination time product |
| PLD: | fluorescent lamps with solar spectrum (trade name of Philips) |
| QE: | quantum efficiency |
| RG630: | red glass filter with a sharp cut-off wavelength at 630 nm |
| $R_p$: | parallel resistance |
| $R_s$: | series resistance |
| $R_{sc}$: | short circuit resistance |
| $\sigma_{photo}$: | photoconductivity |
| SLD: | sodium lamp degradation system |
| SR: | spectral response |
| SSPG: | steady state photocarrier grating method |
| TCO: | transparent conductive oxide |
| VHF-GD: | very high frequency glow discharge |
| $V_{oc}$: | open circuit voltage |
| YAG: | see under Nd-YAG |
| ZnO: | zinc oxide, used in this work as a TCO |

# REFERENCES


[Arch 1991] J.K. Arch, F.A. Rubinelli, J.-Y. Hou, and S.J. Fonash, (1991), J. Appl. Phys., **69**, 7057.

[Arya 1986] R. Arya, A. Catalano, and R.S. Oswald, (1986), Appl. Phys. Lett., **49**, 1089.

[Banerjee 1991] A. Banerjee, S. Guha, A. Pawlikiewicz, D. Wolf, and J. Yang, (1991), AIP Conf. Proc., **234**, 268.

[Beck 1997] N. Beck, (1997), Ph. D. thesis, Institut de Microtechnique, Neuchâtel,

[Beck 1996] N. Beck, N. Wyrsch, C. Hof, and A. Shah, (1996), Journal of Applied Physics, **79**, 9361-9368.

[Beck 1992] N. Beck, N. Wyrsch, E. Sauvain, and A. Shah, 1992, in *European Photovoltaic Solar Energy Coference*, Montreux,

[Beck 1993] N. Beck, N. Wyrsch, E. Sauvain, and A. Shah, 1993, in *Material Research Society Symposium Proceedings*, San Fransisco,

[Bube 1998] R.H. Bube, Photovoltaic Materials, ed., Imperial College Press, London, 1998.

[Crandall 1983] R.S. Crandall, (1983), J. Appl. Phys., **54**, 7176.

[Curry 1998] R. Curry, (1998), Photovoltaic Insiders' Report, **17**, 1.

[Curtins 1989] H. Curtins and M. Favre, in *Amorphous Silicon and related Materials Vol. A)*, edited by H. Fritzsche (World Scientific Publishing Co. Pte. Ltd., Singapore, 1989), pp. 329

[Curtins 1987] H. Curtins, N. Wyrsch, and A. Shah, (1987), Electron. Lett., **23**, 228.

[Dawson 1996] R.M.A. Dawson and C.M. Fortmann, (1996), J. Appl. Phys., **79**, 3075.

References


[Faughnan 1984] B.W. Faughnan and R.S. Crandall, (1984), Appl. Phys. Lett., **44**, 537.

[Favre 1993] M. Favre, (1993), Ph. D. thesis, IMT, Neuchatel.

[Fischer 1994] D. Fischer, (1994), Ph. D. thesis, Institut de Microtechnique, Neuchâtel, Neuchâtel.

[Fischer 1996] D. Fischer, S. Duhail, J.A.A. Selvan, N. Pellaton-Vaucher, R. Platz, C. Hof, U. Kroll, J. Meier, P. Torres, H. Keppner, M. Goetz, A. Shah, and K.D. Ufert, 1996, in *25th IEEE Photovoltaic Specialists Conference*, Washington, 1053

[Flückiger 1995] R.S. Flückiger, (1995), Ph. D. thesis, Neuchâtel.

[Green 1982] M.A. Green, Solar Cells, Operating Principles, Technology and System Applications, ed., Prentice-Hall, Englewood Cliffs, N. J. 07632, 1982.

[Green 1999] M.A. Green, K. Emery, K. Bücher, D.L. King, and S. Igari, (1999), Photovolt. Res. Appl., **7**, 31-37.

[Hack 1985] M. Hack and M. Shur, (1985), J. Appl. Phys., **58**, 997.

[Hattori 1991] K. Hattori, Y. Niwano, H. Okamoto, and Y. Hamakawa, (1991), J. Non-Cryst. Solids, **137&138**, 363.

[Hecht 1932] K. Hecht, (1932), Z. f. Phys., **77**, 16.

[Hegedus 1997] S.S. Hegedus, (1997), Prog. Photovolt. Res. Appl., **5**, 151.

[Hegedus 1994] S.S. Hegedus and J.E. Phillips, 1994, in *First WCPEC*, Hawaii, 654

[Henry 1977] C.H. Henry and D.V. Lang, (1977), Phys. Rev. B, **15**, 989.

[Hubin 1995] J. Hubin and A. Shah, (1995), Phil. Mag. B, **72**, 589.

[Huhin 1992] J. Hubin, A.V. Shah, and E. Sauvain, (1992), Phil. Mag. Lett., **66**, 115.

[Ingram 1996] A.E. Ingram and e. al., 1996, in *Proc. 25th IEEE Photovoltaic Specialists Conference*, 477

[Kleider 1995] J.P. Kleider, C. Longeaud, M. Barranco-Diaz, P. Morin, and P. Roca-i-Cabarrocas, (1995), J. Appl. Phys., **78**, 317.

[Kocka 1994] J. Kocka, M. Vanecek, P. Machacek, A. Fejfar, E. Sipek, Ho-The-Ha, I. Pelant, J. Fric, J. Rosa, Z. Remes, and A. Poruba, (1994), Proceedings, 1st World Conference on PVEC, Hawai,

[Kroll 1995] U. Kroll, J. Meier, H. Keppner, A. Shah, S.D. Littlewood, I.E. Kelly, and P. Giannoulès, (1995), J. Vac. Sci. Technol. A, **6**, 2742.

[Kunz 1995] S. Kunz and e. al., (1995), Proc. of the 13th European Photovoltaic Solar Energy Conference, 733.

[Lang 1991] L. Lang, L. Chen, and A. Catalano, (1991), AIP Conf. Proc., **234**, 275.

[Mahan 1991] A.H. Mahan and M. Vanacek, 1991, in *AIP Conference Proceedings* , **234**, 195

[Meier 1995] C. Meier and e. al., (1995), Proc. of the 13th European Photovoltaic Solar Energy Conference, 831.

[Meier 1996] J. Meier, P. Torres, R. Platz, S. Dubail, U. Kroll, J.A.A. Selvan, N.P. Vaucher, C. Hof, D. Fischer, H. Keppner, A. Shah, K.-D. Ufert, P. Giannoulès, and J. Koehler, (1996), Material Research Society Symposium Proceedings, **420**, 3-14.

[Merten 1998] J. Merten, J.M. Asensi, C. Voz, A.V. Shah, R. Platz, and J. Andreu, (1998), IEEE Trans. Electr. Dev., 45, 423.

[Nowak 1995] S. Nowak and in OFEN, in *Vol.* edited by 1995), pp. 32

[OFEN 1995] OFEN and O.f.d. l'énergie, Statistique suisse de l'électricité, ed., Bern:1995.

[OFES 1997] OFES and O.f.d.l. statistique, Annuaire statistique de la Suisse, ed., 1997.

[Pankove 1984] J.I. Pankove, Semiconductors and Semimetals, ed., London:Academic Press Inc., 1984.

[Pellaton-Vaucher 1998] N. Pellaton-Vaucher, (1998), Ph. D. thesis, Institut de Microtechnique, Neuchâtel, Neuchâtel.

[Platz 1996] R. Platz, D. Fischer, C. Hof, S. Dubail, J. Meier, U. Kroll, and A. Shah, (1996), Mat. Res. Soc. Symp. Proc., **420**, 51.

[Platz 1997] R. Platz, C. Hof, D. Fischer, J. Meier, and A. Shah, (1997), Solar Energy Materials & Solar Cells, **53**, 1-13.

[Rech 1997] B. Rech, (1997), Ph. D. thesis, Forschungszentrum, Jülich.

[Rech 1995] B. Rech, C. Beneking, S. Wieder, T. Eickhoff, and H. Wagner, 1995, in *13th European Photovoltaic Solar Energy Conference* , Nice, 613

[Redfield 1992] D. Redfield, (1992), Material Research Society Symposium Proceedings, 258, 341.

[Rose 1963] A. Rose, Concepts in photoconductivity and allied problems, ed., Interscience Publishers, John Wiley & Sons, 1963.

[Sauvain 1992] E. Sauvain, (1992), Ph. D. thesis, Faculté des Sciences, Neuchâtel, Neuchâtel.

[Shah 1996] A. Shah, (1996), unpublished,

[Shah 1992] A. Shah, J. Dutta, N. Wyrsch, K. Prasad, H. Curtins, F. Finger, A. Howling, and C. Hollenstein, (1992), Mat. Res. Symp. Proc., **258**, 15.

[Shah 1997] A. Shah, E. Sauvain, J. Hubin, P. Pipoz, and C. Hof, (1997), Phil. Mag. B, **75**, 925-936.

[Shimizu 1993] T. Shimizu, (1993), J. of Non-Cryst. Solids, **164-166**, 163.

[Shockley 1952] W. Shockley and W.T. Read, (1952), Phys. Rev., **87**, 835.

[Smith 1959, 1978] R.A. Smith, Semiconductors, 2 ed., Cambridge University Press, 1959, 1978.

[Smith 1988] Z.E. Smith and S. Wagner, in *Amorphous Silicon and Related Materials Vol.* edited by H. Fritzsche (World Scientific Publishing Co. Pte. Ltd., Singapore, 1988), pp. 409

[Smole 1992] F. Smole and J. Furlan, (1992), J. Appl. Phys., 72, 5964.

[Spear 1984] W.E. Spear, H.L. Steemers, P.G.L. Comber, and R.A. Gibson, (1984), Phil. Mag., 50, L33.

[Staebler 1977] D.L. Staebler and C.R. Wronski, (1977), Appl. Phys. Lett., 31, 292.

[Stiebig 1994] H. Stiebig, A. Kreisel, J.-L. Nicque, T. Eickhoff, C. Beneking, and H. Wagner, 1994, in *Twelfth European Photovoltaic Solar Energy Conference*, Amsterdam, 164

[Street 1982] R.A. Street, (1982), Pbys. Rev. Lett., 49, 1187.

[Street 1991] R.A. Street, Hydrogenated Amorpbous Silicon, ed., Cambridge:Cambridge University Press, 1991.

[Street 1986] R.A. Street, J. Kakalios, and T. Hayes, (1986), Phys. Rev. B, 34, 3030.

[Street 1983] R.A. Street, J. Zesch, and M.J. Thompson, (1983), Appl. Phys. Lett., 43, 672.

[Stutzmann 1987] M. Stutzmann, D.K. Biegelsen, and R.A. Street, (1987), Phys. Rev. B, 35, 5666.

[Stutzmann 1985] M. Stutzmann, W.B. Jackson, and C.C. Tsai, (1985), Phys. Rev. B, 32, 23.

[Stutzmann 1991] M. Stutzmann, J. Nunnenkamp, M.S. Brandt, and A. Asano, (1991), Phys. Rev. Lett., 67, 2347.

[Sze 1981] S.M. Sze, Physics of Semiconductor Devices, 2 ed., 1981.

[Takamoto 1997] T. Takamoto and e. al., (1997), Proc. 14th European Photovoltaic Solar Energy Conference, 970.

[Tonon 1991] T. Tonon, X. Li, and A.E. Delahoy, (1991), AIP Conf. Proc., 234, 259.

[Vaillant 1986] F. Vaillant and D. Jousse, (1986), Phys. Rev. B, 34, 4088.

References


[Vignoli 1996] S. Vignoli, R. Meaudre, M. Meaudre, P.R.i. Cabarrocas, C. Godet, and P. Morin, (1996), J. Noo-Cryst. Solids, **198&200**, 474.

[Wallace 1997] R.L. Wallace and e. al., 1997, in , 171

[Walle 1996] C.G.V.d. Walle, (1996), Material Research Society Symposium Proceedings, **420**, 533.

[Wyrsch 1991] N. Wyrsch and A. Shah, (1991), Solid State Comm., **80**, 807.

[Wyrsch 1994] N. Wyrsch and A. Shah, (1994), Proceedings of the 1st World Conference on Photovoltaic energy conversion, 583.

[Xi 1994] J. Xi, D. Shugar, and H. Volltrauer, 1994, in *1st World Conference of Photovoltaic Energy Conversion* , Waikola, Hawaii, 401

[Xu 1989] X. Xu, A. Morimoto, M. Kumeda, and T. Shimizu, (1989), Material Reasearch Society Symposium Proceedings, **149**, 143.

[Yang 1996] L. Yang, M. Bennett, L. Chen, K. Jansen, J. Kessler, Y. Li, J. Newtoo, K. Rajan, F. Willing, R. Arya, and D. Carlson, (1996), Mat. Res. Soc. Symp. Proc., **420**, 839.

[Zeman 1997] M. Zeman, R.E.I. Schropp, and W. Metselaar, 1997, in *Proceedings of the fourteenth European Photovoltaic Solar Energy Conference* , Barcelona, 586

[Ziegler 1997] Y. Ziegler, (1997), Ph. D. thesis, Institut de microtechnique, Neuchâtel, Neuchâtel.

# ACKNOWLEDGMENTS

First of all, I would like to thank Prof. Arvind Shah who has accepted me to conduct this work in his research group. He has been an ideal thesis supervisor who has not only put me on many interesting tracks but who has also helped me with many fruitful discussions.

I also appreciate the acceptance of Prof. N. F. de Rooij, Dr. B. Rech, Prof. W. Rehwald and Dr. P. Seitz to join the examination board and to devote time to the critical reading of this thesis.

A special thank goes to Nicolas Wyrsch who helped me a lot with his scientific competeoce and his ability to present the essential points in a very clear way. He never refused to help me with practical problems at any time.

Diego Fischer has been a very motivatiog person to work with who was able to share his enthusiasm for photovoltaic energy conversion. Particularly, he pushed me at the very beginning of my work on a-Si:H. Thanks for all your inputs.

Essential contributions - namely the biggest part of the samples presented in this thesis were provided by Rainer Platz. He has been a great technologist with a good sense of humor. These statements apply also to Sébastien Dubail (who, too, deposited a large amount of films and cells for me) and to Yvan Ziegler (who produced the hot wire material).

The special, comfortable "ambiance" in Arvinds' group has been great to dive and survive in. All my colleagues and friends from the thin film group - as individuals - deserve a special thanks for making me spend a good time at IMT.

I would like to thank Laurence for accompanying me over the last couple of years and who has definitely contributed in many respects to the successful termination of this "project 2000".

Finally, I would like to thank my parents for their continuous encouragement to lead this work to a good end.